Title
Improved understanding of the climatic and anthropogenic drivers of groundwater depletion and recovery in California's Central Valley

Author
Alam, Sarfaraz

Publication Date
2021

Peer reviewed|Thesis/dissertation

UNIVERSITY OF CALIFORNIA

Los Angeles

Improved Understanding of the Climatic and Anthropogenic Drivers of Groundwater Depletion and Recovery in California's Central Valley

A dissertation submitted in partial satisfaction

of the requirements for the degree

Doctor of Philosophy in Civil Engineering

by

Sarfaraz Alam

2021

ABSTRACT OF THE DISSERTATION

Improved Understanding of the Climatic and Anthropogenic Drivers of Groundwater Depletion and Recovery in California's Central Valley

by

Sarfaraz Alam

Doctor of Philosophy in Civil Engineering

University of California, Los Angeles, 2021

Professor Mekonnen Gebremichael, Chair

The role of climatic and anthropogenic drivers in groundwater storage depletion and recovery in California's Central Valley has been investigated. Specifically, the dissertation addresses three research questions: (1) How does climate change impact the groundwater storage? (2) Can managed aquifer recharge (MAR) mitigate groundwater overdraft? (3) How much of the drought-caused groundwater overdraft in Central Valley has recovered during the post-drought years and what is the role of climate and water management in the fast versus slow post-drought overdraft recovery? In the first part of the dissertation, integrated hydrologic models have been simulated to predict future groundwater storage changes under multiple climate change scenarios and to evaluate the relative contribution of crop water use and surface water inflow to Central Valley regions. It is shown that climate change will accelerate groundwater depletion in the future and an increase in future crop water use will be the dominant cause of future groundwater decline without mitigation measure. In the second part, the impact of large-scale MAR implementation on groundwater overdraft recovery, flood peak, and low flow have been investigated via numerical

experiments. It is shown that MAR has limited capacity to recovery historical groundwater overdraft due to lack of surface water availability in the southern Central Valley (i.e., San Joaquin and Tulare regions). Delivering excess surface water from the delta to the Tulare and San Joaquin region can significantly solve the groundwater overdraft problem. Moreover, MAR can reduce flood peaks, and increase dry season flow. Finally, an ensemble of groundwater storage change estimates has been made using multiple methods and numerical experiments conducted to understand the role of climate and water management to recover drought-caused groundwater overdraft during post-drought years. The result shows that the Central Valley aquifer is not resilient to drought under existing conditions, and it is very challenging to recover drought-caused groundwater overdraft. However, water management measures that restrict groundwater extraction can significantly reduce the groundwater overdraft recovery time.

The dissertation of Sarfaraz Alam is approved.

Dennis P Lettenmaier

William W-G Yeh

Ruopu Li

Mekonnen Gebremichael, Committee Chair

University of California, Los Angeles

2021

This dissertation is dedicated to my family

Table of Contents

List of Figures

List of Tables

ACKNOWLEDGEMENTS

I wish to acknowledge the support and encouragement of my advisor Dr. Mekonnen Gebremichael in guiding me through my doctoral research. I am indebted to the guidance of Dr. Dennis P Lettenmaier, without whom this dissertation would not be possible. I thank Dr. Ruopu Li for providing guidance and insightful suggestions. I also like to thank my dissertation committee member Dr. William W-G Yeh for his valuable suggestions.

I wish to thank many good friends, colleagues, and professors who have shared their knowledge with me during the last couple of years. In particular, I thank Dr. Sanjay Mohanty and Dr. Steve Margulis for valuable suggestions that helped me improve my knowledge and skill. I wish to thank Dr. Akash Koppa for mentoring me and providing me with important suggestions whenever needed. I am indebted to my family for their support and encouragement. I am grateful to my wonderful wife Tasnim Pasha for her support and for being there through the ups and downs during the last almost five years. Without the continuous and unconditional support of my family, I would not be who I am today.

Chapter 2 contains the following published article:

Alam, S., Gebremichael, M., Li, R., Dozier, J. and Lettenmaier, D.P., 2019. Climate change impacts on groundwater storage in the Central Valley, California. Climatic Change, 157, 387–406. https://doi.org/10.1007/s10584-019-02585-5.

Chapter 3 contains the following published article:Alam, S., Gebremichael, M., Li, R., Dozier, J. and Lettenmaier, D.P., 2020. Can Managed Aquifer Recharge Mitigate the Groundwater Overdraft in California's Central Valley? Water Resources Research, 56(8), p.e2020WR027244. https://doi.org/10.1029/2020WR027244.

Chapter 4 contains the following article submitted to Water Resources Research for publication:

Alam, S., Gebremichael, M., Ban, Z., Scanlon, B. R., Senay, G. B. and Lettenmaier, D. P. Post-drought groundwater storage recovery in California's Central Valley. Submitted to Water Resources Research.

VITA

EDUCATION

2013 B.Sc. (Water Resources Engineering), Bangladesh University of Engineering and Technology, Bangladesh

2015 M.Sc. (Water Resources Engineering), Bangladesh University of Engineering and Technology, Bangladesh

2016-2021 Graduate Student Researcher, Department of Civil and Environmental Engineering, University of California, Los Angeles

AWARDS, HONORS & FELLOWSHIPS

2021	UCLA, Outstanding Ph.D. Student Award in Civil & Environmental Engineering
2020	UCLA, Dissertation Year Fellowship
2020	AGU Student Travel Grant
2008-2013	BUET, University Merit Scholarship

PUBLICATIONS

Alam, S., Borthakur, A., Ravi, S., Gebremichael, M. and Mohanty, S., 2021. Managed aquifer recharge implementation criteria to achieve water sustainability. Science of The Total Environment, p.144992. https://doi.org/10.1016/j.scitotenv.2021.144992.

Alam, S., Ali, M., Rahaman, A.Z. and Islam, Z., 2021. Multi-model ensemble projection of mean and extreme streamflow of Brahmaputra River Basin under the impact of climate change. Journal of Water and Climate Change. https://doi.org/10.2166/wcc.2021.286.

Koppa, A., Alam, S., Miralles, D. G. and Gebremichael, M., 2021. Budyko-Based Long-term Water and Energy Balance Closure in Global Watersheds from Earth Observations. Water Resources Research. https://doi.org/10.1029/2020WR028658

Gebremichael, M., Krishnamurthy, P.K., Ghebremichael, L.T. and Alam, S., 2021. What Drives Crop Land Use Change during Multi-Year Droughts in California's Central Valley? Prices or Concern for Water?. Remote Sensing, 13(4), p.650. https://doi.org/10.3390/rs13040650.

Alam, S., Gebremichael, M., Li, R., Dozier, J. and Lettenmaier, D.P., 2020. Can Managed Aquifer Recharge Mitigate the Groundwater Overdraft in California's Central Valley? Water Resources Research, 56(8), p.e2020WR027244. https://doi.org/10.1029/2020WR027244.

Alam, S., Gebremichael, M., Li, R., Dozier, J. and Lettenmaier, D.P., 2019. Climate change impacts on groundwater storage in the Central Valley, California. Climatic Change, 157(3), pp.387-406. https://doi.org/10.1007/s10584-019-02585-5.

Alam, S., Gebremichael, M. and Li, R., 2019. Remote sensing-based assessment of the crop, energy and water Nexus in the Central Valley, California. Remote Sensing, 11(14), p.1701. https://doi.org/10.3390/rs11141701

Cooper, M.G., Schaperow, J.R., Cooley, S.W., Alam, S., Smith, L.C. and Lettenmaier, D.P., 2018. Climate elasticity of low flows in the maritime western US mountains. Water Resources Research, 54(8), pp.5602-5619. https://doi.org/10.1029/2018WR022816.

Alam, S., Ali, M.M. and Islam, Z., 2016. Future streamflow of Brahmaputra River basin under synthetic climate change scenarios. Journal of Hydrologic Engineering, 21(11), p.05016027. https://doi.org/10.1061/(ASCE)HE.1943-5584.0001435.

CHAPTER 1

Introduction

1.1 Background and Motivation

Groundwater contributes more than 36% of the global drinking water supply for millions of people around the world and 42% for irrigation (Alley et al., 2002; Döll et al., 2012). This critical source has been overexploited in many places over the past century, leading to water scarcity (Aeschbach-Hertig and Gleeson, 2012; Famiglietti, 2014; Rodell et al., 2009). Study shows that around 21 out of 37 major aquifers globally are depleted and the depletion is severe in arid and semi-arid regions (Fan et al., 2013; Richey et al., 2015; Wada et al., 2010). Drought accelerates groundwater depletion and adversely impacts natural and human systems (Wilhite and Glantz, 1985). Moreover, agricultural and municipal expansion adds addtionl stress on groundwater resources (Russo and Lall, 2017; Vorosmarty et al., 2000). Declining groundwater is a major threat to environmental and agricultural sustainability and a barrier to the well-being of people living in such regions. Therefore, quantifying groundwater storage changes (i.e. both past and future under climate change), improving the understanding of the causes and consequence of groundwater changes, and identifying ways to reduce groundwater depletion is an important scientific and civil objective.

The primary goal of this dissertation is to improve the understanding of the climatic and anothropogenic drivers of groundwater depletion and recovery in a semi-arid climatic region. Specifically, the dissertation aims to quantify groundwater storage changes under current and future climate, investigate the influence of the changes in different hydrologic components on

groundwater, and identify management measures to mitigate groundwater overdraft problem. The study region selected for the dissertation research is the Central Valley of California. Central Valley is a critically important agricultural region in the USA where the groundwater storage has been declining in the past half-century due to excess groundwater use over natural recharge and frequent drought occurrence (Famiglietti et al., 2011a; Faunt et al., 2016). To halt groundwater depletion, the state has enacted Sustainable Groundwater Management Act in 2014 that requires the groundwater use to be sustainable (California State Legislature, 2014). However, solving the groundwater overdraft problem is sophisticated due to the complex climate-groundwater interaction, the uncertainty in groundwater storage estimations, and limited knowledge on the efficiency of remediation measures. In the following sections, an overview of the challenges and the specific research questions addressed in this dissertation is provided.

1.2 Need for studying groundwater storage changes in a semi-arid region and existing research gaps

Quantifying groundwater storage changes and understanding the role of climate and water management in modulating groundwater changes is challenging due to the lack of in-situ measurements, subsurface hydrogeologic data, groundwater use data, and groundwater-surface water interaction. In semi-arid regions with intensive agriculture, the lack of reliable groundwater storage estimates and limited understanding of groundwater-climate dynamics make it challenging to identify strategies necessary for ensuring agricultural and environmental sustainability. In the subsequent sections, issues related to groundwater storage change that requires detailed investigation are presented.

1.2.1 Understanding the impact of climate change on groundwater storage

Climate change is expected to modulate different components of hydrologic cycle, which can have direct or indirect impact on groundwater recharge and use (IPCC, 2007; Woldeamlak et al., 2007; Zektser and Loaiciga, 1993). The direct impact of climate can come from the change in diffuse recharge from rain and focused recharge from surface water (e.g., wetland, ephemeral streams), while these factors can be modulated by land use and subsurface geology (Taylor et al., 2013). On the other hand, an increase in temperature increases evapotranspiration that can also impact groundwater storage via increasing groundwater extraction volume for irrigation to meet crop water demand. However, the crop water demand also depends on the agricultural practices such as the cropping patterns, irrigation method, and total area covered. Groundwater in agricultural regions that rely heavily on irrigation for crop production (e.g., California's Central Valley) can be particularly vulnerable to changes in surface water availability. As surface water decreases, reliance on groundwater seems to increase, thus threatening the groundwater resources availability. Regions like California where surface water supply is highly dependent on seasonal snowmelt may be particularly vulnerable to an increase in temperature under climate change. Studies show that warming temperature tend to cause earlier snowmelt and earlier peak streamflow (Kapnick and Hall, 2010). Changes in the snowmelt timing and the volume of snow accumulation have important implications on surface water availability. However, the relative contribution of changes in surface water supply (volume and seasonality), and crop water use under future climate were not known, thus limiting the ability to identify appropriate climate change adaptation strategy. Moreover, there has been a limited knowledge of how much additional stress climate change will add to the groundwater storage. The dissertation aims to address these issues (Chapter 2 of the dissertation). Predicting future groundwater storage under climate change and improving

the understanding of the influence of different hydrologic components on groundwater would therefore have direct social implications.

1.2.2 Assessing the role of managed aquifer recharge to recover regionwide groundwater overdraft

Managed aquifer recharge (MAR) is a groundwater management strategy that has the potential to recover groundwater overdraft through recharging excess flood flows (termed Flood-MAR) in the wet seasons to replenish aquifers via artificial recharge, primarily in the form of seasonal land flooding (Sprenger et al., 2017). Recharging surface water started centuries ago (Europe and South America) using ancient methods like sowing and harvesting (known as "careos", "amunas"), while it is still practiced globally using modern methods (Dillon et al., 2019; Martos-Rosillo et al., 2019). MAR is common management strategy preferred for its low implementation cost, low evapotration compared to reservoirs, ability to infiltrate water from multiple sources (Alam et al., 2021; Dillon, 2009; Dillon et al., 2019). But the increase in MAR projects globally is only 5%, whereas the increase in groundwater extraction is much higher (Dillon et al., 2019).

Although MAR has been implemented locally in many places, there has been a limited knowledge of how much the large scale groundwater depletion can be mitigated by MAR. In particular, Central Valley has excess surface water in the stream during winter season that leaves the region (to the Pacific Ocean) without being used or recharged. Additionally, the state enacted Sustainable Groundwater Management Act (SGMA) to mitigate groundwater depletion. Several mitigation measures have been proposed to replenish the overdrafted aquifer, including managing the demand and supply of water resources (Hanak et al., 2018). A key mitigation measure that has been proposed by California's Department of Water Resources (CDWR) is MAR (CDWR, 2018a).

MAR studies in California and elsewhere conducted at the local and farm levels (Dahlke et al., 2018; Ghasemizade et al., 2019; Kourakos et al., 2019) demonstrate the potential of such practices to be scalable to the basin level. Strategies for implementing MAR on a more widespread basis are currently under investigation by CDWR (CDWR, 2018a). However, the benefits and limitations of MAR implementation at the scale of the entire Central Valley are not well understood. There remain key questions, such as the extent to which MAR can replenish existing groundwater overdraft in the Central Valley, and which regions have the greatest potential for MAR.

1.2.3 Understanding the role of climate and water management in post-drought groundwater storage recovery

Groundwater overdraft during droughts is common in semiarid regions globally (Wada et al., 2010), and is expected to be exacerbated by climate change in semi-arid and arid regions (Alam et al., 2019; Wu et al., 2020). Groundwater overdrafts linked to droughts are caused by both reduced groundwater recharge and increased agricultural, industrial, and municipal water demand during droughts (Russo and Lall, 2017; Taylor et al., 2013). While the use of groundwater to mitigate surface water shortages during droughts may be an obvious management response that improves the reliability and robustness of the system, post-drought recovery of groundwater overdraft is key to long-term sustainability. An understanding of the overdraft recovery time and its connection to climate versus anthropogenic factors is critical to developing and implementing sustainable groundwater management plans.

Groundwater storage estimate varies substantially among different methods (Alam et al., 2020; Ojha et al., 2020; Scanlon, et al., 2012), and this has made the understanding of drought recovery challenging. Commonly used methods for groundwater storage change estimation include, (1) observation well measurements (Scanlon, et al., 2012), (2) Gravity Recovery and

Climate Experiment (GRACE) satellite-based estimates (Scanlon, et al., 2012), (3) water balance methods (Xiao et al., 2017), and (4) groundwater simulation models (Brush, 2013; Faunt et al., 2016). Each of the groundwater storage change estimation/measurement methods has its own pros and cons, and there is no single best method that outperforms the others. Past studies of groundwater change in the Central Valley (and many other regions of the world) have relied on only one or two of the above methods. For instance, Xiao et al. (2017) estimated groundwater depletion and post-drought recovery for the 2007-2009 drought using GRACE satellite data and the water balance method. They found groundwater depletion trends to be similar, but recovery rates differed substantially. Therefore, it is important to formally acknowledge differences in results from the different groundwater estimation methods.

Climate and anthropogenic factors can strongly influence groundwater depletion and recovery (Alam, et al. 2019; Hanson et al. 2012; Taylor et al. 2013; Wu et al. 2020). Droughts cause groundwater depletion; the drought recovery period is often calculated from post-drought precipitation duration and magnitude (DeChant and Moradkhani, 2015; Pan et al., 2013). High precipitation during post-drought years increases groundwater recovery, but the effective recovery rate may be hindered by anthropogenic factors, such as increased agricultural and municipal groundwater pumping (Gleeson et al., 2012; Ojha et al., 2020). Although the impacts of drought on groundwater availability have been well studied (Argus et al. 2017; Scanlon et al. 2012; Taylor et al. 2013; Thomas and Famiglietti 2019; Xiao et al. 2017), it is unknown how post-drought groundwater recovery responds to post-drought climate and human activities. An improved understanding of the post-drought groundwater storage recovery can provide key support to the identification of strategies that can accelerate the recovery processes.

1.3 Research Questions

The dissertation aims to address three research questions:

1. How does climate change impact the groundwater storage?
2. Can managed aquifer recharge effectively mitigate the groundwater overdraft?
3. How much has drought-related groundwater overdraft recovered during post-drought years and what is the role of climate and water management strategies in post-drought groundwater recovery?

The research questions are addressed in three chapters (2 through 4). The study domain selected for addressing the research questions is the Central Valley of California. An overview of the dissertation chapters is provided in the following section.

1.4 Dissertation Overview

The dissertation is divided into five chapters. Chapter 1 provides an introduction and the motivation for the dissertation. Chapter 2 presents an assessment of climate change impacts on groundwater storage in California Central Valley. Chapter 3 presents the potential of managed aquifer recharge to mitigate groundwater overdraft and increase environmental benefits. Chapter 4 presents an assessment of drought-related groundwater overdraft recovery during post-drought years and the role of climate versus water management to recover overdraft. Finally, Chapter 5 discusses the conclusions drawn from the research carried out in the dissertation and proposes possible future research.

CHAPTER 2

Climate change impacts on groundwater storage in the Central Valley, California

This chapter has been published in the Climatic Change. © Springer Nature. Used with permission.

Alam, S., Gebremichael, M., Li, R., Dozier, J., & Lettenmaier, D.P. Climate change impacts on groundwater storage in the Central Valley, California. Climatic Change 157, 387–406 (2019). https://doi.org/10.1007/s10584-019-02585-5.

Abstract

Groundwater plays a critical supporting role in agricultural production in the California Central Valley (CV). Recent prolonged droughts (notably 2007–2009 and 2012–2016) caused dramatic depletion of groundwater, indicating the susceptibility of the CV's water supply to climate change. To assess the impact of climate change on groundwater storage in the CV, we combined integrated surface water and groundwater models with climate projections from 20 global climate models and thereby explore the vulnerability of CV groundwater under two climate scenarios RCP4.5 and RCP8.5. We found that groundwater has been declining over the past decades (3 km^3/year on average during 1950–2009). In the absence of future mitigating measures, this decline will continue, but at a higher rate due to climate change (31% and 39% increase in loss rate under RCP4.5 and RCP8.5). The greatest loss (more than 80% of the total) will occur in the semi-arid southern Tulare region. We performed computational experiments to quantify the relative contribution of future crop water use and headwater inflows to total groundwater storage change. Our results show that, without management changes, continuing declines in future

groundwater storage will mainly be attributable to ongoing overuse of groundwater. However, future changes in the seasonality of streamflow into the CV, (small) changes in annual inflows, and increased crop water use in a warmer climate will lead to 40–70% more annual groundwater losses than the current annual average, up to approximately 5 km^3/year.

2.1 Introduction

Global warming poses serious threats to water resources, particularly in the Western U.S (Gleick, 2000). Climate change can directly and/or indirectly affect different components of the hydrological cycle, in which precipitation, snowmelt, and evapotranspiration are linked to agricultural water supply and demand (Garrote et al., 2015). Increases in water demand and decreases in surface water supply caused by a warming climate can negatively affect groundwater storage through increased groundwater exploitation, especially in regions like the Central Valley of California where groundwater is already stressed.

The Central Valley (CV) of California is one of the most productive agricultural regions in the world. On average, sources of irrigation water are about equally divided between surface water and groundwater (Li et al., 2018), but during droughts surface water availability is reduced, and the difference is mostly made up by groundwater, along with some reduction in irrigated area to reduce demand. Throughout the CV, groundwater resources relative to surface water resources vary, partly due to the natural north-south precipitation gradients, with groundwater relatively more important to the south. Surface water comes mostly from streams that originate in the Sierra Nevada Mountains east of the CV (hereafter referred to as headwater watersheds). Precipitation is highly seasonal, mostly occurring from October through March. Pronounced spatial differences exist in terms of the amount and timing of surface water supplies from the headwater watersheds, arising from higher total precipitation in the north and greater winter snowpack storage in the south

of the Sacramento-San Joaquin delta. To address these differences and the overall semi-arid climate, the CV relies on a complex network of reservoirs and manmade canals to store, import and transfer water, especially to its driest southern parts.

In recent decades, a gap has widened between water demand and surface water supply, which was caused by reductions in water available from the Colorado River Basin, a shift from row crops to more water intensive crops, and pervasive droughts over much of the last decade. This gap has been mitigated mostly by the extraction of groundwater, along with the reduction in irrigated areas (Xiao et al., 2017). Overexploitation of groundwater was especially pervasive in southern part of CV. Concerning the long-term viability of agriculture in the CV and the dropping groundwater levels, California State Legislature enacted the Sustainable Groundwater Management Act (SGMA), which requires that groundwater use in the state be managed at sustainable levels (California State Legislature, 2014).

Historically, the area devoted to irrigated agriculture in the CV expanded over a 100-year period from the 1870s to the 1970s, during which the area under irrigation were roughly stable (Olmstead and Rhode, 2017). However, except for exceptionally high runoff years, the water balance in parts of the CV has been in deficit (Famiglietti, 2014; Xiao et al., 2017). This situation worsened during two drought periods in the past decade. Using satellite data from the Gravity Recovery and Climate Experiment (GRACE), (Famiglietti et al., 2011b) estimated that the CV experienced net groundwater depletion of about 20 km^3 during 2003-2010. Xiao et al. (2017) estimated cumulative groundwater storage change (ΔGW hereafter) using multiple data sources, including GRACE data and in situ records, and found a depletion rate of 7.2 ± 1.0 km^3/yr from April 2006 to March 2010 and 11.2 ± 1.3 km^3/yr for the 2012-2016 drought. Other relevant studies support similar findings that CV groundwater has been in decline at least inthe past 50 years (e.g.,

Famiglietti et al., 2011; Scanlon et al., 2012), with most accelerated decline over the last decade. The loss of groundwater in recent droughts is a key indicator of the susceptibility of the CV groundwater system to climate variability and change, to an extent that has not previously been estimated.

The objective of this study is to assess the historic changes in groundwater storage and to estimate the additional stress likely to be imposed by future climate change within CV over the next century. In general, there are two important factors that affect CV groundwater, these are - (i) climate change, which has resulted in changes in headwater runoff patterns associated with earlier snowmelt, and increased evaporative demand (VanRheenen et al., 2004), and (ii) crop evolution (change in crop area and patterns), resulting in increased crop water use (Alam et al., 2019a). In this study, we disentangle these effects over the historic records and determine how much additional stress future climate may impose.

To address these issues, we use a suite of global climate model outputs archived for the Fifth Assessment Report of the Intergovernmental Panel on Climate Change (IPCC). We test projections both for modest global emissions increases (RCP4.5) and a more draconian scenario (RCP 8.5). Compared with previous efforts (e.g. Hanson et al., 2012; Massoud et al., 2018), we use a full suite of climate models and scenarios to represent future climate conditions that will affect CV groundwater in the coming decades. We use a hydrology model to represent the effects of headwater watersheds in producing streamflow into downstream reservoirs and subsequent releases from reservoirs that produce surface flows into the CV. Finally, we represent the implications of future surface runoff into the CV on groundwater use. Our domain is the entire Sacramento-San Joaquin-Tulare lowland and upland domain (SSJT, see Fig. 2.1), as described in the next section.

2.2 Study area

The study area consists of the entire CV from north of Redding to the Tulare River basin lowlands (see Fig. 2.1). In total, the study area encompasses approximately 160,000 km^2, around one third of the area of California. Most of the CV is nearly flat or in low-relief, contrastive with the surrounded high-elevation headwater watersheds. Strong precipitation gradients characterize the transition from the valley floor to the mountains, and a subtler precipitation gradient exists from the humid north to the semi-arid south (Bales et al., 2006).

Averaged over the domain, more than 75% of the average annual precipitation occurs between October and March (Cooper et al., 2018). Notwithstanding that headwater basins to the south are more snow-dominated than those to the north, northern watersheds generate more than two-thirds of the total annual inflow to the CV. This imbalance has motivated the construction of dams and conveyance structures that transfer water from the north to the south. This complex network of surface storage and conveyance structures control the basinwide surface water distribution throughout the year. The reservoirs store high winter and spring flows, and release them during the high-demand summer season, while providing flood protection and environmental services (mostly supplementing summer low flows). There are around 18 major reservoirs located in headwater watersheds (shown in Fig. 2.1), and five major hydrologic regions (HR) in CV, including Sacramento (SC), San Joaquin (SJ), Tulare (TL), Delta and East-Delta (Brush and Dogrul 2013). In this study, we compared groundwater storage changes in three major hydrologic regions: Sacramento, San Joaquin and Tulare.

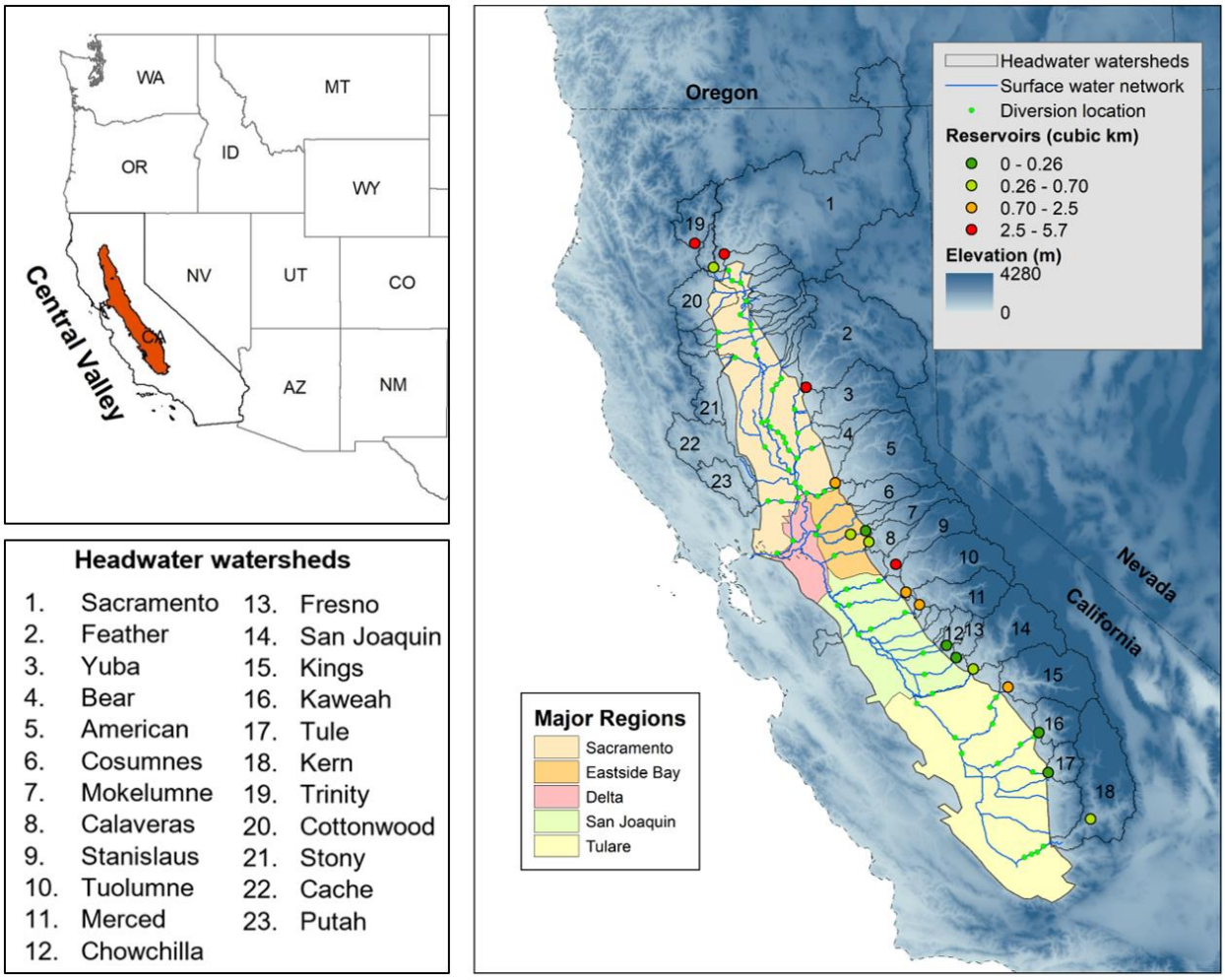

Figure 2.1. Map showing Central Valley and its surrounding watersheds (headwater watersheds). The five major hydrologic regions and rivers flowing through them are shown in the map to the right. Headwater watersheds and major reservoirs we represent in the study region are also shown (right). Blue shades indicate elevations of headwater watersheds

2.3 Approach and data

2.3.1 Modeling approach

We used a range of climate model projections and hydrologic and water resources management models to evaluate groundwater storage changes in major hydrologic regions. In general, our headwaters-to-groundwater modeling framework can be divided into three major components, which include models representing the headwater watershed, headwater reservoir regulation, and integrated surface water-groundwater. We linked each of the components forced

with different climate projections and scenarios. A conceptually similar modeling approach was taken by Hanson et al. (2012), which showed that such a model integration can effectively estimate potential changes in groundwater due to climate change over the CV. The steps we followed are to (1) identify representative climate models and extract downscaled climate variables; (2) simulate headwater watershed runoff using the Variable Infiltration Capacity (VIC) model (Liang et al., 1994); (3) model headwater reservoir storage and releases using a reservoir simulation model (CVmod: Van Rheenen et al. 2004); (4) model the integrated surface water-groundwater system using the California Central Valley Groundwater-Surface Water Simulation Model (C2VSIM: Brush et al., 2013); and (5) assess historical and future change in groundwater storage in CV (Fig. 2.2).

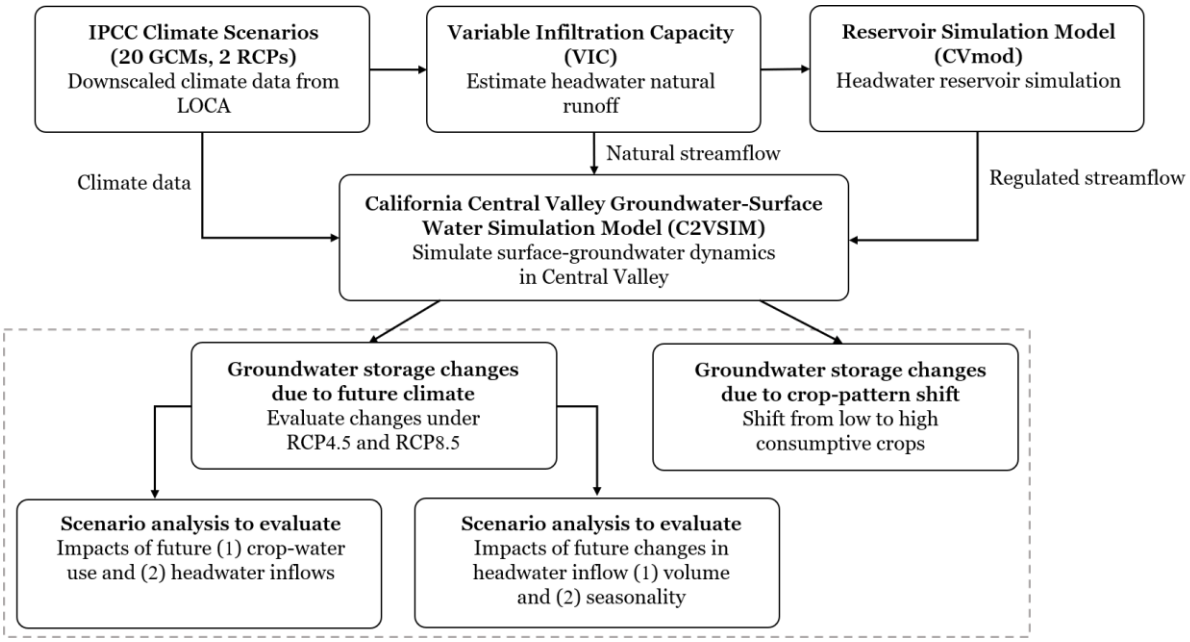

Figure 2.2. connectivity and flow of data in our integrated modeling system. Items in the dashed box are the key.

2.3.2 Headwaters to groundwater modeling framework

The headwater watersheds in our modeling framework are represented by the VIC model - a physically based semi-distributed hydrological model that solves the land surface water and energy budgets at the grid cell level (Liang et al. 1994). While there are other models like Noah-MP (Niu et al., 2011) and BCM (Flint and Flint, 2007) that could be used to simulate headwater watershed hydrology, we selected the VIC model because it has a long history of success in numerous studies, including those conducted for the CV system (VanRheenen et al., 2004; Xiao et al., 2017). For the current study, we used VIC simulations by (Pierce et al., 2018) that are available at daily time step and 1/16th degree (6 km) spatial resolution for both historical (driven by the Livneh et al. (2015) gridded historical dataset of 6 km resolution) and future periods (driven by LOCA downscaled climate projection for 32 climate models by Pierce et al. 2014 at 6 km resolution). We obtained the VIC simulation data from the Cal-Adapt online portal (Cal-Adapt, 2018). We aggregated VIC-simulated daily runoff to monthly to generate inflows to reservoirs and other CV inflow points. Hereafter, we refer to VIC-simulated headwater watershed flows as inflows to the CV, which are regulated by reservoirs (where they exist) or otherwise flow directly to the CV. To verify the accuracy of VIC-simulated headwater watershed flows, we compared annual flows from major watersheds with available unimpaired flow estimates (CDWR, 2016). They are generally in agreement (see Table A1 and Figure A1 in supplementary information). We then used the headwater inflows as inputs to the headwater reservoir model (where reservoirs exist) and surface water-groundwater model (in headwater watersheds without reservoirs).

We simulated headwater reservoir operation using the reservoir simulation model CVmod (VanRheenen et al., 2004). CVmod operates at a monthly time step. The model takes natural inflows from surrounding headwater basins (observed or simulated by a hydrological model such

as VIC) as inputs, and simulates reservoir storage and releases based on operations related to flood control, hydropower production, navigation, instream flow requirement for fish, and water supply demands. We calibrated CVmod to historical reservoir operations (releases and storage). We also extended the model to represent four additional reservoirs in the Tulare basin (Pine Flat, Isabella, Success, and Kaweah Lake), calibrated with historical flows, and evaluated performance relative to observed reservoir storage and releases. We ran CVmod using VIC simulated headwater inflows to obtain reservoir release and storage for both historical and future climate simulations (Fig.1 shows reservoirs considered in this study). Details of model performance are given in Text A2, Table A2 and Figure A2 of supplementary information.

We used C2VSIM to simulate CV surface water and groundwater dynamics. C2VSIM, originally developed by CDWR, has a long history of development and applications in climate change studies (Brush et al., 2013; Brush and Dogrul, 2013; Dale et al., 2013; Miller et al., 2009a). The model simulates groundwater flows in three layers on finite element grids, and dynamically couples with a one-dimensional simulation of land surface hydrologic processes, streamflow, vertical movement in the vadose zone, lakes, and flows from adjacent ungauged watersheds (Brush and Dogrul, 2013). The groundwater flow equations are solved at 1392 finite element grids (51,000 km^2) and land surface hydrologic processes are computed at 21 water balance subregions. We used a coarse grid version of the model with element sizes ranging from 5.4 km^2 to 87 km^2 (average 37 km^2). The model estimates water demand given irrigated land use as determined by agricultural management parameters, crop types, water supply from surface water diversions groundwater pumping, and climatic forcing. Brush et.al. (2013) calibrated C2VSIM for the period 1975-2003 to produce a good match between simulated and observed streamflow, groundwater heads, and head differences between wells. C2VSIM runs for the period October 1921 to September 2009 at

a monthly time step (see Brush et al. 2013 for details). While there are other models like CVHM (Faunt et al., 2009) that could be employed for simulating groundwater processes, we selected C2VSIM because of (i) its greater temporal coverage for the current study and (ii) a long history of successful applications.

Among the many input data to C2VSIM, the ones we adjusted were precipitation, crop evapotranspiration (ETc), crop types, surface water diversions, urban water demand and, inflow from surrounding watersheds. To demonstrate the direct impacts of climate change on agriculture and groundwater resources, we set urban and agricultural land use patterns, and irrigation efficiency to 2003 values. However, given that urban water demand is anticipated to increase in the future (Johnson, 2009), we applied a 1.2% annual rate of increase in urban water demand, similar to Hanson et al. (2012), from year 2000 through 2098. We computed ETc as the product of the crop coefficient (Kc) and reference crop evapotranspiration (ETo) following Allen et al. (1998). The mean values and seasonal variations in Kc are obtained from Brush et al. (2004) and ITRC (2003). We estimated ETo using the Penman-Monteith equation and following Allen et.al. (1998) at 1/16-degree spatial resolution for the study region. This ETo calculation requires air temperature, vapor pressure deficit, relative humidity, solar radiation, and wind speed (Eq 1).

$$ET_0 = \frac{0.408\Delta(\mathrm{Rn} - \mathrm{G}) + \gamma \frac{900}{\mathrm{T} + 273} u_2 (e_s - e_a)}{\Delta + \gamma(1 + 0.34u_2)} \qquad (1)$$

In equation 1, Rn is net radiation, G is ground heat flux (assumed zero), T is mean daily air temperature at 2 m height (℃), u_2 is wind speed at 2 m height, e_s is saturation vapor pressure, e_a is actual vapor pressure, Δ is the slope of the saturation vapor pressure curve, and γ is the psychrometric constant.

We extracted all the required variables over CV from the VIC model (driven by Livneh et al. (2015) data for the historical period and LOCA climate projections from Pierce et al., 2014) for the future. We temporally aggregated ETo to obtain monthly data from daily time series and extracted the subregion averaged ETo. 12 major crop types are used by C2VSIM including virtual crops that aggregate multiple actual crops (e.g. grains, orchard, field crops, truck crops). To verify that C2VSIM performed well during the historical simulation driven by the Livneh et al. (2015) data, we compared our groundwater storage change results with previous studies (shown in section 2.4).

Additionally, C2VSIM requires user-defined surface water diversion information along the stream network (shown in Fig. 2.1). Previous studies of the CV and its contributing watersheds used relatively simple methods to estimate surface water deliveries. For instance, Hanson et al. (2012) estimated future diversions based historical analogs (partitioning years into wet and dry periods), Miller et al. (2009) used historic diversion statistics (mean, median). We developed a simple linear programming (LP) model with surface water networks similar to C2VSIM to estimate surface water diversions (Fig. 2.1 showing the network and diversion locations; a more detailed description of the diversion locations available in Brush and Dogrul, 2013). The objective of the LP model is to maximize the surface water delivery under constraints like mass balance, and maximum/minimum instream flows (see Text A3 of supplementary information). We used upstream headwater watershed flows as the upstream boundary to the LP model. We first ran the LP model at a monthly time step for the projection period and then applied the surface water diversion outputs to C2VSIM. In C2VSIM, surface water deliveries are used first to meet demand, and any deficit in surface water supply is then met by pumping groundwater.

2.3.3 Climate models, and crop and hydrologic scenarios

To account for the uncertainty associated with future projections from different GCMs, we performed a preliminary analysis to select suitable climate models for this study. We compared the empirical cumulative distribution functions (ECDFs) of mean annual runoff (VIC-simulated annual total runoff averaged over 2006-2099 for the Sacramento, San Joaquin, and Kings Rivers for RCP 8.5) among different combinations of GCMs (for more information refer to Text A4 and Figure A3 of supplementary information). Based on our comparison we selected 20 GCMs that capture most variability out of the 32 GCMs archived in the Coupled Model Intercomparison Project phase 5 (CMIP5; the selected GCMs are shown in Table A3 of supplementary information). We considered both RCP 4.5 and RCP 8.5 global emissions scenarios. We first ran integrated chain of models for the historical period (1950-2009), where land use and cropping patterns vary annually (referred to as "Hist" hereafter). Next, we ran the models with historical climate (1950-2009) and assumed fixed (to 2003 levels) agricultural practices and cropping patterns (referred to as "Baseline"). To assess the impact of climate change, we ran the models with future climate forcings (2010-2098) based on projections for RCP4.5 and RCP8.5 (we refer to this simulation as 'CCR' hereafter), where we assumed fixed (at 2003 levels) agricultural practices and cropping pattern. We also conducted scenario analyses to examine future climate impact on groundwater storage. We analyzed the simulation results for three future periods: beginning of century (BOC; years 2010-2039), mid-century (MOC; years 2040-2069) and end of century (EOC; years 2070-2098). The formulation of scenarios is detailed in sections 2.3.3.1 and 2.3.3.2 as well as in Table 2.1.

Table 2.1. Summary of the scenarios considered in this study.

Scenario	Description	Period
Hist	Historical climate and cropping pattern	1950-2009
Baseline	Historical climate and cropping pattern for 2003	1950-2009
CCR	Climate change run (future forcing + 2003 cropping pattern) for RCP 4.5 and RCP 8.5	2010-2098
FC	Future crop-water use (CCR forcing over CV + headwater inflows as Hist + 2003 cropping pattern)	2010-2098
FI	Future inflows (Hist forcing over CV + headwater inflows as CCR + 2003 cropping pattern)	2010-2098
I_SC	Headwater inflows seasonality change (seasonality as CCR + mean annual volume as Hist) + 2003 cropping pattern	2010-2098
I_AC	Headwater inflows annual volume change (mean annual volume as CCR + seasonality as Hist) + 2003 cropping pattern	2010-2098
CS	Cropping shift (future forcing + 40% and 60% shift from row to tree crops)	2010-2098

2.3.3.1 Future crop-water use and headwater inflow change scenarios

The amount of groundwater being pumped to meet agricultural demands in the CV is essentially a balance between the crop water demand, precipitation, surface water supply from headwater watersheds and delta outflow to the Pacific. Crop evaporative demand increases with temperature, or precisely, with temperature-dependent variables such as the vapor pressure deficit, net radiation, and the slope of the vapor pressure relationship with temperature. Historically, crop-water demand in the CV has been met primarily by surface water (~51%) and groundwater (~49%) (Li et al. 2018). As climate continues to evolve, both demand and supply are expected to change, the magnitudes of which will exhibit inter-region variability. In general, there are two main factors that control the CV aquifer response to climate: crop-water use (crop evaporative demand) and supply from headwater watersheds (headwater inflow hereafter). A good understanding of the groundwater changes attributable to these factors is necessary to design proper mitigation measures, as required by SGMA. Here, we conducted two scenario analysis to quantify the relative contribution of these factors to future ΔGW. The scenarios are (1) current crop-water use and future inflows (FI), and (2) current inflows and future crop water use (FC). Both the scenarios

require current and future input data (inflow and crop water use) of equal time span, however, the historical data spans 60 years (1950-2009) and future data spans 90 years (2010-2099). To solve this issue of varying time length, we generated synthetic time series data that we used as a proxy for current crop-water use and headwater inflow. To do so, we randomly sampled the baseline (1950-2009) historical analysis to generate time series of monthly data for 30 years. We repeated the random sampling two more times to create 90 years of data (we used the same 30 years data for each future period for consistency). After performing the experiments, we calculated the change associated with future crop-water use (FC) from the difference in CCR and FI, whereas the changes due to future inflow are taken as the difference between the CCR and FC scenarios.

2.3.3.2 Future headwater inflow volume and seasonality change scenarios

Both the volume (of annual inflow to the CV) and timing (seasonality) of headwater inflows are expected to change in the future. An understanding of the relative contribution of headwater inflow volume and seasonality to groundwater storage change is important to design potential mitigation measures like managed aquifer recharge, as suggested by SGMA. Moreover, the effect of these projected changes on groundwater storage have not been quantified previously. Here, we conducted two scenario analyses by adjusting the projected inflows to quantify relative importance of headwater inflow volume versus seasonality. We multiplied the projected headwater inflows (2010-2098) by perturbation ratios between projected inflows and historical inflows following Wang et al. (2011) and Miller et al. (2003). The scenarios are described as follows:

Annual inflow volume adjustment

We determined annual perturbation ratios (A_c) from the 30-year (1971-2000) historical mean annual inflows (R) and 30-year projected mean annual inflows (R'_c) for three future periods (2010-2039, 2040-2069 and 2070-2099). We then multiplied the projected inflows ($R'_{cij},\ c =$

2010-2039, 2040-2069 and 2070-2099, i $= 1,\ldots,12$ for each month, j $= 1,..,90$ years) by these ratios. The modified time series (T_{cij}) consists of inflows that have the same annual mean as historical (1971-2000), but with seasonality as projected for the future period.

$$A_c = \frac{R}{R'_c} \qquad (2)$$

$$T_{cij} = A_c \times R'_{cij} \qquad (3)$$

The modified inflows (VIC-simulated) corresponding to each GCM were used as input to the CVmod (for CV tributaries where reservoirs exist) or C2VSIM (where no reservoirs exist). We refer to this scenario as I_SC hereafter. The ΔGW attributable to future inflow volume change is later determined from the difference in ΔGW estimated by CCR and I_SC scenarios.

Monthly inflow perturbation

We also generated headwater inflow time series that keep the projected annual inflow volumes unchanged in the future, with monthly (mean) fractions of mean annual inflows the same as in the historical period (1971-2000). We determined the mean monthly fractions of annual flows from the 30-year historical period ($B_i, i = 1, \ldots,12$ for each month). We then multiplied the projected annual flows (R'_j) by the fractions (B_i) to obtain inflow time series (G_{ij}) with the historical seasonality. Accordingly, the annual volumes remained as projected for the future period.

$$G_{ij} = B_i \times R'_j \qquad i = 1,..,12; j = 1,..,90 \qquad (4)$$

The modified inflows (VIC-simulated) were used as inputs to the CVmod (for CV tributaries where reservoirs exist) or directly to C2VSIM (where no reservoirs exist). We refer to this scenario as I_AC hereafter. The ΔGW attributable to future inflow seasonality change is later determined from the difference in ΔGW estimated by CCR and I_AC scenarios.

2.3.4 Cropping pattern scenario

We quantified the ΔGW that is attributable to the historic evolution of crop (area and patterns) from 1950 through 2009. We did this by finding the difference in groundwater storage change estimated from two sets of simulations: (i) crops evolve as they did during the historical period (this is basically the 'Hist' simulation), and (ii) crops remain fixed at year 1950 conditions (all other inputs remain same as 'Hist') or Hist_50 hereafter. Moreover, we quantified the climate related ΔGW during historical period that can come from changing crop water use (as ET changes with climate) and headwater inflow (in the form of seasonality and volume). We estimated historic ΔGW attributable to the change in crop water use (due to climate) from ETo trend, whereas we estimated the effect of headwater inflow change as the difference between total change and crop related changes.

In addition, we quantified the ΔGW that would occur due to a cropping shift from mostly row crops to tree crops (together with future climate). For the scenario analysis, we specified 40% and 60% row crops (classification of row and tree crops based on Xiao et al. 2017) to high water consumptive tree crops (orchard). One motivation behind choosing 40% change is from Xiao et al. (2017), who showed that during 2007-2016 there was an average 40% shift from row crops to tree crops, suggesting that much of the change we "project" has already occurred. In our case, we applied the shift relative to the baseline cropping pattern (2003). We ran the models with 40% and 60% crop shifts for all (20) future GCM climate scenarios (referred to hereafter as CS). The difference between the CS and CCR scenarios (ΔGW) is due to a shift from row to tree crops.

2.4 Results and discussion

2.4.1 Analysis of historical changes in groundwater storage

Fig. 2.3 (a,b) shows historical (1950-2009) changes in precipitation, headwater inflows, and cumulative changes in groundwater storage (ΔGW). The historical (1950-2009) groundwater depletion rate ΔGW is around 3.0 km^3/yr, with interannual variability in that increases during the latter half of the record (1980-2009) due to intermittent wet and dry years (as seen in the precipitation and inflow time series shown in Fig. 2.3a). For the baseline scenario (2003 cropping patterns), the simulated ΔGW rate is -3.1 km^3/yr. The baseline groundwater depletion rate is slightly higher than the historical rate, mainly due to difference in the historical evolution of land-use and cropping patterns; the historical run considers changes (i.e. agricultural area increased monotonically between 1950 through 1975, then became relatively stable) while the baseline run considers land-use and cropping patterns to be fixed at 2003 levels.

We compared the simulated ΔGW from C2VSIM with other available estimates. The simulated changes (mean trend) in ΔGW for April 2006 to September 2009 from C2VSIM is -8 km^3/yr, compared to -7.9 ± 1.3 km^3/yr by Xiao et al. (2017) and -7.8 km^3/yr by Scanlon et al. (2012). GRACE-based estimates include -7.2 ± 1 km^3/yr by Xiao et al. (2017) and -6.0 km^3/yr by Famiglietti et al. (2011) for the period April 2006 to March 2010 which is also close to our simulated estimate of ΔGW. Fig. 2.3c compares monthly GRACE ΔGW from Xiao et al. (2017) and C2VSIM; it is visually evident that C2VSIM reasonably captures the increasing/decreasing trends.

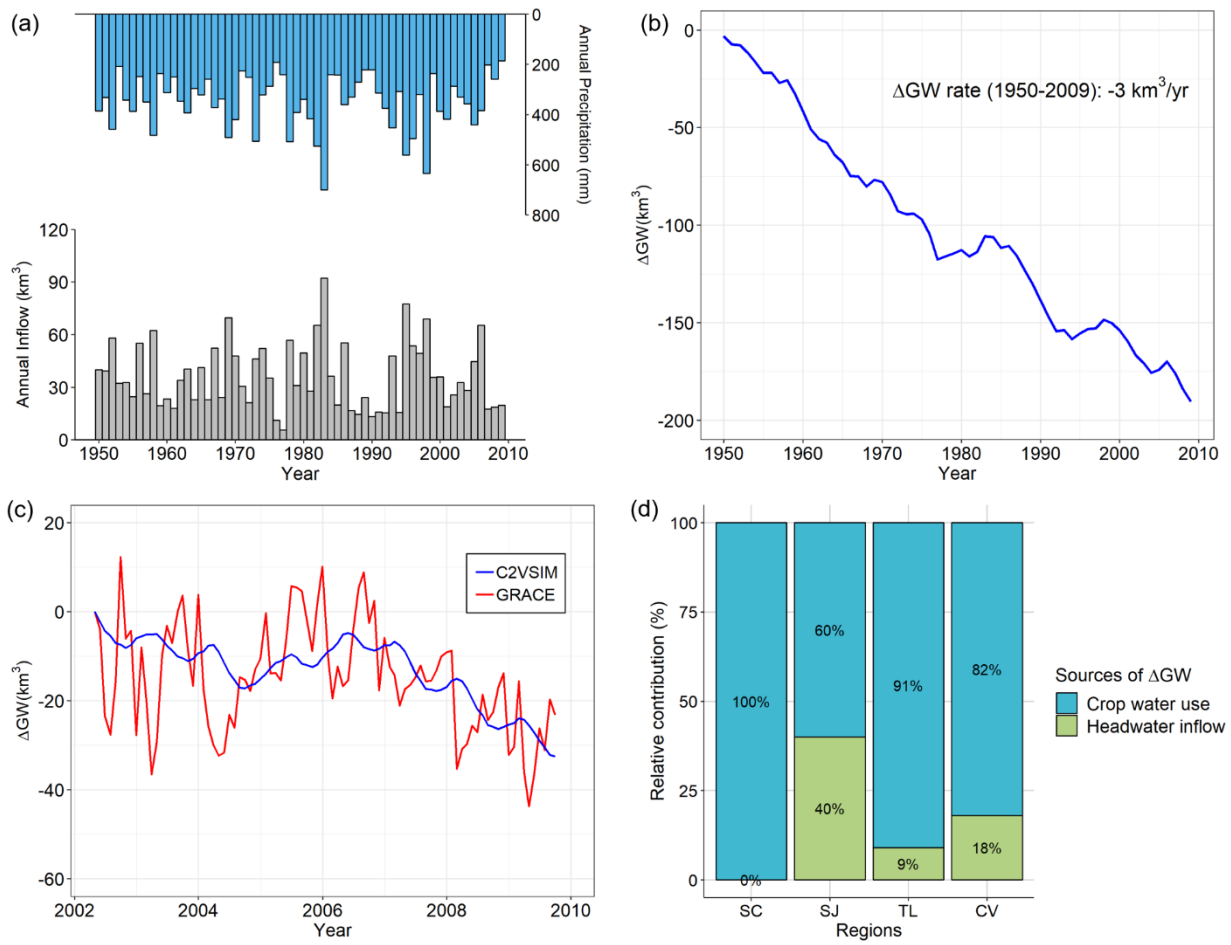

Figure 2.3. Historical estimate of (a) annual precipitation and inflows, (b) annual ΔGW, (c) ΔGW comparison between C2VSIM simulation and GRACE estimation at monthly timestep, and (d) relative contribution of historical crop water use versus headwater inflow to total ΔGW.

We estimated the relative contribution of crop water use (evolution of crop area, cropping pattern and climate related changes) and headwater inflow change (volume and seasonality) to the historical groundwater overdraft (section 2.3.4 discusses the method of separating the individual effects), as shown in Fig. 2.3d. On average, the relative contribution of crop water use and headwater inflow to ΔGW for the entire CV is around 82% and 18% respectively. We found that the crop water use-related groundwater loss almost entirely comes from historical evolution (increase) in crop area and shift in cropping patterns, whereas climate-related increase in crop water use is negligible (no significant trend exists in reference crop evapotranspiration). Moreover,

our regionwide analysis shows that the relative contribution of historical crop evolution and headwater inflow (i) for SC was around 100% and 0%, (ii) for SJ was around 60% and 40%, and (iii) for TL was around 91% and 9%.

2.4.2 Changes in hydrology

Fig. 2.4 shows mean annual changes (%) in precipitation (P), headwater inflows (I) and reference evapotranspiration (ETo) for all 20 climate models and scenarios during three future periods (BOC, MOC, and EOC) compared with the historic climate reference period (1971-2000). Multi-model precipitation estimates over CV have a median annual decrease of -2.2% and -4.4% for RCP4.5 and RCP8.5 respectively near EOC. However, the variability of the multi-model estimates is quite high (standard deviations of 8.9% and 15.2% for RCP4.5 and RCP8.5 respectively). On the other hand, temperature increases in the future will increase crop evaporative demands (here we have shown ETo change as proxy). Climate change will cause ETo over the CV to increase by 6.6 ± 1.5% and 10.5 ± 1.8% over the CV near the end of the century (EOC) for RCP4.5 and RCP8.5 respectively. The rate of ETo increase is higher in RCP8.5 due to continuing increase in temperature, whereas, the rate of increase decreases slightly after mid-century (MOC) in RCP4.5. Additionally, projected changes in temperature and precipitation over the headwater watersheds results in varying impacts on headwater inflows (I). Mean annual inflows have negative trends but high variability especially towards the end of the century, with changes of -4.20% ± 12% and -4.37% ± 19% at MOC; -3.59% ±16% and -8.19% ± 23% at EOC for RCP4.5 and RCP8.5 respectively (changes of hydrologic variables shown in Table A4 of supplementary information).

Headwater inflow changes can be both positive and negative (in contrast to ETo which increases in all models). The variability (standard deviation) of future inflow changes is higher

than the median in all cases; the headwater runoff projections range from negative to positive depending on the GCM. Moreover, there is a contrasting trend in the cool season (October through March) versus the warm season (April through September) flows where cool season flows are expected (in the median) to increase, and warm season flows are expected to decrease. The variability in multi-model estimates increases towards the end of century (percentage changes in seasonal inflows are shown in Fig. 2.4). The median changes in annual inflows is negative, this is dominated by warm season decreases versus cool season increases (volumetric changes in inflow are shown in Figure A4 of supplementary information). To get an idea of multi-model agreement as to the sign of the median change, we calculated the number of concordant minus discordant pairs, divided by the numbers of pairs for annual precipitation, annual and seasonal inflows (shown in Figure A5 and Figure A6 of supplementary information). We found that there is little agreement in the annual estimates of inflows (concordance 0.1-0.3) and precipitation (concordance 0.1-0.6, lowest during EOC) among models over the CV. There is, however, greater agreement at the seasonal level of inflow changes (concordance in warm season 0.9-1 and cool season 0.4-0.9). On average, concordance for decreases in inflow during the warm season is higher than for increases in inflow during the cool season.

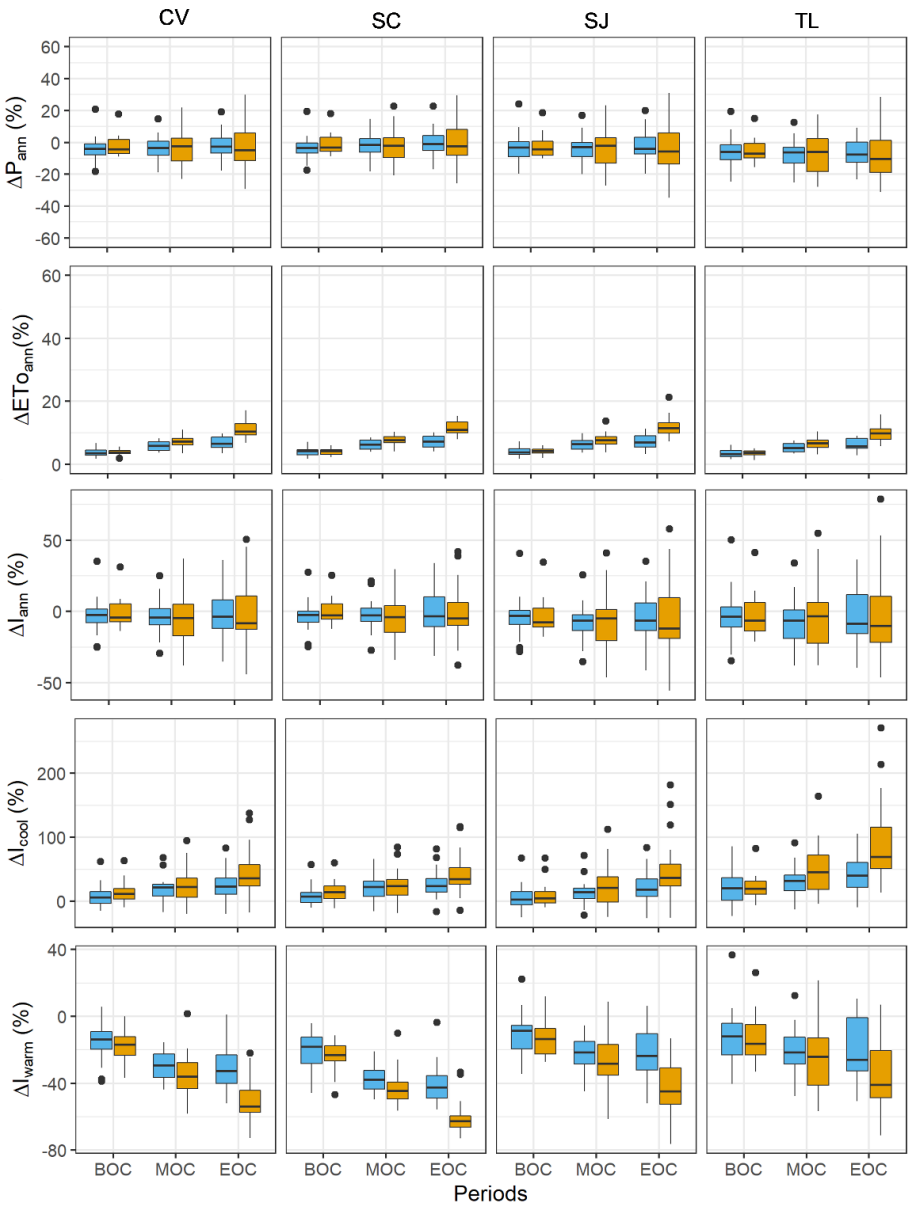

Figure 2.4. Changes in annual precipitation (P_{ann}), ETo and headwater inflow (I_{ann}) in CV and major regions for three future periods relative to 1971-2000. Seasonal variation in inflows are shown in bottom two rows. (sky-blue: RCP4.5, brown: RCP8.5). Horizontal axis represents three future periods - beginning of century (BOC; 2010-2039); middle of century (MOC; 2040-2069); end of century (EOC; 2070-98).

At the regional level, changes in precipitation are smaller (in absolute value) in the Sacramento than in the San Joaquin and Tulare, where across-GCM variability is also larger (Fig. 2.4). Similarly, mean annual runoff decreases in SJ and TL, whereas there is no clear trend in the

multi-model median for SC (percent changes in annual volume are higher in TL and SJ than in SC). However, the multi-model median of headwater inflows in all the regions increases during the cool season and decreases during the warm season, with a high degree of concordance in both measures.

2.4.3 Projected climate change impacts on groundwater storage

We quantify ΔGW for the projection period (2010-2098) where the forcings come from 20 climate models and 2 RCP scenarios. Fig. 2.5a shows ΔGW for the entire CV and its major hydrologic regions. It is visually evident that in both RCP scenarios, the CV is expected to go through a continuous groundwater depletion with higher multi-model variability towards the end of the century. Median ΔGW at the end of the century (2098) is expected to be -373 ± 88 km^3 for RCP4.5 and -406 ± 116 km^3 for RCP8.5. Furthermore, we fit linear regressions and estimated trends in ΔGW over the future periods (Fig. 2.5b). The long-term (2010-2098) median (over GCMs) trend in ΔGW is -4.1±1.1 km^3/yr for RCP4.5 and -4.4±1.4 km^3/yr for RCP8.5 respectively. These represent median trend increases of 31% and 39% compared to the baseline trend (2003 cropping patterns) for RCP4.5 and RCP8.5 respectively. The rate of depletion and uncertainty is higher during EOC, with a median rate ΔGW of -4.4±1.1 km^3/yr (RCP4.5) and -4.9±1.4 (RCP8.5) km^3/yr, which is equivalent to increases by 40% and 56% increase in ΔGW depletion rate compared to the baseline trends (2003 cropping patterns), respectively. Overall, there will be 40-70% increase (interquartile range of all percent changes) in GW depletion over the entire CV.

The rate of groundwater decline under future climate change scenarios is not uniform across the CV. The southernmost part (the TL region) will experience higher groundwater declines compared to the central and northern parts (SJ and SC). On average, due to future climate conditions, TL will experience 88% more groundwater decline than either SJ and SC. Separating

the results according to the major hydrologic regions of CV, median rates of change in ΔGW in TL during the projection period are -2.5 ± 0.7 km^3/yr (RCP4.5) and -2.5 ± 0.9 km^3/yr (RCP8.5), which is equivalent to 26% and 28% increases in ΔGW depletion rate compared to the baseline trends (-2.0 km^3/yr) for RCP4.5 and RCP8.5 respectively in TL. The second highest depletion is expected in SJ where long-term rate of ΔGW change are -0.78±0.2 km^3/yr (RCP4.5) and -0.86±0.3 km^3/yr (RCP8.5), which is equivalent to 49% and 65.7% increases in ΔGW depletion rate compared to baseline (-0.52 km^3/yr) for RCP4.5 and RCP8.5 respectively. ΔGW in SC is even smaller, with rate of change in ΔGW is expected to be -0.38±0.11 km^3/yr (RCP4.5) and -0.48 ± 0.14 km^3/yr (RCP8.5), which is an increase in ΔGW depletion rate by 31.3% and 63.5% compared to baseline (-0.29 km^3/yr) for RCP4.5 and RCP8.5 respectively. Groundwater losses (in absolute value) are higher for all regions at the end of century (2070-2098) and higher for RCP8.5 than for RCP4.5. In particular, the median (over GCMs) ΔGW rates will increase by 44.4%, 47.1% and 33.3% respectively under RCP4.5, and 80.9%, 53.9% and 47.5% for SC, SJ, and TL, respectively under RCP8.5 at the end of century.

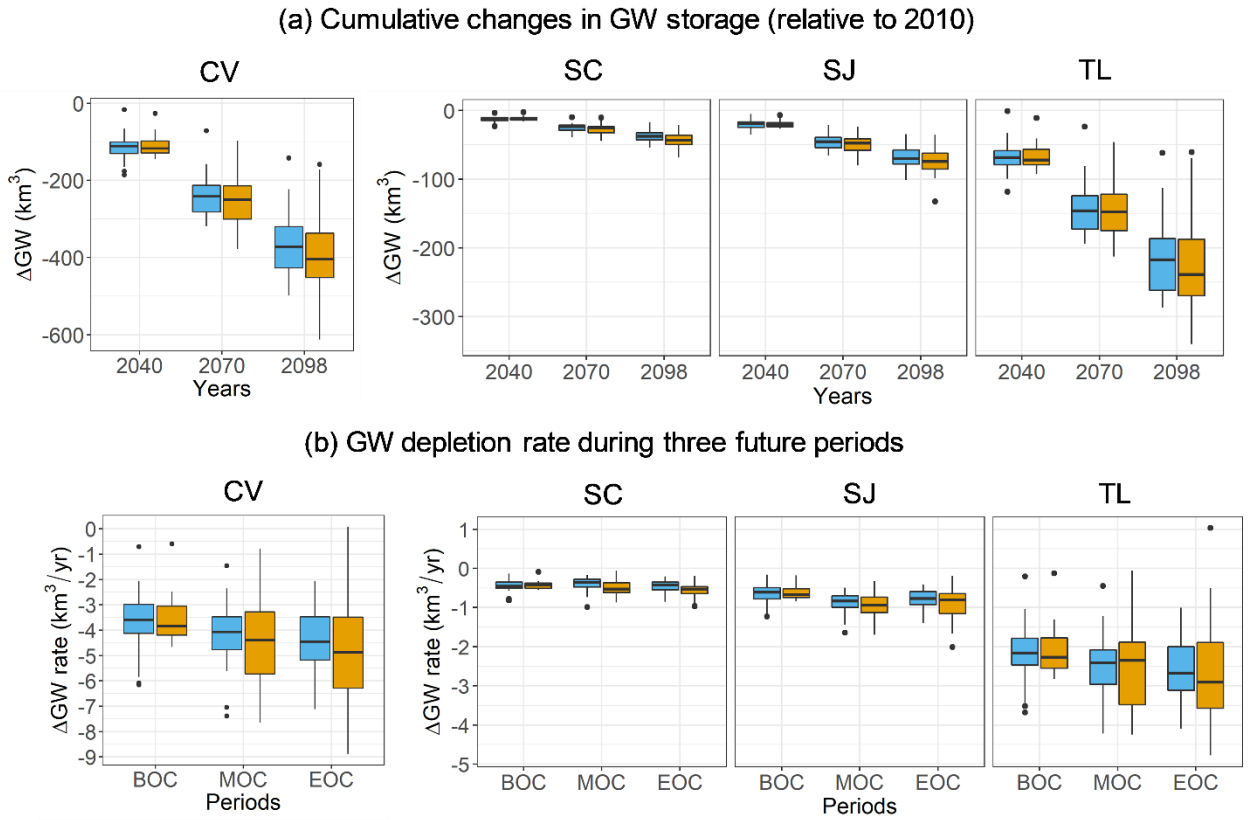

Figure 2.5. ΔGW (relative to 2010) in CV and major regions for RCP4.5 (sky-blue) and RCP8.5 (brown). The boxplots represent ΔGW obtained by forcing the chain of models with forcing from 20 climate models (ΔGW till 2040, 2070 and 2098 reported in the plot). (b) ΔGW rate during three future period. Whiskers represent min (max) value or 1.5 times interquartile range from first (third) quartile, whichever is bigger (smaller).

There are three main elements of the climate change contribution to groundwater storage: 1) changes (increases) in crop water demand due to warmer temperatures, 2) the effect (mostly negative) of changes in annual mean inflows to the CV, and 3) changes in the seasonality (generally, more flow in winter and less in spring and summer) of the inflows to CV. We discuss these elements in the following sections.

2.4.4 Role of future crop-water use versus headwater inflows

We analyzed the effect of changes in the demand (crop-water use) versus supply (surface water inflows) component of the CV water budget. Fig. 2.6 shows the annual average ΔGW

(additional) between FC (future crop-water use) and FI (future inflow) scenarios for three future periods. Here, we first calculated the difference in groundwater anomalies (between CCR and FI or FC) and determined the median of the multi-model ensembles, then we took the mean of the annual changes for each future period.

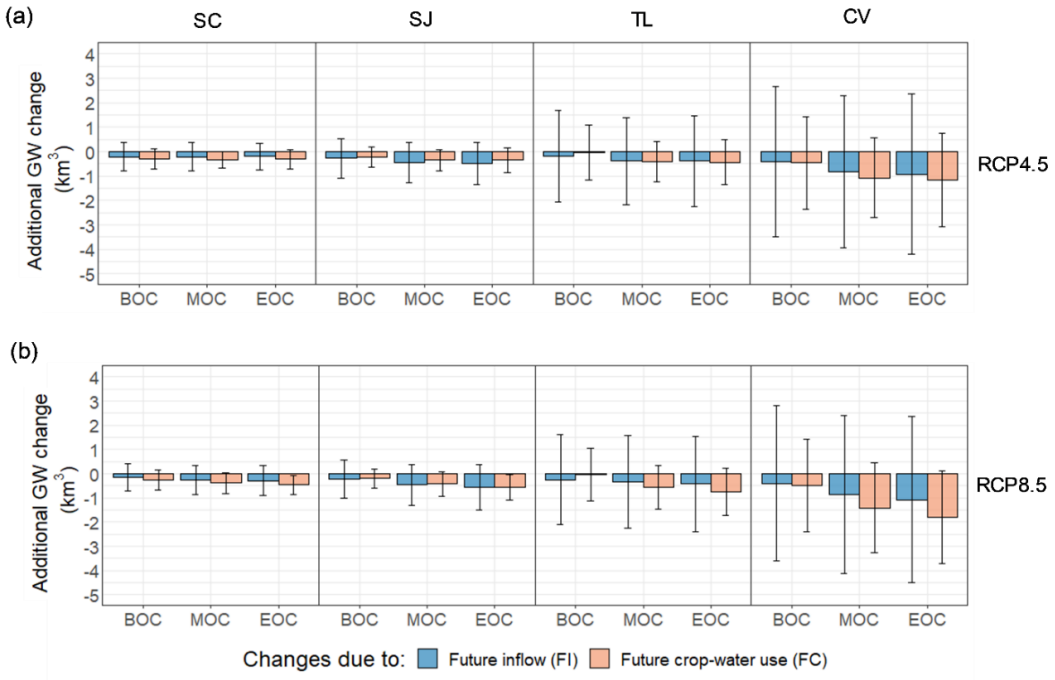

Figure 2.6. Additional changes in groundwater storage (annual) due to future crop-water use and inflow under RCP4.5 (a) and RCP8.5 (b) compared to historical (averaged over three future periods). The barplot represent average changes, and the whiskers show the interannual variability (one standard deviation).

In all cases, climate change is expected to increase ΔGW (in absolute value). We found that future crop-water use (change) will have a greater (negative) impact on total groundwater storage in the CV than inflow changes (FI) (predominantly during the middle to end of the century under RCP8.5); the relative contributions attributable to FC and FI are around 60% and 40% respectively. At a regional level, future crop-water use will have greater (negative) impact in SC (on average 60% of ΔGW), whereas future inflow will have almost equal or greater (on average 50-60% of change) impact (negative) in SJ (except RCP8.5 during EOC), indicating that the SJ is

susceptible to both inflow changes and increased crop-water use. However, the changes in groundwater in TL due to future inflow changes and crop-water use changes are almost the same at BOC and MOC, and changes (negative) due to crop-water use is higher at EOC (on average the relative contribution is 50%). We found similarities in the relative effect of FI and FC in snow dominated regions (SJ and TL) as opposed to the rain dominated region (SC). Our results also indicate that the interannual variability (hence uncertainty) in all cases is higher for FI, which is due to higher uncertainty in inflows (as shown in Fig. 2.4) and relatively less uncertain future increase in crop-water use (because temperature rises in all cases).

2.4.5 Role of headwater inflow volume and seasonality shifts under future climate

Fig. 2.6 shows the effect of FI and FC, where FI is made up of a combination of changes in annual inflow volumes, and changes in seasonality. Both effects contribute to ΔGW. To determine the relative magnitude of these effects, we conducted an experiment in which we partitioned the future inflows into seasonal and annual changes (I_SC: seasonality changes in the future, and I_AC: annual volume changes in the future). Fig. 2.7 shows the changes in annual average groundwater storage (additional) due to future inflow seasonality (I_SC) and annual volume (I_AC) (higher negative ΔGW means greater groundwater loss) changes. We followed the same process discussed in the previous section (but between CCR and I_SC or I_AC) and compared the changes (Fig. 2.7). We found that ΔGW change attributable to FI is about 80% from future headwater seasonality changes and 20% from future annual volume changes. The greatest effect of seasonality changes (more than 80%) is in SC and SJ. On the other hand, inflow volume changes have almost equal effect as seasonality changes in the TL region. We noted that the effect of changes in natural inflows are mediated to varying degrees by headwater regulation; this mediation is much greater for seasonality as contrasted with volume changes. One potential

measure to reduce the negative impact of future headwater inflow seasonality is to recharge excess cool season flow through managed aquifer recharge or MAR (DWR Flood-MAR whitepaper). Recent work has shown that Flood-MAR or Ag-MAR can be a promising solution to mitigate the effect of climate change on groundwater storage (Kocis and Dahlke 2017; Gailey et al. 2019; Fogg et al. 2018).

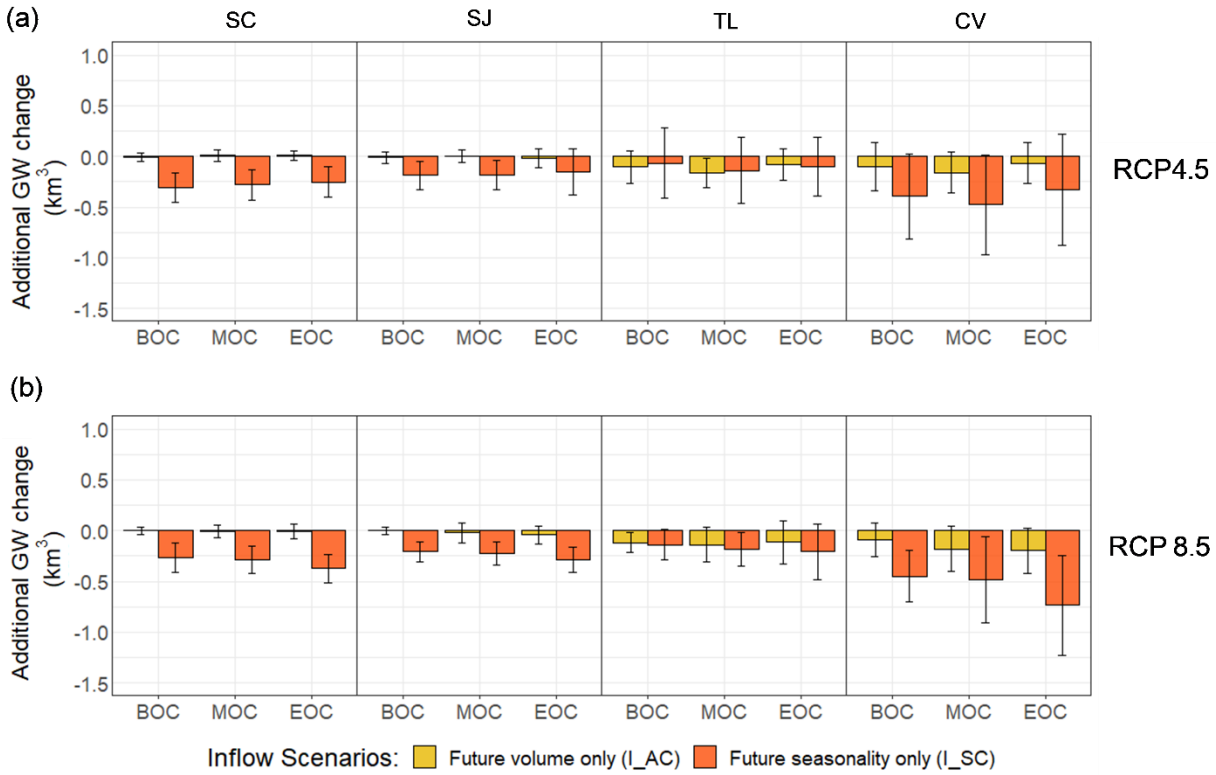

Figure 2.7. Additional changes in groundwater storage (annual) due to future inflow volume and seasonality changes for RCP4.5 (a) and RCP8.5 (b) compared to historical (averaged over three future periods). The barplot represents average changes, and the whiskers show the interannual variability (standard deviation).

2.4.6 Crop-shift scenario

We compute the ΔGW associated with a 40% and 60% shift towards tree crops (see section 2.3.4) for all climate models (RCP8.5 scenario only). In general, a shift towards tree crops is expected to increase water use requirements, but some of the increased water demand is due to climate change, so we partitioned the climate- and crop change-related components. We found that

a 40% shift towards tree crops (compared to 2003) causes an additional 0.91 km^3/yr groundwater loss, which is equivalent to a 29% increase in ΔGW (in absolute value) compared to the baseline ΔGW rate. The Groundwater depletion rate from the combination of future climate (RCP8.5) and crop-shift (40%) shows that the relative contributions of climate and crop-shift are about 58% and 42% respectively. However, it is important to note that the 40% shift we considered is with respect to the 2003 cropping pattern. As noted above much of this shift is already in place as of 2018 (see Xiao et al. 2017). For this reason, we also tested a scenario with 60% crop-shift (row to tree), the results of which are that groundwater declines at a rate of (increase relative to baseline) 1.39 km^3/yr (equivalent to 44% increase in groundwater depletion rate relative to the baseline). While the shift towards trees from row crops causes increased groundwater loss in all the major regions, the percentage changes are greatest in SJ (46% and 70% increase for two crop-shift scenarios), and the absolute changes are (by far) the largest in TL (0.55 km^3/yr and 0.83 km^3/yr for 40% and 60% shifts respectively).

2.5 Summary and Conclusions

Groundwater plays a critical role in the Central Valley's agricultural production and environment. The vulnerability of groundwater to climate in the Central Valley is evident from the drastic decline of this resource over the past few decades (Xiao et al. 2017), during which average annual groundwater loss has exceeded 3.0 km^3/yr. Given this backdrop, our objective was to assess historic changes in groundwater storage and to estimate the additional stress likely to be imposed by future climate change within the CV. Our methodology involved (1) simulation of surface and groundwater in the region using chain of integrated models (C2VSIM, CVmod and VIC), (2) forcing the models with climate model projections under different climate change scenarios

(RCP4.5 and RCP8.5), and (3) simulation experiments for cropping pattern change scenarios. Based on our simulations, we conclude that:

- Groundwater storage in CV has been declining in recent decades (1950-2009) at an average rate of about 3 km^3/yr. This decline in groundwater has resulted from a combination of gradual increases in crop water use (82% of the overdraft) due to increased crop area (and shifts towards more water intensive crops) and changes in headwater inflow seasonality and volume (18% of the overdraft in aggregate).

- In the absence of mitigation measures, over the future period (2010-2098), groundwater loss is likely to continue, but at an increased rate. Assuming no (further) change in crop types (relative to 2003), the long-term (2010-2098) rate of groundwater decline in CV under future climate will increase from about 3.0 km^3/yr to 4.1 ± 1.1 km^3/yr (RCP4.5; modest greenhouse emission scenario) and 4.4 ± 1.4 km^3/yr for RCP8.5 (worst scenario), or 31-39% higher than our base case with 2003 crop patterns.

- Groundwater declines are associated both with (1) increased groundwater pumping due to increased crop-water demands associated with rising temperatures (and to a lesser extent, reduced precipitation), and (2) reduced surface water supply to CV from headwater watersheds. We found that, absent mitigating measures, the dominant cause of future groundwater declines will be increases in future crop-water (~60% of total change). We noted that the projections of headwater inflow changes are much more uncertain (hence projections variable) as they are dominantly associated with precipitation changes, whereas projections of crop water use, which are dominated by temperature changes, are less uncertain.

- Groundwater declines, both in the past and projected for the future, are dominated by the Tulare (TL) region, which has accounted for roughly 80 percent of the historical decline. However, the sensitivities of future groundwater loss to climate-related crop water use and inflow changes are not necessarily greatest in the TL basin.

California's new Sustainable Groundwater Management Act (SGMA) mandates that groundwater depletions be brought into balance. Increases in crop water use, and reduced surface water availability associated with climate warming constitute an additional stress on the system; depending on specifics, these additional stresses will increase the current imbalance by one-third to one-half. These additional stresses will need to be addressed by efforts to formulate the sustainable surface and groundwater management strategies that will be required to comply with the mandate of SGMA.

Acknowledgements:

We are grateful to Dr. Tariq Kadir and Dr. Emin Dogrul from the California Department of Water Resources for technical assistance in the use of C2VSIM. We are also grateful to the kind help from Dr. Alan Hamlet at the University of Notre Dame for his assistance with CVmod.

CHAPTER 3

Can Managed Aquifer Recharge mitigate the groundwater overdraft in California's Central Valley?

Alam, S., Gebremichael, M., Li, R., Dozier, J. and Lettenmaier, D.P., 2020. Can Managed Aquifer Recharge Mitigate the Groundwater Overdraft in California's Central Valley?. Water Resources Research, 56(8), p.e2020WR027244. https://doi.org/10.1029/2020WR027244.

Abstract:

Groundwater plays a critical role in sustaining agriculture in California's Central Valley (CV). However, groundwater storage in the CV has been declining by around 3 km^3/year over the last several decades, with much larger declines during the 2007–2009 and 2012–2015 droughts. Managed Aquifer Recharge (MAR) can potentially mitigate existing overdraft by recharging excess streamflows (during flood periods) to the aquifers. However, the degree to which the existing CV groundwater overdraft might be mitigated by MAR is unknown. We applied a coupled surface water-groundwater simulation model to quantify the potential for groundwater overdraft recovery via MAR. To quantify the potential benefit of MAR, we used the coupled surface water-groundwater model to simulate water allocation scenarios where streamflow above the 90th or 80th percentiles was reallocated to aquifers, subject to constraints on the maximum depth of applied water (0.61 and 3.05 m). Our results show that MAR could recover 9–22% of the existing groundwater overdraft CV-wide based on a 56-year simulation (1960–2015). However, the impact

of MAR varies strongly among regions. In the southern CV where groundwater depletion is most serious, the contribution of MAR to the overdraft recovery would be small, only 2.7–3.2% in the Tulare basin and 3.2–7.8% in the San Joaquin basin. However, transferring excess winter flow from the northern to the southern CV for MAR would increase the overdraft recovery to 30% in San Joaquin and 62% in Tulare. Our results also indicate that MAR has the potential to supplement summer low flows (52–73%, CV-wide) and reduce flood peaks.

3.1 Introduction

Groundwater is an important freshwater source for more than 1.5 billion people globally (Alley et al., 2002). As the population grows and irrigated agriculture expands, reliance on groundwater continues to increase (Gorelick and Zheng, 2015; Rodell et al., 2009; Siebert et al., 2010). Overexploitation of groundwater due to increasing demand and climatic stresses (i.e. drought) in recent decades has had major, sometimes irreversible, impacts to many aquifers around the world (Taylor et al., 2013). For example, according to (Wada et al., 2010), groundwater storage depletion rates have doubled over the past 50 years in arid and semi-arid regions of the world. Such large-scale depletion threatens sustainable agricultural development, as well as environmental and ecological health. Climate change is likely to further increase groundwater depletion rates by increasing irrigation water use and altering the timing and volume of streamflows (Alam et al., 2019d; Hanson et al., 2012). Therefore, there is a critical need to identify vulnerable locations most affected by groundwater overdraft and measures to mitigate existing groundwater depletion.

The Central Valley (CV) of California, our study region, is one of the most agriculturally productive regions in the U.S. (Figure 1). It produces more than half of the fruits, nuts, and vegetables grown in the U.S. Almost half of the area in the CV is irrigated (~30,351 km^2), using

surface water, groundwater, or a combination of both. Surface water comes from upstream watersheds that surround the CV, the availability of which generally decreases from north to south following a north-south precipitation gradient. The regional imbalance in the surface water supply is mitigated somewhat by a complex surface water transfer network (Brown et al., 2009). Nonetheless, surface water alone is insufficient to meet water demands, and the deficit has been met by groundwater pumping, which now substantially exceeds recharge (Famiglietti et al., 2011a; Li et al., 2018). Historically, groundwater has played a vital role in sustaining high agricultural productivity in the CV, especially during drought years.

Overexploitation of groundwater in the CV has resulted in progressive groundwater depletion. Long-term groundwater depletion rates have been estimated by several studies: about 3 km^3/year by (Alam et al., 2019d), 2.5 km^3/year by (Hanak et al., 2017), 1.4-3 km^3/year by (CDWR, 2013), and 0.6-1.85 km^3/year by (Faunt et al., 2009). GRACE satellite-based estimates show a depletion rate of around 20 km^3 (or about 2.2 km^3/year) over the period 2003-2011 (Famiglietti et al., 2011a). Scanlon et al. (2012) estimated that the depletion rate in CV increased to about 8.9 km^3/year during the 2006-2009 drought, and (Xiao et al., 2017)estimated a depletion rate of 11.2 ± 1.3 km^3/year during the 2012-2016 drought. Groundwater depletion in CV is expected to increase by about 2 km^3/year at the end of the century as the climate changes (Alam et al., 2019d), absent implementation of mitigation measures. To minimize the impact of climate change and ensure groundwater sustainability, the California legislature passed the Sustainable Groundwater Management Act (SGMA) in 2014 to regulate the use of groundwater resources and to restore groundwater to an “acceptable level” by 2040 for critically over-drafted basins and 2042 for high and medium priority basins.

Several mitigation measures have been proposed to replenish the existing groundwater overdraft, including managing the demand and supply of water resources (Hanak et al., 2019). A key mitigation measure that has been proposed by California's Department of Water Resources (CDWR) is Managed Aquifer Recharge (MAR), which would use excess flood flows (termed Flood-MAR) in the wet seasons to replenish aquifers via artificial recharge, primarily in the form of seasonal land flooding (CDWR, 2018a; Sprenger et al., 2017). The benefits of MAR have been broadly recognized and have already been implemented in some parts of the CV (Dillon, 2009; Dillon et al., 2019; Bridget R. Scanlon et al., 2016). MAR has the potential to replenish aquifers, reduce land subsidence risk, increase drought resilience, and lower flood-related risks (Chinnasamy et al., 2018; Hashemi et al., 2015; Niswonger et al., 2017; Ronayne et al., 2017; Bridget R. Scanlon et al., 2016). MAR studies in California and elsewhere conducted at the local and farm levels (e.g., Bachand et al., 2014; Dahlke et al., 2018; Ghasemizade et al., 2019; Kourakos et al., 2019) demonstrate the potential of such practices to be scalable to the basin level. Strategies for implementing MAR on a more widespread basis are currently under investigation by (CDWR, 2018a). However, the benefits and limitations of MAR implementation at the scale of the entire CV are not well understood. There remain key questions, such as the extent to which MAR can replenish existing groundwater overdraft in the CV, and which regions have the greatest potential for MAR.

Here, we address the question of how much of the CV's groundwater overdraft can potentially be mitigated by MAR and how much the recovery may vary among regions and subregions of the CV. In addition, we examine the additional benefits of MAR for low flow augmentation and flood reduction.

3.2 Study Area

Figures 1a and 1b show the location of the CV region of California, which covers an area of about 53,600 km^2. As shown in Figure 1c, the CV generally has low relief and is surrounded by high-elevation watersheds (hereafter headwater watersheds) in the Sierra Nevada. Surface water from these headwater watersheds flows into the CV through natural stream networks, and eventually enters the San Francisco Bay-Delta (hereafter Delta).

As shown in Figure 2.1c, CDWR divides the CV into five major hydrologic regions: Sacramento (SC, 15,900 km^2), Delta (DL, 2,900 km^2), East Delta (EZ, 3,660 km^2), San Joaquin (SJ, 10,020 km^2), and Tulare (TL, 21,200 km^2). The Sacramento, San Joaquin, and Tulare regions are located in the northern, central, and southern parts of CV respectively. The Delta and East-Delta hydrologic regions are located in the central CV and provide outlets to the Delta that drain excess surface water (remaining water that is not diverted for agricultural or municipal use) flowing through the rivers in the CV. As shown in Figure 2.1d, CDWR has further divided the region into 21 subregions for hydrologic studies. Here, we refer to each subregion using the IDs shown in Figure 2.1d (e.g., subregion 1 to be referred to as SR-1).

The long-term rainfall map (Figure 2.1d) shows that there is a strong precipitation gradient from the headwater watersheds to the valley floors, and from the northern part (which is mostly semi-humid) to the southern part (which is mostly semi-arid) of the region. The headwater watersheds in the north are generally rain-dominated and contribute most of the surface water flowing to the CV, while the southern headwater basins are snow-dominated. The north-south contrast in water demand and supply motivated the construction of the Central Valley Project (CVP) and State Water Project (SWP) aqueducts that transfer water from the Delta to the south via hundreds of miles of aqueducts. CVP, built in the 1970s and managed by the U.S. Bureau of

Reclamation, is a multipurpose project consisting of dams, reservoirs, pumping plants, and aqueducts. The Friant Kern Canal (245 km length) and Delta Mendota Canal (188 km length) are the major CVP canals carrying water southward. SWP, currently operated by CDWR, is also a multipurpose project that was built about the same time as the CVP. The California Aqueduct (length about 715 km) is the major SWP canal that conveys water from north to south.

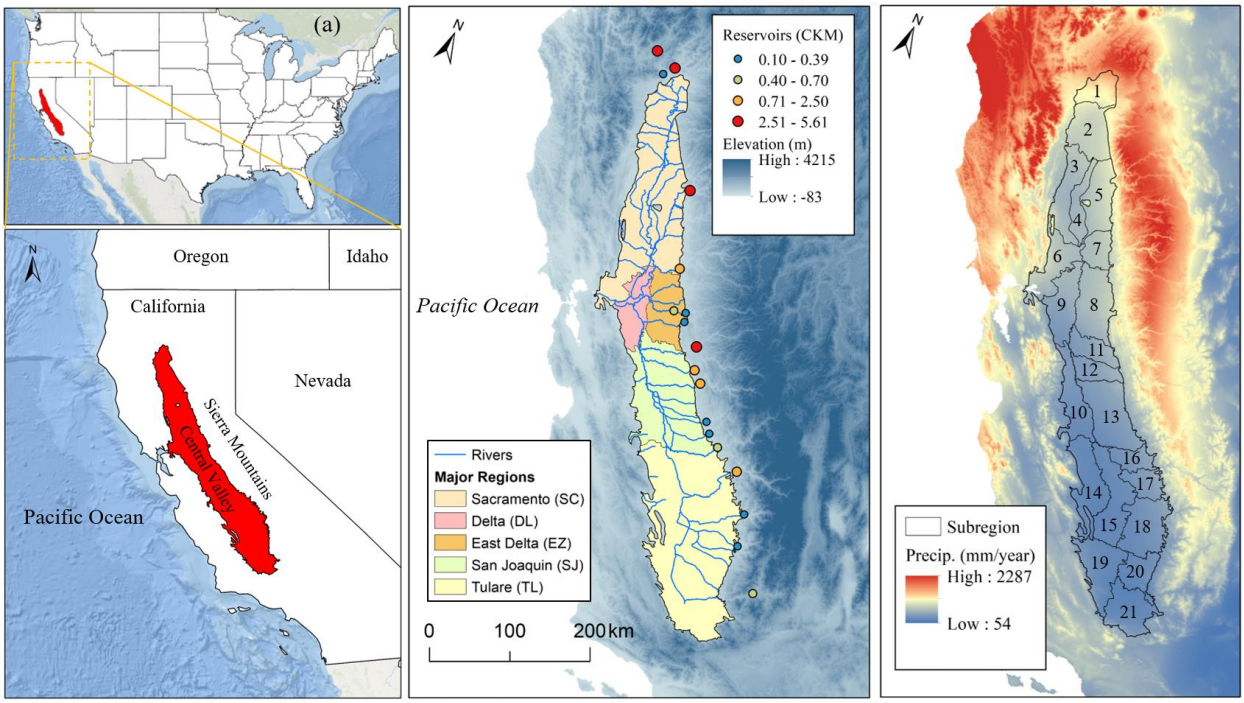

Figure 3.1. (a) Location of the CV in the U.S.; (b) CV location in California, (c) major hydrologic regions (HR), major reservoirs, and river networks within the CV. Blue shade represents elevation; and (c) 21 subregions (SR) of the CV, where the numbers represent subregion numbers.

There is also a temporal mismatch between rainfall and crop seasons: most of the precipitation across the entire CV falls during the period of November to March, while irrigation demand is mostly in the summer (July to September). This mismatch is mitigated by some 18 major headwater reservoirs (locations shown as circles in Figure 1c), which store winter flows for release during the summer (Alam et al., 2019). In addition to supplying water during the low-flow

season, the reservoirs provide additional benefits in the form of flood protection and environmental services. The surface water that enters the CV is diverted at several locations to satisfy agricultural, municipal, and environmental needs taking into account water rights and legal requirements. Surface water flow in excess of the diverted water is discharged (exclusively in high-flow seasons) to the San Francisco Bay through the Delta.

3.3 Methodology

Our methodology involves numerical modeling experiments that use a coupled hydrologic model to simulate surface hydrology and groundwater dynamics. Figure 2 shows the five key steps of our modeling approach. The first step is to identify potential MAR sites based on soil properties and feasible locations for diverting streamflows to the recharge sites. The second step considers different water diversion rules (i.e., the maximum amount of water that can be diverted from the streams to the MAR sites). The third step is to conduct numerical modeling experiments using the coupled hydrologic model, CDWR's California Central Valley Groundwater-Surface Water Simulation Model (C2VSIM), and taking into consideration operational information such as suitable MAR sites, diversion locations, and diversion rules identified in previous steps. The fourth step is the analysis of model simulation results focusing on: (i) groundwater recovery, (ii) changes in the water balance, and (iii) low-flow augmentation, flood-risk reduction, and potential crop damage. In the following sections, we discuss each of these steps in further detail.

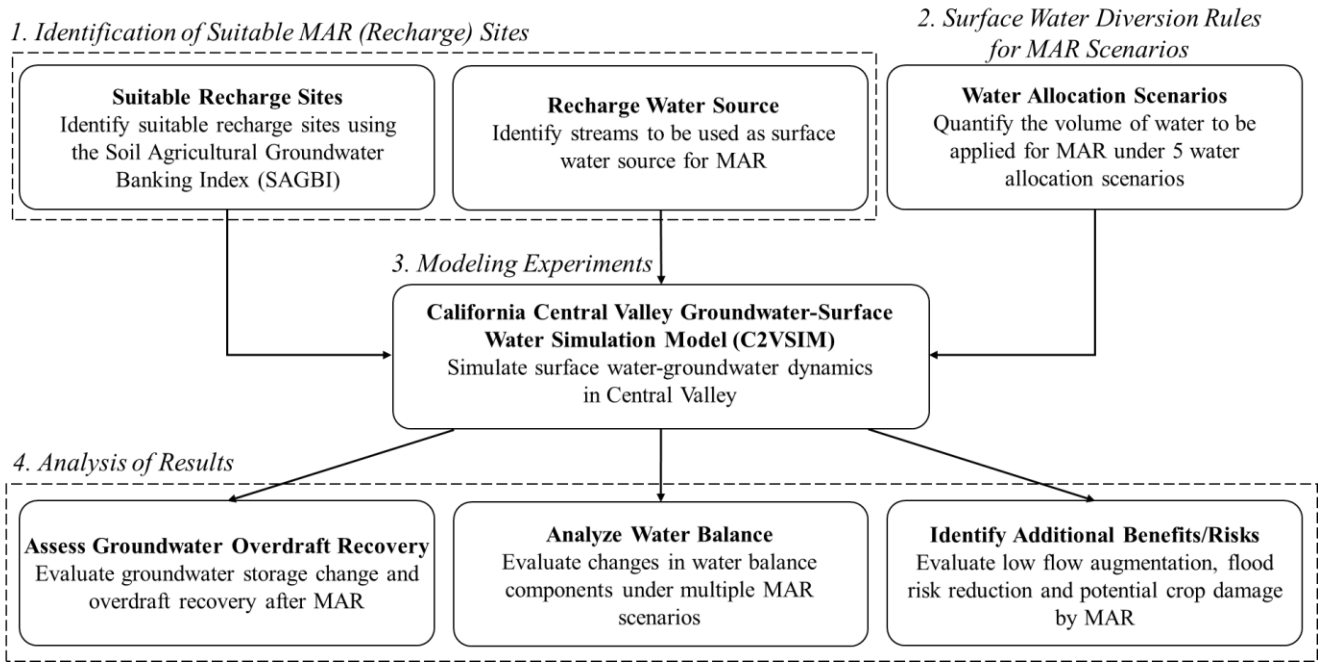

Figure 3.2. The flowchart used in our modeling experiment.

3.3.1 Model description

C2VSIM was developed by applying the Integrated Water Flow Model (IWFM) software (Dogrul et al., 2017) to the entire CV. We chose this model for a number of reasons. First, it was developed, calibrated, and validated for the CV, taking into account the main hydrological processes in the region. Second, the use of C2VSIM facilitates the communication and transfer of results to CDWR. CDWR has made Flood-MAR a priority, and is soliciting inputs from the community (an example is the October 2019 Flood-MAR Public Forum organized by).

C2VSIM is an integrated surface water and groundwater model that is capable of simulating hydrologic processes including surface runoff, streamflow, land surface, root zone and vadose zone processes, and saturated groundwater flow (Brush et al., 2013). Its core is a finite element solver, which has been implemented at both coarse-grid (C2VSIM-CG) and fine-grid (C2VSIM-FG) resolutions. We used a beta version of C2VSIM-FG (C2VSim-FG beta2) that has

been developed using IWFM version 2015 (hereafter, we refer to this version of C2VSIM-FG as C2VSIM). Originally calibrated by Brush et al. (2013), C2VSIM has been applied in multiple previous studies in the region (e.g., Alam et al., 2019; Dogrul et al., 2016; Ghasemizade et al., 2019; Kourakos et al., 2019).

C2VSIM dynamically calculates agricultural and urban water demands, links these to groundwater pumping and surface water diversions, and adjusts water deliveries based on demands. C2VSIM requires user-inputs for precipitation, evapotranspiration, irrigation method, crop distribution, population, boundary inflow, and surface water delivery. The model calculates the runoff, return flow, infiltration, vertical movement of soil moisture in the root zone, and aquifer recharge. The amount of crop water demand unmet by surface water and root zone soil moisture is dynamically supplemented by groundwater pumping. Crop water demand is calculated based on crop evapotranspiration rates, irrigation efficiency, stream diversion, precipitation, and crop distribution. Surface water delivery is user-defined in C2VSIM, suggesting that the applied water for MAR is an input to the model. However, the model has the capability of adjusting the actual delivery based on water availability in the stream. For example, if the allocated surface water delivery (as input) is higher than the available streamflow in a month, the model adjusts the volume of water that is available for MAR. The unsaturated zone in C2VSIM is divided into the root zone and the deep unsaturated zone where the flow in the root zone is computed dynamically using a tipping bucket model's one-dimensional unsaturated flow equation. A portion of the water applied for irrigation can flow through the vadose zone and reach the saturated zone through infiltration and deep percolation. The model also allows the application of MAR water directly to the saturated zone as deep percolation, which we follow in a manner similar to other recent studies (Ghasemizade et al., 2019; Kourakos et al., 2019). This allows the model to be computationally

efficient and thereby suitable for multi-decadal analysis of the impacts of MAR (Ghasemizade et al. 2019).

C2VSIM simulates all the major infrastructure that substantially affects the movement of water within the CV. In C2VSIM, surface water deliveries are specified at 414 locations, which include diversions for agriculture, urban, MAR, and regional export/import via natural streams and aqueduct/canals. Diversions from major infrastructure include Delta export to both CVP and SWP, the Delta-Mendota Canal to different water districts, DMC to Mendota pool, California Aqueduct diversion (e.g. Kern county via Cross Valley Canal or CVC), CVC diversions, and Friant-Kern canal diversion (to Kings, Tule, Kaweah and Kern Rivers), among many others. In addition, the model also considers existing MAR projects including the California Aqueduct diversion to the Kern water bank and Arvin-Edison water storage district, Kings River diversion (to Fresno, Alta Irrigation District), and many others (see (Brush et al. (2013) for detail). Among the existing recharge projects, the Kern water bank and Arvin-Edison are relatively large (areas of 81 km^2 and 526 km^2 respectively) with maximum annual recharge capacities of 0.56 and 0.19 km^3/year respectively, and cumulative storage volume ranges between 1 km^3 to 2 km^3 (Christian-Smith, 2013; B. R. Scanlon et al., 2012).

Figure 3 shows the major processes represented by C2VSIM. C2VSIM uses four vertical layers in the subsurface. The top layer represents the unconfined aquifer and the bottom two layers represent confined aquifers. The confined and unconfined aquifers are separated by a thin layer of Corcoran clay in parts of the modeling domain. Horizontally, the region is divided into finite element computational polygons, which have irregular shapes. Each corner of a finite element is called a groundwater node. C2VSIM uses the Galerkin finite element method to solve the governing equation at each groundwater node. Stream connectivity in C2VSIM is defined by a

series of inflow and outflow nodes, which represent the locations where the water is received from surface runoff, return flow, and other nodes, and where the water is diverted for irrigation and other downstream nodes. Stream-aquifer interactions depend on the head gradient between the stream stage and groundwater head, and streambed conductance.

The model operates at a monthly time step. We used the baseline period of 1960-2015 (water years). Therefore, our analyses are derived from 56 years of historical data (inputs) and corresponding monthly simulations.

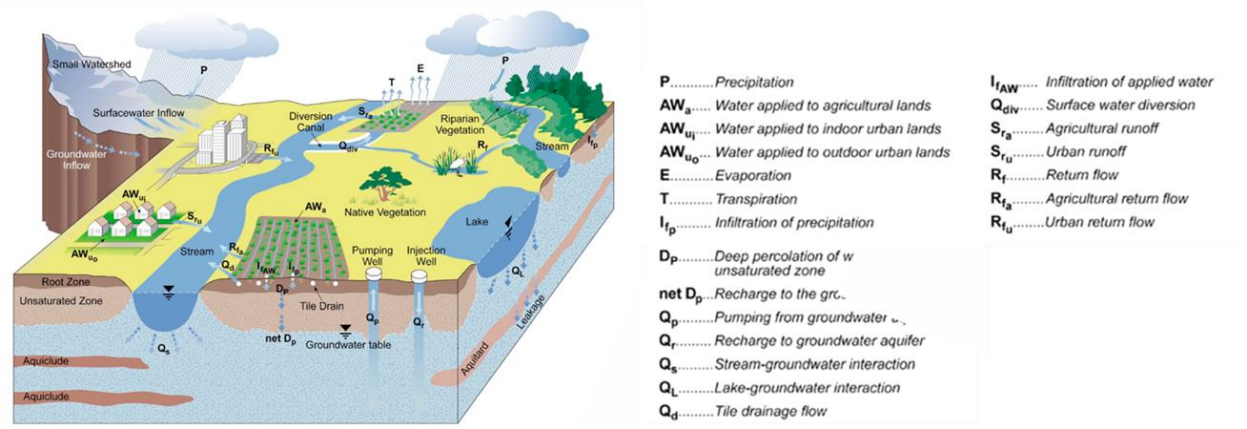

Figure 3.3. Major hydrologic processes modeled by the C2VSIM (IWFM manual).

3.3.2 Identification of suitable MAR (recharge) sites

We identified suitable recharge sites within each subregion using a two-step process. First, we identified potential sites suitable for recharge based on soil properties - this step classified the land into MAR-suitable and MAR-unsuitable areas. Then, we identified diversion locations on the streams within each of the 21 CDWR subregions (subregions without any stream were considered MAR-unsuitable regardless of suitability based on soil properties). The physical and geological characteristics of a recharge site determine the efficiency of groundwater overdraft recovery by MAR (Ghasemizade et al., 2019). Recharge sites that consist of relatively coarse-grained soils (e.g.

sand and gravel) have higher recharge rates compared to sites with fine-grained soils (e.g., clay). However, the selection of suitable recharge sites must be based on physical and geologic characteristics of the entire soil column, as the geologic formation of aquifers is heterogeneous both spatially and vertically (Fogg, 1986; Maples et al., 2019).

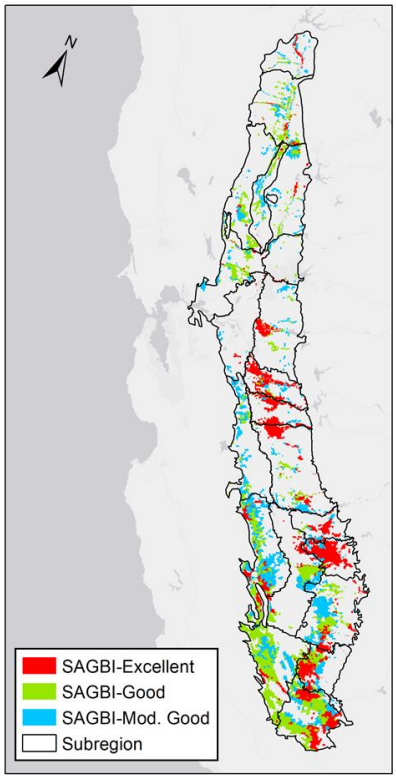

Figure 3.4. SAGBI classified excellent, good, and moderately good recharge sites in CV.

Table 3.1 Mar recharge site areas and water diversions by regions (in km3/yr) for MAR under different scenarios. Here, SC, EZ, SJ, TL and CV represent Sacramento (SC), East-Delta (EZ), San Joaquin (SJ), Tulare (TL) and Central Valley (CV) respectively.

Regions	SC	EZ	SJ	TL	CV
MAR recharge site areas (km^2)					
SAGBI-Excellent	317	770	2166	4844	8097
SAGBI-Good	1720	106	377	5209	7412
SAGBI-Moderately Good	1262	145	1060	3553	6020
Total area	3298	1021	3602	13607	21529
Water allocation in MAR scenarios (km^3/yr)					
R90_2ft	0.85	0.16	0.18	0.20	1.40
R80_2ft	1.44	0.26	0.32	0.30	2.32
R90_10ft	1.85	0.38	0.22	0.21	2.65
R80_10ft	3.17	0.61	0.42	0.30	4.50

We used the recharge-potential classification recommended by the Soil Agricultural Banking Index (SAGBI) that takes soil properties into account (O'Geen et al., 2015). The SAGBI classifies lands within the CV into six groups according to their suitability for MAR: excellent, good, moderately good, moderately poor, poor, and very poor. The SAGBI classification is based on the following factors: deep percolation, root zone residence time, chemical limitations, topographic limitations, and surface conditions. We used the unmodified version of the SAGBI (O'Geen et al., 2015) that considers the soil permeability derived from the USDA-NRCS Soil Survey Geographic Database (SSURGO) and ignores the effect of agricultural tillage. Since the focus of our study is to test the full potential (i.e. maximum) of MAR for groundwater overdraft recovery, we only considered locations with excellent, good, and moderately good soil suitability as potential recharge sites (see Figure 4). Because the SAGBI map identifies agricultural lands suitable for recharge, our MAR application is also known as agricultural managed aquifer recharge or Ag-MAR (hereafter, we will use MAR to refer to Ag-MAR). Table 3.1 shows the distribution of recharge sites we identified using SAGBI in major regions of the CV. The total recharge site area is highest in the TL region (roughly 4 times the recharge area of SC or SJ). Based on SAGBI, we found that there are more recharge sites with excellent suitability than there are good and moderately good recharge areas. Kourakos et al. (2019) studied the effect of MAR in SR-3 using some of the SAGBI recharge areas which range between 42 and 154 km^2, whereas the potential recharge area we use in the entire SR-3 is 704 km^2. Ghasemizade et al. (2019) conducted numerical experiments with MAR scenarios in SR-18 with a recharge area ranging between 313 and 1023 km^2, which is roughly comparable with 1660 km^2 of suitable recharge areas we identified in SR-18. Although the SAGBI classification provides the best available information on the soil's MAR

potential, we acknowledge that there are uncertainties associated with the representation of subsurface geologic structures that might not be well captured by SAGBI (Maples et al., 2019).

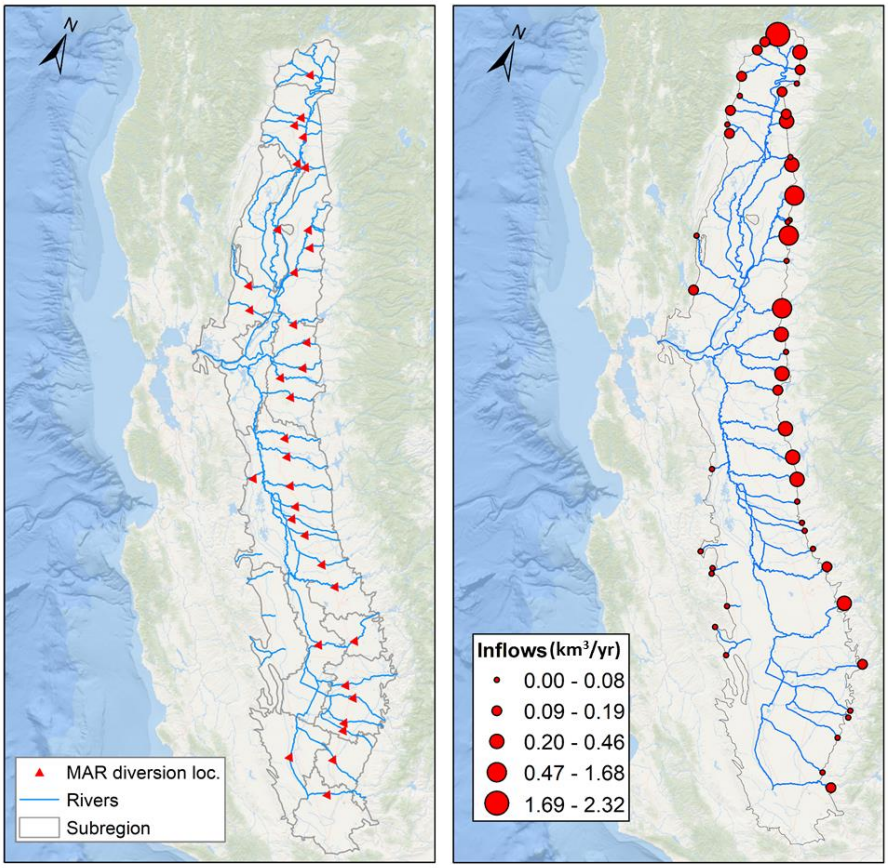

Figure 3.5. (a) Surface water diversion locations for MAR. (b) November-March headwater watershed inflow in km3/year for the period 1960-2015.

Given the purpose of our study, we assumed that all the recharge sites within a given subregion would be uniformly recharged, provided that there is at least one stream crossing the region (more discussion below). However, in reality, the depth of water that can be applied to a recharge site may be limited by additional factors, such as the height of berms or the depth of recharge basins, conveyance structure capacity from hydraulic engineering perspectives, and crop sensitivity to stagnant water (for agricultural lands).

In the CV, the surface water originating from the headwater watersheds flows through interconnected rivers and enters the immediate downstream subregion, where it serves as a potential source of recharge water. We identified locations on the rivers where recharge water could be diverted to the MAR sites. Each subregion has either one, multiple, or no rivers crossing it (see Table B1 of Supplementary Material, which lists the diversion streams for each subregion). Assuming that all rivers crossing a given subregion could provide recharge water to that subregion, we identified only one diversion location on each river for each subregion (a subregion with no river is deemed unsuitable for MAR). For our modeling experiments, we identified exact diversion locations on the rivers for each subregion based on a simplified rule that the locations should have the minimum distance between a river and the center of recharge sites (diversion locations shown in Figure 5a; detailed selection criteria described in Text B1 of the Supplementary Information).

3.3.3 Surface water diversion rules for MAR scenarios

Surface water availability in the CV is highest during the winter (November through March) because most of the CV's annual precipitation occurs during this season. Figure 5b shows the annual average streamflow entering the CV from the headwater watersheds during the winter. The figure shows that the streamflow volumes are higher in the northern headwater watersheds compared to southern headwater watersheds. Once this streamflow enters the CV, the water flows through connected rivers shown in Figure 5b, where it is diverted for agricultural and municipal purposes with the remaining water finally draining to the Delta. During 1960-2015, the average volume of winter Delta outflow was about 18 km^3/year. Delta outflow (on average) increases from December to January, and then remains stable up to March. There must be a minimum flow into the Delta to meet environmental and legal requirements. Flows above this requirement after

meeting all the needs are referred to as “excess flow” (see Figure A1 of Supplementary Material for Delta outflow variability).

Surface water diversion rules for MAR depend on two factors: (1) streamflow requirements to meet environmental and legal restrictions in the streams and the Delta, and (2) allowable depth of water at the recharge sites that can realistically be retained for recharge and would not affect the production of winter crops if the land is used for agricultural purposes. Here, we made assumptions and used theoretical values to incorporate these two factors as discussed below.

With respect to the first factor, no fixed rule is available in most streams flowing to the CV as to how much excess flow might be diverted for MAR without causing environmental conflicts. However, there is a general consensus that streamflow above the 90^{th} percentile threshold (during the period November to March) could be considered for MAR allocation (Baker et al., 2004; Kocis and Dahlke, 2017; Olden and Poff, 2003; USGS, 2016). Therefore, we calculated the 90th percentile of winter flow at each diversion location (shown in Figure 5a), and considered winter flows that exceeded the 90th percentile threshold for MAR application in corresponding subregions (referred to as the R90 scenario). We tested a less restrictive threshold, the 80th percentile (R80 scenario), as well. At a field scale, the volume of water that can actually be applied depends on the existence of a conveyance system and its capacity to carry water to the recharge sites. We assume the allocated water can be delivered to the MAR sites even if there is no existing conveyance system for delivery, i.e., a lack of conveyance system is not a constraint. As noted in section 3.4.8, in this respect we provide a maximum or bounding estimate of the potential of MAR.

MAR can negatively affect winter crops in the recharge sites if the sites are agricultural land and water is left stagnant for long periods. However, most of the recharge sites we identified are located in agricultural lands. On agricultural lands, water is retained by building a berm

(elevated border using soil) that generally has a height of 0.153 m or 6 inches (Flores-López, 2019). If water is applied each day, assuming all water is recharged, the total depth it can hold in a month is 2.29 m or 15 ft (6-inch × 30-days). To be conservative but also realistic, assuming recharge over 2/3 of the month, such a recharge site can allow up to 3.05 m (or 10ft) recharge in a month. Here, we adopted a maximum depth of 3.05 m (10 ft) as well as a more restrictive option of 0.61 m (2 ft) per month in our scenario experiments. In both scenarios, we applied water uniformly to all recharge sites.

To implement both scenarios, we followed a two-step process to determine the actual volume of water to be applied. In the first step, we quantified the volume of water available from a stream above the threshold (90th or 80th percentile). Second, we calculated the maximum volume of water allowed to be delivered to the recharge site in a given scenario, which is the product of the recharge area and maximum allowable depth (0.61 or 3.05 m). If the water available is less than the maximum allowable delivery, all water is delivered; otherwise, the application volume is equal to the maximum allowable delivery.

In summary, we considered four diversion rules:

- 90th percentile threshold with 0.61 m (or 2-ft) application depth (R90_2ft)
- 90th percentile threshold with 3.05 m (or 10-ft) application depth (R90_10ft)
- 80th percentile threshold with 0.61 m (or 2-ft) application depth (R80_2ft)
- 80th percentile threshold with 3.05 m (or 10-ft) application depth (R80_10ft)

The availability of surface water for recharge has been identified as one of the most critical factors to the success of MAR (Perrone and Rohde, 2016). Earlier studies have quantified the

volume of surface available for MAR using both monthly and daily streamflows. CDWR (2018) estimated regionwide water available for recharge using a hydrological model (WEAP) in combination with gage measurements. The study used simulated monthly streamflow from WEAP, and estimated water available for recharge considering both unlimited and limited conveyance capacities (i.e. based on historical maximum diversion). On this basis, they found 0.82 and 0.27 km^3/year water available for recharge in SC and SJ_TL (SJ and TL together) respectively under limited conveyance capacity. CDWR (2018a) found 5 and 0.85 km^3/year water available for recharge in SC and SJ_TL respectively considering unlimited conveyance capacity. Kocis and Dahlke (2017) estimated the amount of water available for groundwater recharge using daily streamflows and found 2.0 and 1.2 km^3/year water available for recharge in SC and SJ_TL. Table 3.1 shows our estimate of annual average water diversions for MAR during 1960-2015 for each major region. We calculated the water available for recharge based on simulated monthly streamflow from C2VSIM. The diversion volumes are higher in the north, due to higher excess water availability. In contrast, the diversion volumes in the south are less variable due to relatively low winter inflows. In our case, we used a monthly time step, as did CDWR (2018). We found that water available for MAR in SC is 0.85 and 1.85 km^3/year under R90_2ft and R90_10ft scenarios respectively. For SJ_TL, our estimated water available for recharge are 0.38 and 0.43 km^3/year under R90_2ft and R90_10ft scenarios. Our estimate under the R90_2ft scenario is close to CDWR's estimate. In comparison with Kocis and Dahlke (2017), under the R90_10ft scenario, our estimate for SC is close (1.85 versus 2.0 km^3/year) but lower in SJ_TL (0.43 versus 1.2 km^3/year). The higher value by Kocis and Dahlke (2017) is most likely attributable to the daily time step they used. We acknowledge that the use of a monthly timestep can lead to a lower estimate of water available for recharge in some years due to not being able to capture peak flows

from short term storms. However, we argue that the consideration of the 80th percentile threshold rather than the 90th percentile compensates for some of the time step-related differences.

In the above scenarios, streams (originating from headwater watersheds) crossing each sub-region are considered "source" water for MAR in each sub-region. Due to the spatial variability of rainfall (see Figure 1d), subregions in the northern part of CV are expected to receive more recharge water compared to subregions in the southern part. Similarly, northern regions contribute more excess Delta flow than the southern regions. We added one additional scenario in which the streamflows in the Delta that exceeded the 90th percentile threshold after the R90_2ft scenario being implemented were transferred to the southern subregions in the SJ and TL basins. We labeled this scenario as "R90_2ft_WT". In our case, we assumed that the existing infrastructure is capable of transferring water to the south (SJ and TL) for MAR.

In all the MAR scenarios described above, we limited our analysis to 56 years (1960-2015) a period that includes historical crop/land-use change and infrastructural developments. However, there are differences in infrastructural developments and crop/land use between the last decade and a few decades earlier. For example, SWP and CVP were fully developed by the mid-1980s, after which the Delta operation was different than before. Moreover, there have been changes in cropping patterns (mostly transition of row crops to tree crops) and some other land uses over the decades. To expand our analysis to potential future conditions, we conducted additional experiments with crop/land use and infrastructure development representative of the recent past. To do so, we performed three additional simulations with land use and cropping patterns fixed at the year 2009 (here, we assume 2009 land use is representative of current conditions). These three simulations are (1) base_cf: base simulation with fixed cropping and land use pattern, (2) R90_2ft_cf: R90_2ft simulation with fixed cropping and land use pattern, (3) R90_10ft_cf:

R90_10ft simulation with fixed cropping and land use pattern. We consider the post-1980 period (1980-2015) for the above scenarios, which is representative of current (expected) infrastructural development. The differences between in R90_2ft_cf (and R90_10ft_cf) and base_cf provide an insight into the expected groundwater changes if infrastructural development and water footprint stay the same for the recent and future periods.

3.4 Results and discussion

3.4.1 Surface water delivery under MAR

In section 3.3.3, we discussed the volume of water allocated for MAR in different regions of CV. The volume of water that is actually diverted depends on the water availability in the stream. Table 3.2 presents the regionwide distribution of actual volumes of MAR delivery simulated by C2VSIM. We found that the actual volume of water delivered is nearly the same as the allocation in all the regions. For example, water allocations for SC under the R90_2ft and R90_10ft scenarios are 0.85 and 1.85 km^3/year, whereas the actual delivery is 0.82 and 1.77 km^3/year respectively. We found that the actual delivery under the R90_2ft scenario for SC and SJ_TL were close to those reported by CDWR (2018), i.e. SC (CDWR: 0.82 vs. ours: 0.82 km^3/year) and SJ_TL (CDWR: 0.27 vs. ours: 0.29 km^3/year). We also found that the actual volume of deliveries in TL did not increase as the depth of water application increased from 0.61 m (or 2 ft) to 3.05 m (or 10 ft). This is attributable to the fact that the total recharge area is large enough to allocate all the water for either threshold depth (0.61 m or 3.05 m).

Table 3.2. Actual volume of water delivery (km3/year) for MAR in all major regions.

Regions	R90_2ft	R80_2ft	R90_10ft	R80_10ft
SC	0.82	1.37	1.77	3.04

EZ	0.15	0.22	0.28	0.40
SC_EZ	0.97	1.59	2.05	3.44
SJ	0.18	0.32	0.22	0.42
TL	0.11	0.15	0.11	0.15
SJ_TL	0.29	0.47	0.32	0.57
CV	1.25	2.06	2.37	4.01

Note: SC_EZ: SC and EZ together, SJ_TL: SJ and TL together

3.4.2 Groundwater storage change

3.4.2.1 Baseline groundwater storage change during 1960-2015

First, we quantified the groundwater storage change between the end-years of the baseline period, 1960 and 2015, for each of the subregions (Figure. 6a). The change in groundwater storage varies within the region. In general, the southern region (almost half of the CV) has the most serious groundwater overdraft problem, while the northern region has exhibited little to no change in groundwater storage in recent decades. The groundwater overdraft in the southern CV is severe: the largest overdraft of 0.71 km^3/yr in SR-18 in the TL. The next largest overdrafts are between 0.41 km^3/yr and 0.40 km^3/yr in SR-10 (SJ basin) and SR 17 (TL basin) respectively. The north-south gradient in groundwater overdraft is due to increasing gaps in surface water supply and agricultural water demand. On average, CV groundwater storage has decreased by about 3.1 km^3/year during 1960-2015. We estimated that groundwater storage has been changing at a rate of 0.28, -1.01, and -2.28 km^3/year in the SC, SJ, and TL regions respectively from 1960-2015. The regionwide distribution of groundwater change was also estimated by Faunt et al. (2009), who used the CVHM model for CV groundwater depletion. They found that groundwater storage had changed at a rate of 0.04, -0.03, and -2 km^3/year in the SC, SJ, and TL respectively from 1962-2003. Hanak et al. (2018) estimated groundwater changes in SJ and TL from 1986-2015 and found that groundwater storage had changed at a rate of -0.2 and -2 km^3/year in SJ and TL respectively. Overall, our estimated groundwater storage depletion rate in CV is higher compared to Hanak et

al. (2017) and Faunt et al. (2009). Regional comparison with other studies shows that our estimated groundwater storage change rate is similar for TL, higher in SC and lower in SJ.

3.4.2.2 4.2.2 Impact of MAR on groundwater storage change in subregions

We evaluated the groundwater storage changes for the R90 (R90_2ft and R90_10ft) and R80 (R80_2ft and R80_10ft) MAR scenarios. The spatial distribution of groundwater storage change for MAR scenarios have similar patterns as the base scenario. We found that the groundwater storage change under R90_2ft, R90_10ft, R80_2ft, and R80_10ft scenarios was -2.8 km^3/year, -2.6 km^3/year, -2.6 km^3/year and -2.4 km^3/year respectively during 1960-2015. We also calculated the percent change in groundwater storage by MAR for each subregion using Equation (1),

$$\text{GWC}(\%) = \frac{\sum_{i=1}^{N} \Delta GW_{i,MAR} - \sum_{i=1}^{N} \Delta GW_{i,base}}{abs(\sum_{i=1}^{N} \Delta GW_{base})} \times 100 \qquad (1)$$

where, GWC represents the groundwater storage change in percentage after MAR application compared to the base condition. The term GWC also represents groundwater overdraft recovery (%) when there is an overdraft in the base simulation. ΔGW_i represents groundwater change in a given month i compared to previous month. N is total number of months (N=672 months in our case) and abs represents the absolute value.

Figure 6b-e show GWC under R90_2ft, R90_10ft, R80_2ft, and R80_10ft scenarios. In SC_EZ, subregions 2 to 8 show higher GWC, which is due to a higher amount of water applied to areas with relatively small or no groundwater overdraft. Results from the base scenario show that only SR-6, SR-7, and SR-8 have an existing groundwater overdraft (Figure 6a) in SC_EZ. MAR would mitigate more than half of the existing groundwater overdraft in SR-6 (GWC 73%-100%) and SR-8 (GWC 56%-100%), and up to 25% in SR-7. The rate of groundwater storage change is

low in SJ and TL subregions, except for SR-11 and SR-12 that show higher change. The low percentages for most of the SJ and TL subregions (Figure 6b-e) are due to low net groundwater recharge compared to a relatively high existing overdraft. In TL, only SR19 shows high (compared to the rest of the domain) GWC, which is due to relatively low groundwater storage change in the base scenario compared to other subregions in TL.

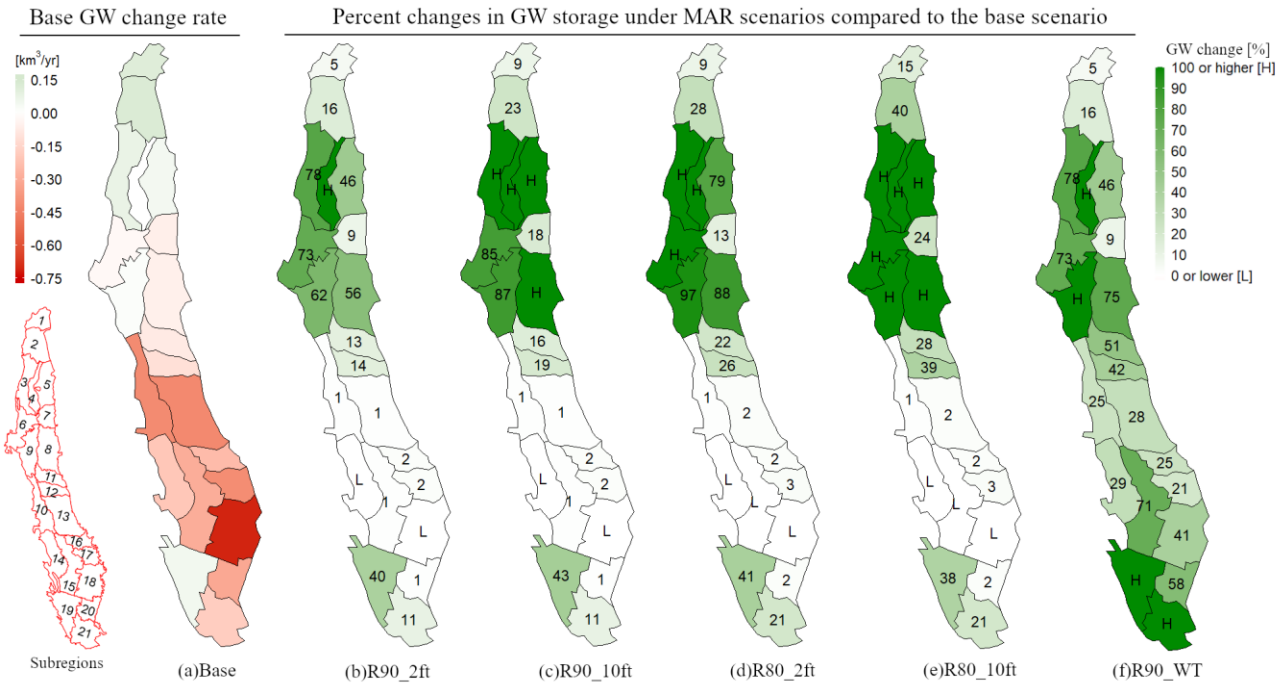

Figure 3.6. (a) Groundwater storage change rates (km3/year) in the base simulation (year 1960-2015), where the unit km3/year represents the annual average groundwater change in a subregion. (b-f) Groundwater storage changes (%) compared to base conditions for R90_2ft, R90_10ft, R80_2ft, R80_10ft, and R90_WT scenarios respectively. The inset map on the left corner shows the subregion IDs.

3.4.2.3 Impact of MAR on groundwater storage change in major hydrologic regions

Figure 7a shows the percent change in groundwater storage in each of the major hydrologic regions (HRs) (see Figure A2 in Supplementary Material for the cumulative difference in groundwater storage between MAR and base scenarios). Groundwater storage change is calculated

using Equation (1). We found MAR can recover 8.9% and 14.1% of the CV's total groundwater overdraft (we use the term overdraft when base scenario shows groundwater loss) under the R90_2ft and R80_2ft scenarios, respectively. The recoveries under R90_10ft and R80_10ft are 14% and 22.2%. Groundwater storage change is highest in SC_EZ, ranging from 27.5% to 57.3% under the R90 scenarios (R90_2ft and R90_10ft) and, 56% to 101% under R80 scenarios (R80_2ft and R80_10ft). The relatively high change in SC_EZ is attributable to the higher availability of excess surface flow. In SJ, the overdraft recoveries range from 3.2% to 7.8%. Recoveries are even lower in TL, where only 2.7% to 3.2% of the existing overdraft can be recovered by any scenario. Our findings indicate that the lack of floodwater (without water transfers from the Delta) is the key reason for low groundwater overdraft recovery (in SJ and TL), rather than the lack of recharge sites (assuming implementation of MAR at all selected locations). Low groundwater recovery in SJ and TL is due to low water availability combined with high existing overdrafts, which is also evident in other studies (e.g. Ghasemizade et al., 2019). It appears that SJ and TL will require measures in addition to MAR to mitigate the existing overdraft. These include, for example, moving from crisis-driven responses (e.g. groundwater overexploitation during drought) to the enactment of mitigation measures (e.g. conjunctive management, cropping pattern shift, irrigation efficiency) (Christian-Smith et al., 2015). Xiao et al. (2017) showed that a shift in cropping pattern (predominantly row crops to tree crops) has contributed to enhanced groundwater depletion during the 2012-2015 drought. Alam et al. (2019) estimated an increase in groundwater depletion rate of 0.93 km^3/year for a 40% shift from row to tree crops. Further study is required to assess the combined effect of demand management along with MAR.

3.4.2.4 Groundwater storage change under water transfer scenario R90_2ft_WT

As described in section 3.3.3, we quantified the volume of water leaving the Delta above the 90th percentile (excess flow) after implementing the region-wide R90_2ft scenario, which is about 2.2 km^3/year (see Figure A3 of Supplementary Material for the cumulative difference in Delta outflow between MAR and base scenarios). We applied this water to the recharge sites of SJ and TL. The total volume of transferred water applied to SJ is on average 0.41 km^3/year and TL is 1.79 km^3/year under the R90_2ft_WT scenario. Figure 6f shows the spatial distribution of groundwater storage changes under the R90_2ft_WT scenario. We found that SR-15, 18, 19, and 21 show higher groundwater storage changes. Figure 7a compares the groundwater storage change percentage between water transfer scenario R90_2ft_WT and non-water transfer scenarios. We found that the R90_2ft_WT scenario significantly increases groundwater storage change (or overdraft recovery) in SJ and TL; specifically the groundwater overdraft recovery increased to 63%, 62% and 30% (under R90_2ft_WT scenario) from 9%, 3% and 3% (under R90_2ft scenario) in CV, TL, and SJ respectively.

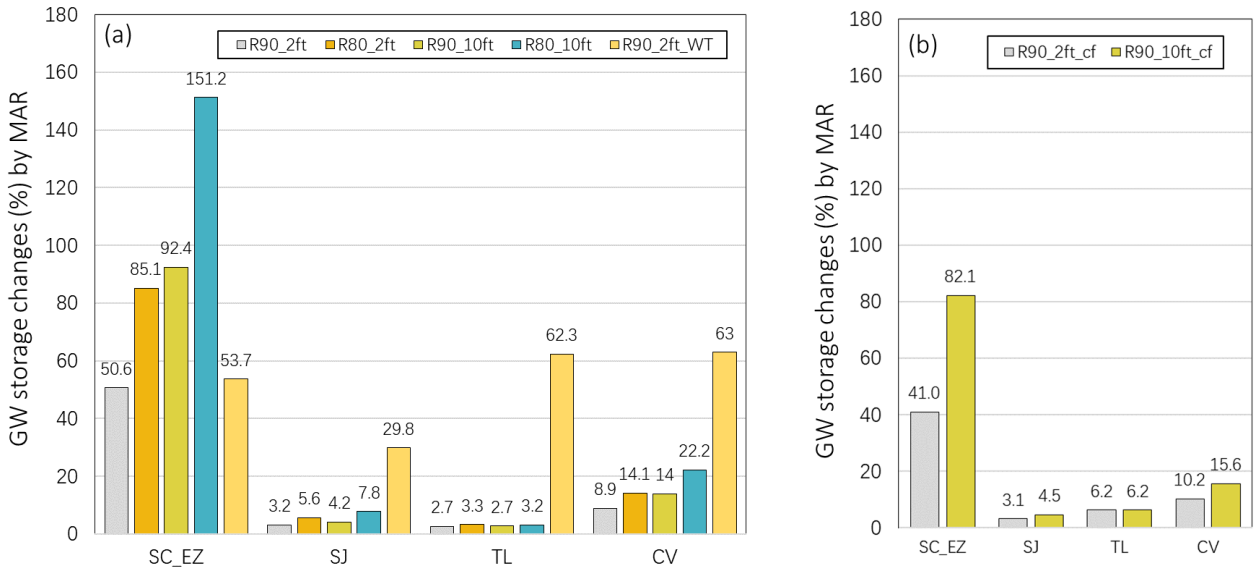

Figure 3.7. Groundwater storage changes (%) estimated by multiple MAR scenarios, (a) R90_2ft, R80_2ft, R90_10ft, R80_10ft scenarios, and R90_2ft_WT, (b) R90_2ft_cf and R90_10ft_cf scenarios.

3.4.2.5 Groundwater storage change under current crop/land use scenario

Figure 7b shows the groundwater storage changes due to MAR under current crop/land use and infrastructural development (i.e. R90_2ft_cf and R90_10ft_cf scenarios). We found that the groundwater storage increases for R90_2ft_cf and R90_2ft_cf scenarios are similar to the R90_2ft and R90_2ft scenarios over the entire CV. A regional comparison shows that the groundwater storage increase, compared to the R90_2ft (and R90_10ft) scenario, is lower in SC_EZ, however, it is almost the same in SJ and higher in TL. The results from this experiment indicate that MAR will provide similar benefit (in terms of aquifer storage recovery) in the near future (assuming water supply remains less variable in the next 30–40 years) as it could have done in the past.

3.4.3 Changes in groundwater balance components

Groundwater storage change in an aquifer is the result of a balance among deep percolation, stream-aquifer interaction, return flow, net subsurface flow, and groundwater pumping. These

groundwater balance components are expected to vary among regions. Here, we calculated the cumulative difference in each of the groundwater balance components between MAR and the base scenario using equation (2).

$$\text{Cumulative change } = \frac{\sum_{i=1}^{N} Var_{i,MAR} - \sum_{i=1}^{N} Var_{i,base}}{Total\ years} \qquad (2)$$

where VAR_i represents a particular water balance component for month i. Total years considered are 56 (1960-2015). The units of cumulative change are km^3/year.

Figure 8 shows the yearly cumulative change in water balance components relative to base conditions in the major regions (i.e., SC_EZ, SJ, and TL) of the CV under the R90_2ft scenario. We show the comparison for R90_2ft only because this scenario's results are representative of the relative contribution of each of the water balance components. In Figure 8, three variables, diversion, deep percolation, and GW flow to stream, show relatively high changes after MAR implementation. Diversion indicates how much water is diverted (from a stream) for MAR. Deep percolation is the portion of diverted water (for MAR) that reaches the saturated zone. Figure 8 shows that the water diversion for MAR is higher in SC_EZ compared to SJ and TL. This is due to higher surface water availability in SC_EZ. As surface water diversions to MAR sites increase, deep percolation also increases in all regions, with a higher rate in SC_EZ and SJ (see Figure A4 of Supplementary Material) than in TL.

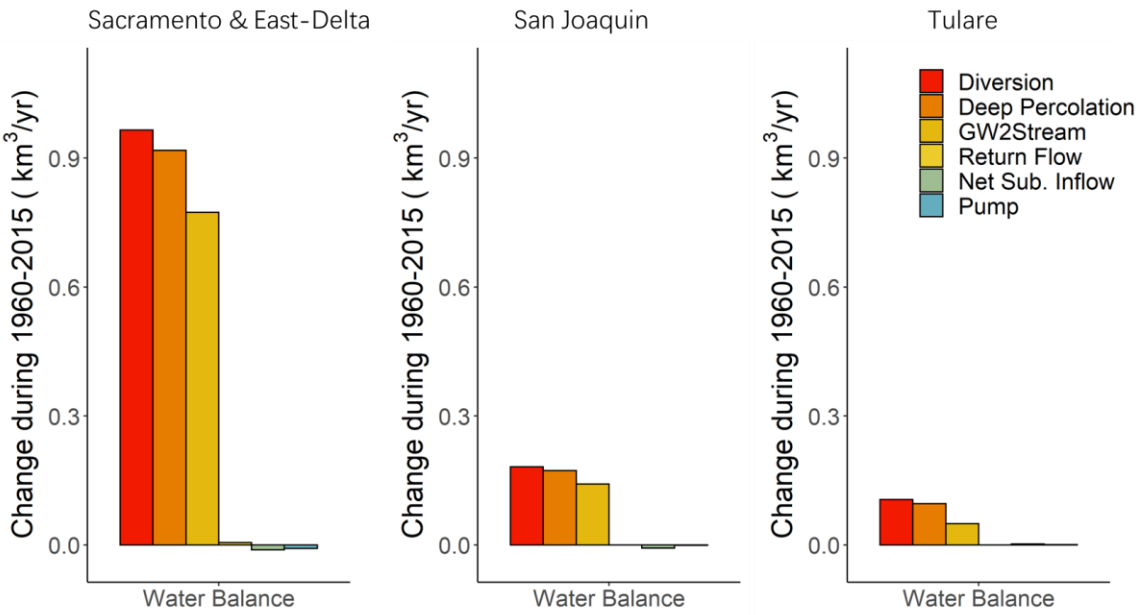

Figure 3.8. Change in water balance components for R90_2ft scenario compared to base condition averaged over 1960-2015. The water balance components shown here include diversions for MAR, deep percolation, lateral flow from groundwater flow to stream (GW2Stream), net subsurface inflow from neighboring subregions (Net Sub. Inflow), and pumping.

The increase in deep percolation also increases lateral flows from groundwater to stream (discussed in the next section). Furthermore, we found that the effect of MAR is not significant on other water balance components, such as return flow, net subsurface inflow, and pumping. The effect of MAR on pumping was low at the regional scale, similar to the finding by Ghasemizade et al. (2019). MAR's influence on groundwater pumping depends on the spatial distribution of MAR sites, head differences between streams and aquifers, hydraulic connectivity, and distances between the MAR sites and streams (Ghasemizade et al., 2019). With MAR, it is possible that streams will not lose as much water to the aquifer due to higher groundwater elevations, which will increase the availability of streamflow for other uses, which in turn could result in a greater decrease in pumping. On the other hand, we found that the regional change in groundwater head after MAR (especially in TL) is modest, therefore the effect on groundwater pumping likely would

be small (see Figure A5 for temporal distribution of pumping). We do note that a local level study by Scanlon et al. (2016) on the effect of MAR projects in the southern CV (e.g. Arvin-Edison Water Storage District, Kern Complex, Rosedale-Rio Bravo and others) shows that groundwater depletion near the MAR projects is much less than the regional depletion. The Scanlon et al. (2016) study also shows that MAR together with conjunctive surface-groundwater use can reduce groundwater pumping rates. We argue that a regional scale decrease in groundwater pumping is only possible when MAR projects can significantly reduce the regionwide depletion ofgroundwater head, which did not occur in our simulated results.

3.4.4 Changes in stream-aquifer interaction

The net volume of groundwater overdraft recovery is influenced by stream-aquifer interactions (i.e. flow exchange between stream and aquifer). According to Darcy's Law, two factors are important to determine the direction and volume of subsurface flow: (1) horizontal hydraulic conductivity, and (2) head difference between the groundwater table and the connected stream. Higher hydraulic conductivity results in relatively fast movement of subsurface water, and greater positive head differences result in greater movement of water from the aquifer to the stream. In our simulations, all regions had increased flow from the aquifers to the streams (Figure 8) with MAR. To better demonstrate how stream-aquifer interactions vary among regions and over time, we calculated cumulative stream-aquifer interactions using equation (2) for each major CV region.

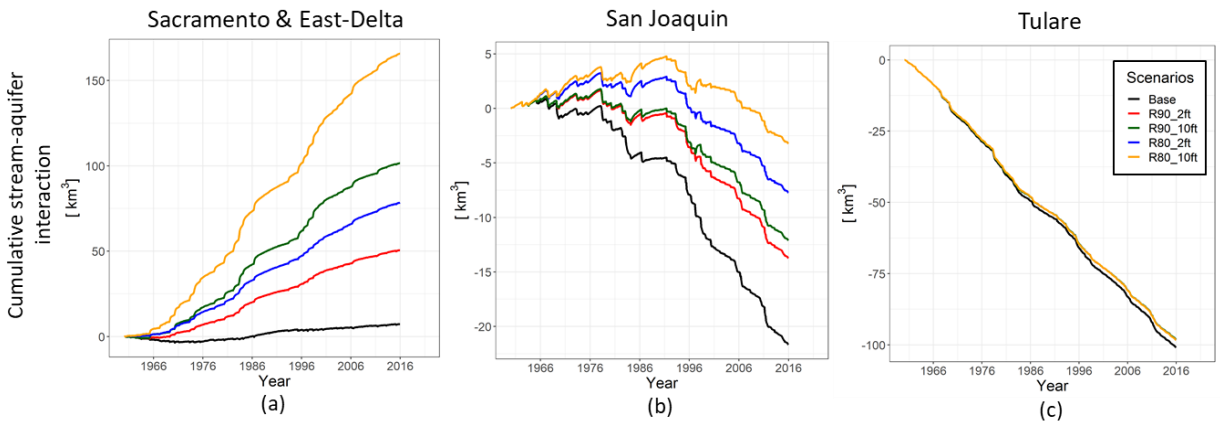

Figure 3.9. Cumulative stream aquifer interactions in SC_EZ (left), SJ (middle) and TL (right) for the base and MAR scenarios. A positive value indicates flow from groundwater to stream, a negative value indicates vice versa.

Figure 9 shows the cumulative stream-aquifer interactions in SC_EZ, SJ, and TL during 1960-2015. The increase in deep percolation (as shown in Figure 8) associated with MAR raises the groundwater table relative to the base scenario, thereby changing the relative head difference between surface water and the groundwater table. This changes the stream-aquifer dynamics compared to the base scenario. In SC_EZ, the cumulative stream-aquifer interaction is close to 0 for the base condition, but groundwater flow from the aquifer to stream increases under MAR scenarios (Figure 9). This suggests that a fraction of groundwater recharge by MAR returns back to the stream through subsurface flow (or baseflow). In both SJ and TL, cumulative stream-aquifer interactions are negative under the base scenario, which indicates that the groundwater table is lower than the stream stage and there is a net flow from stream to the aquifer in the base condition. As MAR is implemented, the rise in the groundwater table leads to the change in hydraulic head difference and baseflow between the stream and the aquifer. In SJ, the cumulative stream-aquifer exchange is relatively balanced during 1960-1978 under the base condition. However, due to intensive groundwater extraction in SJ in the later part of the simulation period, the groundwater table dropped substantially and resulted in net negative baseflow even with the implementation of

MAR. In TL, the aquifer had been so severely overexploited that it is essentially disconnected from the stream, in which case the recharge rate is theoretically independent of the water table position (Brunner et al., 2009; Winter et al., 1998) and thus insensitive to MAR (as shown in Figure 9c).

3.4.5 The effect of MAR on low flow augmentation

Summertime (July-September) low flow is an important source of water for fisheries and ecosystem environmental flow. Baseflow (or lateral groundwater flow) from aquifers is an important, often primary, source of summertime low flow. MAR enhances baseflow by increasing net groundwater storage in the aquifers, which can play a vital role in sustaining streamflows during water-scarce drought years. MAR's ability to enhance low flows varies among regions due to variations in soil characteristics (e.g. horizontal and vertical hydraulic conductivity). We analyzed the baseflow change after MAR implementation for our entire simulation period (1960-2015), as well as for 2007-2009 and 2012-2015 drought periods. By comparing the modeled baseflow and the observed summertime streamflow entering the Delta (a proxy of net baseflow during summer), we found the model is in good agreement with observations (see Figure A6 of Supplementary Information).

Figures 10 a-f show the spatial distribution of the percent changes in baseflow for the entire simulation period and for the two drought periods. We found that the baseflow increases in almost all subregions in the SC, but is highest in SR-2, SR-5 and SR-6, located around Sacramento River (SR-2 and SR-4) and Feather River (SR-5). In SJ, relatively large increases in baseflow occur in SR-10 and SR-12, near the San Joaquin River (SR-10) and Merced River (SR-12). In TL, stream-aquifer interactions are weaker, which cause the baseflow to have very low or no change (discussed in Section 3.4.5).

Figures 10g-i show bar charts of the percent changes in baseflow. The figures show that there is a net increase in baseflow of about 47% and 78% under the R90_2ft and R80_2ft scenarios, respectively, during 1960-2015 in CV (Figure 10g). The northern region (SC_EZ) generally has the greatest increases in baseflow due to higher MAR-induced groundwater storage. Baseflows increase by about 37% and 62% in SC_EZ and 7% and 13% in SJ under the R90_2ft and R80_2ft scenarios, respectively, during 1960-2015 (Figure 10g). In TL, the baseflow increases are relatively small (~1%). Therefore, MAR appears to be a promising way to ensure environmental and ecological flows. In addition, we also computed the baseflow changes under R90_10ft and R80_10ft scenarios during 1960-2015 (not shown in Figure 10), which are about 85% and 146% in SC_EZ and 9% and 18% in SJ respectively. As a comparison, Ghasemizade et al. (2019) found the ratio of baseflow increase and MAR water delivery volume to be 0.38-0.49 in SR-18 (for the period of 1921 to 2009), whereas we found the ratio to be 0.30-0.39 for the same subregion.

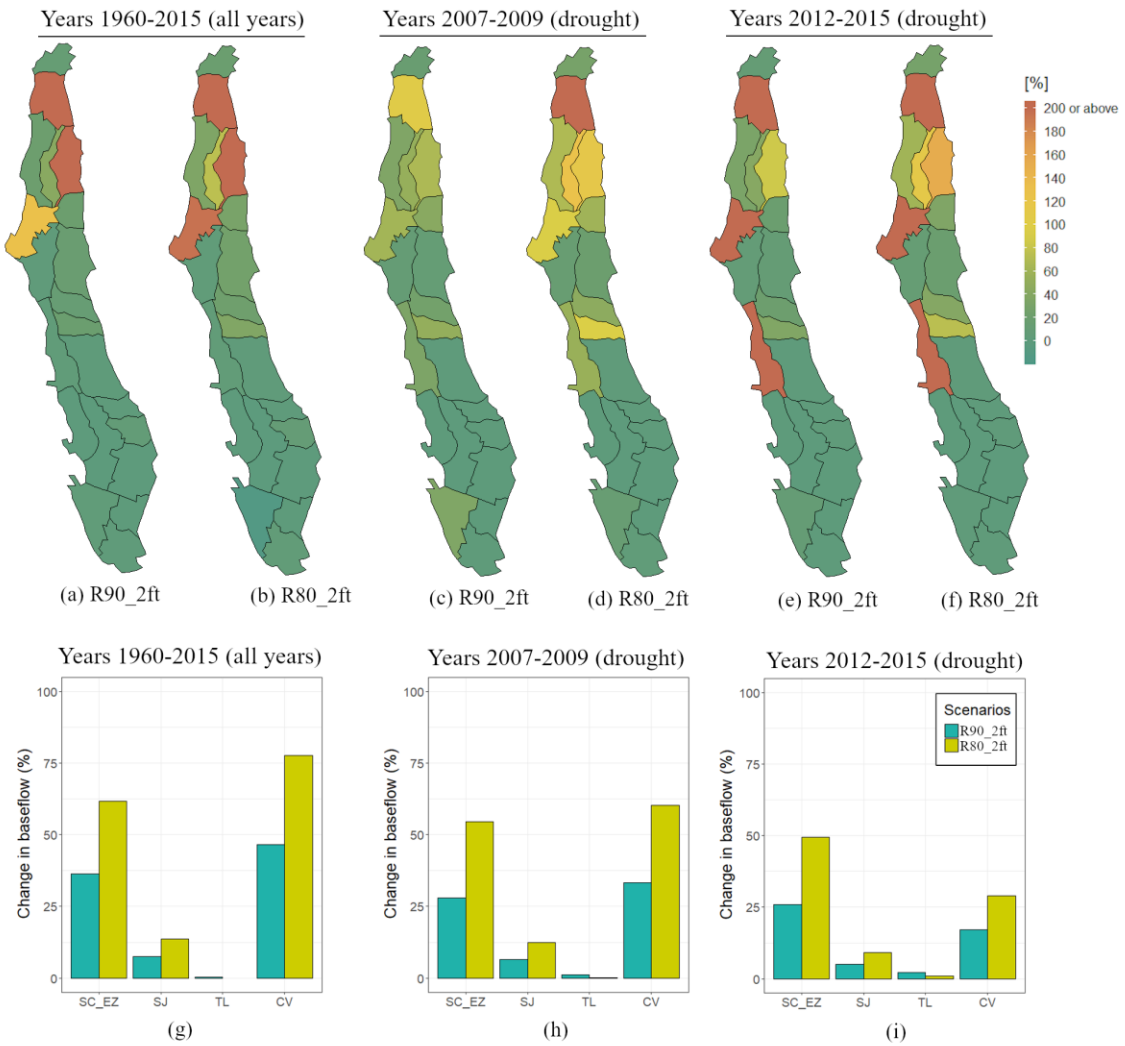

Figure 3.10. Summertime (July-September) baseflow changes in percentages. (a-f) Spatial distribution of baseflow changes for the entire study period 1960-2015 (a-b), the 2007-2009 drought (c-d) and the 2012-2015 drought (e-f). (g-i) Baseflow changes in major hydrologic regions.

MAR is intended to promote drought resilience through groundwater banking in the wet years (Scanlon et al. 2016). To evaluate the extent to which this would be the case, we compared baseflow changes during the 2007-2009 and 2012-2015 droughts. Figures 10h-i show the percent changes in baseflow during the 2007-2009 and 2012-2015 droughts, respectively. The baseflow increase due to MAR is substantial in most of the subregions during the drought years. We found that MAR would increase baseflow over the entire CV by around 28% (R90_2ft) and 60%

(R80_2ft) during the 2007-2009 drought, and around 17% (R90_2ft) and 29% (R80_2ft) during the 2012-2015 drought. SC has the highest enhanced baseflow among all regions. As the baseflow increase was found to be positively related to the amount of water applied for MAR, almost all of the subregions show higher increases under the R80_2ft than R90_2ft scenario. However, baseflow increases in SR-15 and SR-19 are lower under the R80_2ft than the R90_2ft scenario. This is because MAR diversion nodes for both subregions are located downstream of other diversion nodes that deliver MAR to other subregions first. Kings River delivers MAR water to SR-17 first and then SR-15, whereas Kern River delivers MAR water to SR-21 first and then SR-19. In SR-15 and SR-19, the actual volumes of water applied for MAR are 0.01 and 1.36 km^3 lower in the R80_2ft scenario than in the R90_2ft scenario. Overall, MAR can augment summertime low flows, especially during drought periods, by as much as 52% without water transfer and 73% if excess flows are delivered from north to south. This finding confirms that MAR could enhance drought resilience and sustain environmental flows in the CV.

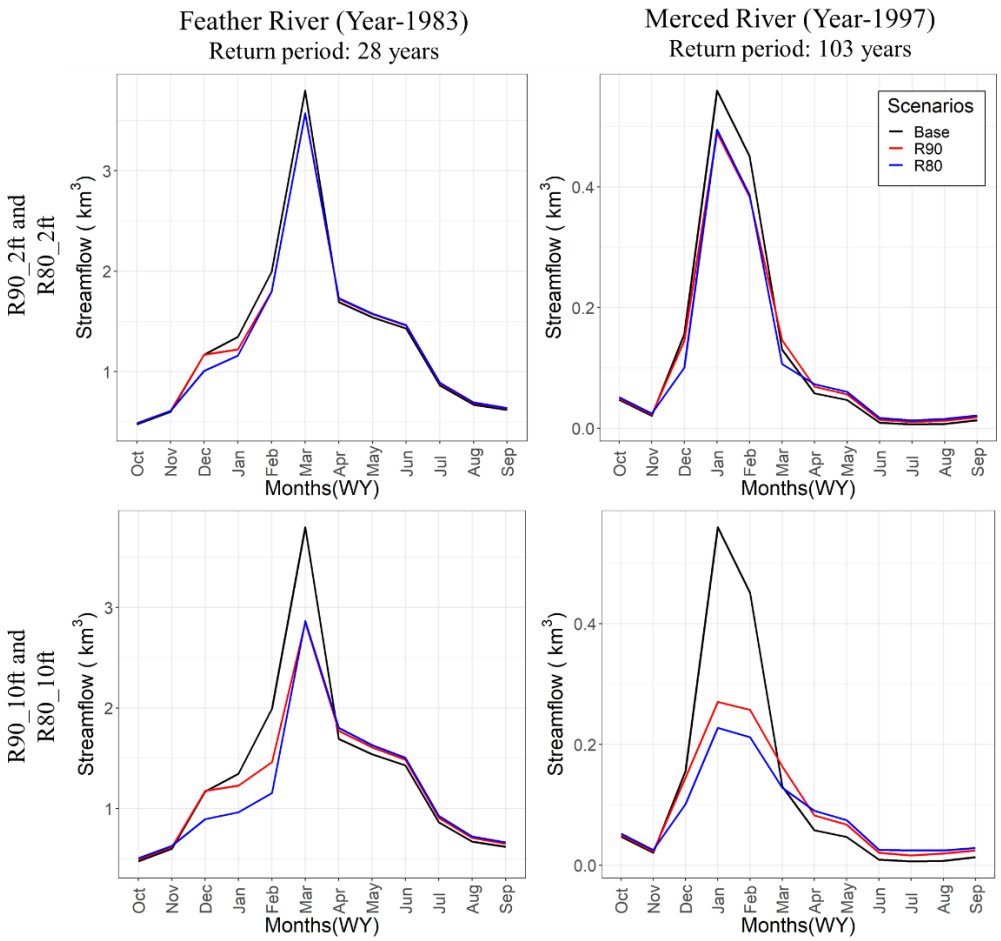

Figure 3.11. Monthly hydrograph for two wet years (1983 and 1997) near the outlets of Feather River (top row) and Merced River (bottom row). In all the plots, the black line represents the base simulation, and the red and blue lines in the top row represent R90_2ft and R80_2ft scenarios respectively and in the bottom row represent R90_10ft and R80_10ft scenarios respectively

3.4.6 The effect of MAR on flood risk reduction

MAR could reduce flood peaks by diverting high flows from the streams. Figure 11 shows the monthly hydrograph of the Feather River in 1983 and the Merced River in 1997 – two major flood events in the CV. The peak discharge in both basins usually occurs between January and March. We found that the peak discharge decreases in all cases with the MAR implementation. The comparison of the scenarios with different maximum depths (2ft and 10ft) show that much greater reduction in flood peak occurs (Figure 11) when the maximum allowable depth is increased

from 2ft to 10ft, especially during the extreme Merced River flood of 1997 (an estimated return period of 103 years). Overall, we found peak flow decreased by around 10%-40% (during February-March) in Feather River and 12%-59% (during January-February) in Merced River.

3.4.7 Potential crop damage due to waterlogging

MAR implementation raises the water table, which can threaten crops if the water table enters the root zone. Root zone waterlogging can have multiple negative consequences, such as reduced aeration, slowed bacterial activity, and increased plant vulnerability to diseases. We identified locations that are at risk of crop damage due to root zone waterlogging. The average root zone depth for both row and tree crops is 1.5 m in the model, which was also used by Ghasemizade et al. (2019). As a metric of risk, we calculated the number of additional months when the water table was below the threshold depth under MAR scenarios during the growing season (Figure 12) and the winter seasons (Figure A7 of the Supplementary Information). All the subregions in SC have some (non-zero) risk associated with rootzone water logging. In SJ, areas in subregions 11-13 shows increased waterlogging, but the waterlogging is not expected to last more than about 20% of the growing season months. In TL, there are a few areas in subregions 18 and 19 that show increased waterlogging (mostly <40% of the time waterlogged) under R90_2ft_WT scenario. Despite the waterlogging expected to occur in some areas under R90_2ft_WT scenario, most places in the domain encounter waterlogging during less than 5% of the growing season. This analysis indicates that more detailed investigation of the waterlogging problem will be warranted in the future work. Although the rules we use to determine where excess flows are to be applied do not consider waterlogging, the model and the scenario settings could be further refined to reduce the extent and magnitude of waterlogging risk.

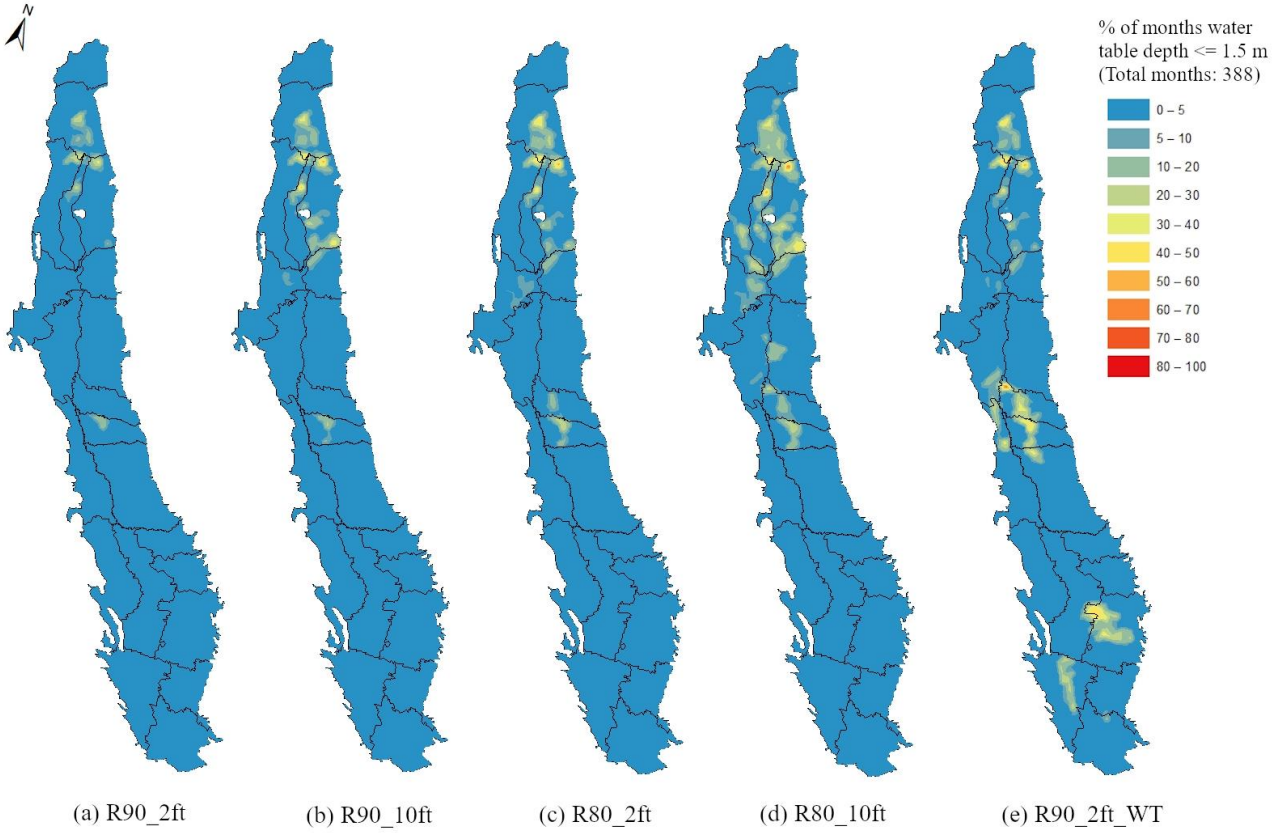

Figure 3.12. Percent of growing season months (April through October) for which the water table enters the rootzone due to the implementation of different MAR scenarios.

3.4.8 Limitations and future research

Our results are based on several important assumptions, which infer certain limitations to our findings. First, we assume that there are adequate water delivery facilities to convey surface water to the MAR recharge sites when flood water is available for recharge. Clearly, this may not always be the case, and in this respect our results are indicative of the maximum potential of MAR. Second, we used a monthly time step for the model (a C2VSIM limitation), which limits our ability to capture peak streamflows that arise from short-term storm events. While our results show that there could be considerable flood protection benefits from the use of MAR, further studies (at shorter time steps) are needed to reliably quantify those benefits. Third, in our computations, we

assume that the areas selected for MAR would be available for recharge regardless of policy and social constraints that may limit the use of that land (Deitch and Dolman, 2017; Foster and Garduño, 2013; Li et al., 2016). These constraints include, but are not limited to, legal/regulatory frameworks, groundwater governance structure, local water policies, landowners' participation willingness, existing water rights, and coordination among agencies (see CDWR 2018b for more detail). As is the case for our assumption of adequate conveyance infrastructure, these considerations suggest that our results are best interpreted as an upper bound on the potential of MAR to mitigate groundwater overdrafts. Fourth, we note that the depth of water to be applied was not differentiated among different SAGBI classes. The differences in recharge rates among specific recharge sites might result in variable benefits of MAR. A more detailed investigation is needed to determine the effects of such differences on the field-scale potential for MAR. Lastly, we did not link the role of MAR to climate change. However, this was partially addressed in a previous study (Alam et al., 2019d). An expected increase in the winter inflows to the CV may be expected to provide more water for MAR in the future.

3.5 Summary and Conclusions

Groundwater plays a vital role in the Central Valley's water supply, especially during drought periods. Over our 56-year study period (1960-2015), groundwater storage in the CV has progressively decreased by an average of around 3 km^3/year. MAR has the potential to replenish groundwater through the application of high winter flows to agricultural lands. Our objective was to evaluate the potential of groundwater overdraft recovery and other ancillary benefits through a regionwide implementation of MAR. We conducted numerical experiments using a surface water-groundwater hydrological model and assuming wintertime flows exceeding the 90th (R90

scenarios) and 80th (R80 scenarios) percentiles were available to be applied for MAR. Based on our simulations, we conclude that:

- MAR could potentially recover 9 – 22% (for R90 and R80 scenarios) of the existing groundwater overdraft aggregated over the entire CV. The effect of MAR varies among regions. In the northern CV (i.e. Sacramento) where groundwater depletion is not a major problem (compared to the southern CV), the effect of MAR is high. In southern CV (i.e. San Joaquin and Tulare) where groundwater overdraft is large, MAR cannot solve the problem. We find that the contribution of MAR to the reduction of the historic groundwater overdraft would be about 3 – 8% in the San Joaquin (SJ) region, and even less (about 3%) in the Tulare (TL) region. The primary cause of low groundwater recovery in the southern CV (SJ and TL regions) is the lack of adequate headwater supply in relation to the large existing groundwater overdraft.

- The application of MAR using streamflow crossing each region is not expected to effectively mitigate the groundwater overdraft problem in the southern CV. However, MAR could mitigate a much greater portion of the groundwater overdraft through the delivery of excess winter flow from northern CV to southern CV for MAR. We investigated the effect of delivering excess winter Delta outflow (over the 90th percentile) to the southern CV for MAR, this would enhance groundwater overdraft recovery by 63% in CV, 30% in SJ, and 62% in TL.

- The application of MAR would have ancillary benefits in addition to groundwater overdraft recovery. MAR can augment summertime low flows, especially during drought periods by as much as 52% without water transfer and 73% if excess flows are delivered from north to south. Moreover, we tested the effect of MAR on streamflow of Feather River and

Merced River during two large flood events, showing that MAR effectively reduces the flood peaks by 10% – 40% in Feather River and 12% – 59% in Merced River.

Acknowledgements:

We acknowledge the University of California Research Initiatives Award LFR-18-548316 for supporting this work. We are grateful to Dr. Emin Dogrul and Dr. Tyler Hatch from the CDWR for technical assistance in the use of C2VSIM.

CHAPTER 4

Post-drought groundwater storage recovery in California's Central Valley

This chapter has been submitted to Water Resources Research for review in its current form.

Alam, S., Gebremichael, M., Ban, Z., Scanlon, B. R., Senay, G. B. and Lettenmaier, D. P. Post-drought groundwater storage recovery in California's Central Valley. Submitted to Water Resources Research.

Abstract

Groundwater depletion is a major threat to agricultural and municipal water supply in California's Central Valley. Recent droughts during 2007–2009 and 2012–2016 exacerbated chronic groundwater depletion. However, it is unclear how much groundwater storage recovered from drought-related overdrafts during post-drought years, and how climatic conditions and water management affected recovery times. We estimated groundwater storage change in the Central Valley for April 2002 through September 2019 using four methods: GRACE satellite data, a water balance approach, a hydrologic simulation model, and monitoring wells. We also evaluated the sensitivity of drought recovery to different climate scenarios (recent climate ± droughts) and future climate change scenarios (20 GCMs and 2 RCPs). Central Valley groundwater loss ranged from 19 km^3 (2007 – 2009) to 26 km^3 (2012 – 2016) (median of four methods). Aquifer storage recovery was 34% and 13% of the overdraft during the 2010–2011 and 2017–2019 post-drought years. Numerical experiments show that recovery times are sensitive to climate forcing, with longer recovery times for a future climate scenario that replicates historical climatology relative to

historical forcing with no-drought. Recovery times for groundwater pumping restrictions at 30th to 50th percentiles of historic groundwater depletion were reduced by ~2× relative to no pumping restrictions under no-drought future climatology. This study highlights the importance of considering water management within the context of climate change scenarios to determine future drought recoveries.

4.1 Introduction

Groundwater overdraft during droughts is common in semiarid regions globally (Wada et al., 2010), and climate change is expected to further accelerate groundwater depletion in these regions (Alam et al., 2019; Wu et al., 2020). Groundwater overdrafts linked to droughts are caused both by reduced groundwater recharge and increased agricultural, industrial, and municipal water demand (Russo and Lall, 2017; Taylor et al., 2013). The impact of drought on groundwater can be especially severe in irrigated agricultural regions with limited surface water supply. There is a critical need to understand drought impacts on groundwater and to identify measures to improve resiliency to droughts (Taylor et al., 2013).

Recovery of groundwater is critical for long term environmental and agricultural sustainability. However, aquifers in semi-arid regions such as the U.S. High Plains and northeastern India have shown limited resilience to drought events — the groundwater depletion during droughts are typically not fully recovered (Famiglietti et al., 2011; Rodell and Famiglietti, 2002; Scanlon et al., 2012; Voss et al., 2015). Limited recovery can be attributed to excess groundwater use that in some regions exceeds the net volume of water supplied during wet post-drought years. For instance, groundwater in the Central and Southern High Plain aquifers (USA) has been declining over the past few decades (39 km^3 during 2002 to 2017), and there has been very low overdraft recovery during this time (i.e., 2006 through 2010) (Rateb et al., 2020). In

contrast, there are also some regions that show rapid groundwater recovery during post-drought years (e.g., Texas Gulf Coast) (Rateb et al., 2020). Irrespective of the recovery pattern (rapid versus slow), precipitation and related surface water supply are key to overdraft recovery as high precipitation promotes greater groundwater recovery. Additionally, precipitation events affected by large scale climatic conditions, such as the El Niño Southern Oscillation (ENSO) (2 to 7-year cycle) or the North Atlantic Oscillation (NAO) (3 to 6-year cycle) have been found to influence groundwater level variability in many aquifers globally, e.g., North Atlantic Coastal Plain principal aquifers (USA), Northwest India, Southwest British Columbia and other regions (Asoka et al., 2017; Fleming and Quilty, 2006; Kuss and Gurdak, 2014; Perez-Valdivia et al., 2012). However, the complex interplay between climatic conditions (e.g., precipitation) and the nature of groundwater recovery is modulated by water management (e.g., groundwater pumping, reservoir regulation), and varying hydrogeologic conditions. To our knowledge, there is no study that investigates the groundwater recovery associated with droughts and its connection to precipitation and water management practices, particularly in highly managed aquifer (e.g., Central Valley of California).

California's Central Valley (CV)—one of the richest agricultural regions in the world—has experienced frequent droughts over the past half century, with the last decade marked by two major drought periods: 2007–2009 and 2012–2016 (Famiglietti, 2014; Faunt et al., 2016; Thomas et al., 2017). Despite the droughts, agricultural water consumption in the CV did not decrease during the drought years (Alam et al., 2019a; Gebremichael et al., 2021). The effects of drought instead were mitigated by supplementing or replacing surface water supply sources with groundwater (Famiglietti et al., 2011; Ralph & Dettinger, 2012). Increased water demand over time compounded by ongoing climate change have resulted in long-term groundwater depletion in

the CV, which was accelerated during the 2007–2009 and 2012–2016 droughts (CDWR, 2013; Hanak et al., 2017; Xiao et al., 2017). The historic chronic groundwater depletion (Faunt et al., 2009) motivated the State Legislature to enact the Sustainable Groundwater Management Act (SGMA), which mandates sustainable groundwater use (California State Legislature, 2014). While the use of groundwater to mitigate surface water shortages during droughts may be an obvious management response that improves the reliability and robustness of the system, post-drought recovery of groundwater overdraft is key to long-term sustainability. To ensure post-drought groundwater storage recovery and develop a sustainable groundwater management plan that increases groundwater resilience, there is a critical need for improved understanding of (1) how much groundwater was recovered during post-drought years, and (2) the influence of climate versus anthropogenic factors on post-drought groundwater recovery.

A major constraint in understanding post-drought groundwater recovery is the lack of reliable groundwater storage data on a regional scale. Groundwater storage change estimates for the CV vary substantially among different methods (Alam et al., 2020; Ojha et al., 2020; Scanlon, et al., 2012), and this has made understanding of drought recovery challenging. Commonly used methods for groundwater storage change estimation are, (1) well measurements (Rateb et al., 2020; Scanlon et al., 2012), (2) Gravity Recovery and Climate Experiment (GRACE) satellite-based estimates (Rateb et al., 2020; Scanlon et al., 2012), (3) water balance methods (Xiao et al., 2017), and (4) hydrologic simulation models (Brush, 2013; Faunt et al., 2016). Each of these methods has its own strengths and weaknesses. Well data provide direct measurements of groundwater levels, yet such measurements are scarce in many places, lack continuous long-term measurements, and calculation of groundwater storage from well measurements is prone to large uncertainties because of lack of knowledge of aquifer storage coefficients and order of magnitude variations in storage

coefficients between unconfined and confined aquifers. Continuous estimates of groundwater storage change (2002 to present) can be derived from the GRACE satellites which measure terrestrial water storage (TWS); however, the GRACE footprint is large (~150,000 km^2), limiting small scale groundwater storage change estimation (Long et al., 2016; Longuevergne et al., 2007). Another approach to estimate regional groundwater storage change is through the water balance method (WB), which sums the influxes (precipitation, inflow) and subtracts the outfluxes/storage changes (evapotranspiration [ET], outflow, in soil moisture, snow, and surface water) over a prescribed domain (Xiao et al., 2017), closes the water balance (and hence provides groundwater storage change estimates compatible with the other hydrological components), yet it is subject to estimation errors from each of the water balance components. Hydrologic models simulate continuous groundwater storage changes, and are ideal to perform scenario experiments (Dogrul et al., 2016; Faunt et al., 2016). However, such simulations are subject to errors resulting from model's approximation to physical process, parameter estimation, and input data accuracy.

In summary, each of the groundwater storage change estimation/measurement methods has its own pros and cons, and there is no single method that is likely to outperform others. Past studies of groundwater change in the CV (and many other regions of the world) have relied on only one or two of the above methods. For instance, Xiao et al. (2017) estimated groundwater depletion and post-drought recovery for the 2007–2009 drought using GRACE satellite data and the WB method. They found groundwater depletion trends for the two methods were similar, but recovery rates differed substantially. We argue that in order to fully understand post-drought groundwater storage recovery, it is important to formally acknowledge differences in results from the various groundwater estimation methods, but to use multiple methods to the maximum extent possible. This can be done through the use of all available groundwater estimation methods and by

identifying and acknowledging agreements and disagreements in the results. To our knowledge, no study has been performed on CV that examines and compares groundwater depletion and recovery rates from all four-groundwater storage change estimation methods.

Climate and anthropogenic factors can strongly influence groundwater depletion and recovery (Alam, et al. 2019; Hanson et al. 2012; Taylor et al. 2013; Wu et al. 2020). Droughts cause groundwater depletion; the drought recovery period is often calculated from post-drought precipitation duration and magnitude (DeChant and Moradkhani, 2015; Pan et al., 2013). High precipitation during post-drought years reduces post-drought recovery period, but the effective recovery rate may be hindered by anthropogenic factors, such as increased agricultural and municipal groundwater pumping (Gleeson et al., 2012; Ojha et al., 2020). Although drought impacts on groundwater availability have been well studied (Argus et al. 2017; Scanlon et al. 2012; Taylor et al. 2013; Thomas and Famiglietti 2019; Xiao et al. 2017), it is unknown how groundwater recovery during post-drought years relates to post-drought precipitation. In addition to degree of recovery of groundwater storage, the rate at which groundwater recovery occurs is a key indicator of the resilience of the groundwater system. Rapid recovery indicates that an aquifer is resilient to extreme climate conditions such as drought. In contrast, slow recovery can be threatening as another drought event may begin before full recovery from a previous drought. In the past few decades, there were a few wet spells over California, but it is unknown if such wet spells are sufficient for recovery of groundwater overdraft during droughts, and if not, what measures could be implemented to assure full post-drought groundwater overdraft recovery. The overdraft recovery duration and its relationship with precipitation amount in the CV aquifer is currently unknown.

The objective of this study is to address the following questions: (1) how much of the groundwater storage overdraft related to recent droughts in the CV was recovered during post-drought years? and (2) what is the role of precipitation and water management strategies in rapid versus slow post-drought groundwater storage recovery? We address these issues using the four methods summarized previously. We also isolate the impact of future climate on groundwater storage recovery from drought using different scenarios (historical climatology, no drought, wet years only) and climate change impacts using 20 Global Climate Models (GCMs) and two Representative Concentration Pathways (RCPs) from the IPCC Fifth Assessment Report. Our outcomes are intended to provide insights into drought resiliency that could help in developing groundwater management plans mandated by SGMA (California State Legislature, 2014).

4.2 Study area

The CV, located along a north-south transect in California, drains three major watersheds that deliver water to the CV region: the Sacramento, San Joaquin, and Tulare (SSJT watersheds) (Figure 4.1a). The CV is a flat valley of about 54,000 km^2 area surrounded by mountains: the Sierra Nevada to the east and the Coastal range to the west. The climate of this region is Mediterranean, with most precipitation occurring in the winter (November through March), out of phase with evaporative demand which is high in the summer (July through September) (Cooper et al., 2018). The two major droughts of the past two decades (2007–2009 and 2012–2016) resulted in 38.6% of California being in severe to exceptional drought categories (according to the U.S. Drought Monitor) between 2007–2009, and 68% between 2012–2016, suggesting 2012–2016 drought was relatively more severe. See supporting information (SI), Figure B1.

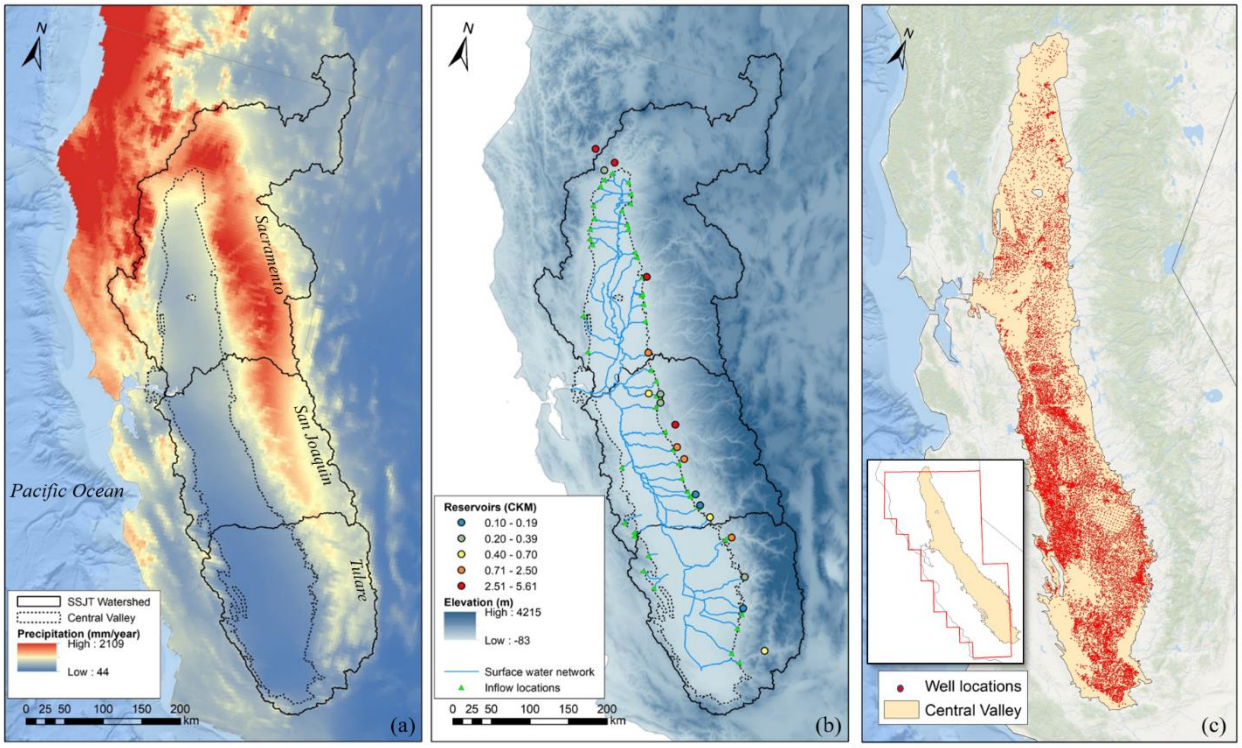

Figure 4.1. Study area: (a) Central Valley boundary and Sacramento-San Joaquin-Tulare (SSJT) watersheds, with long term mean annual precipitation (averaged over 2000-2018; source http://worldclim.org/); (b) Locations of major reservoirs (CDEC, 2020), with elevation, surface water network, and inflow locations to the CV; (c) Location of groundwater wells (total 23,048) in the CV (CASGEM, 2021). The inset in Figure 4.1c shows the GRACE analysis region (red border).

Precipitation generally decreases both from north to south and through headwaters along valley to mountain transects (Figure 4.1a). Generally, headwater watersheds are considerably wetter than valley bottoms. About half (~28,000 km^2) of the CV is irrigated. The source of water is a mixture of surface and groundwater (Hanak, 2011). The contrast in north-south water demand and supply motivated the construction of headwater reservoirs and infrastructure that convey surface water from the Sacramento-San Joaquin River Delta in the north to the south with infrastructure known as the State Water Project (SWP) and the federal Central Valley Project (CVP). Most of the surface water supply to the CV is generated in the headwater watersheds. More than 50 reservoirs (20 reservoirs in the Central Valley Project and 34 in the State Water Project)

regulate inflows from the headwaters to the CV (CDWR, 2014; USBR, 2014). Surface water from headwater watersheds enters the CV at ~50 locations (Figure 4.1b). Excess surface water after meeting all demands (agricultural, municipal, and industrial) is released to the San Francisco Bay via the Delta.

The CV aquifer contains unconsolidated sedimentary deposits in stream channels, alluvial fans, and flood plains (Farrar and Bertoldi, 1988). The aquifer material in the western CV (coastal) is relatively fine grained whereas the material in the eastern CV is much coarser grained (granite and volcanic). Lenses and beds of fine-grained material (Corcoran clay) are found predominantly in the southern Tulare Basin and the western San Joaquin Basin, and restrict vertical flow of groundwater (Planert and Williams, 1995).

4.3 Data and Method

We produced multiple estimates of groundwater storage (GWS) change and conducted numerical experiments to quantify the role of climate and water management on groundwater overdraft recovery following drought. Our approach follows three steps:

(1) Estimate GWS changes using four different methods,

(2) Conduct numerical experiments with different climatic conditions and water management options to estimate the time for GWS recovery from drought,

(3) Conduct numerical experiments to estimate the time for GWS recovery under future climate change.

In Step (1), we estimated GWS changes using the four methods: GRACE satellite data, WB, model simulation, and well measurements. In Steps (2) and (3), we performed numerical experiments.

4.3.1 Metrics for measuring post-drought groundwater storage recovery

Metrics for estimating groundwater storage recovery time and volume following drought can take multiple forms. For instance, groundwater recovery can be measured with respect to the historical average condition or some other threshold level. In our case, we measure the post-drought groundwater recovery with respect to the pre-drought GWS level (see Figure C6, SI for detail). We used the following metrics for measuring recovery: GWS recovery volume (ΔGWS_{recov}), GWS depleted during drought ($\Delta GWS_{drought}$), GWS recovery percentage $\left(R_f\right)$, and GWS recovery duration (D_{rec}):

$$\Delta GWS_{recov} = GWS_{post\_drought} - GWS_{drought\_end} \quad (1)$$

$$\Delta GWS_{drought} = GWS_{drought\_end} - GWS_{drought\_start} \quad (2)$$

$$R_f = \frac{\Delta GWS_{recov}}{|\Delta GW_{drought}|} \times 100\% \quad (3)$$

$$D_{recov} = t_{post\_drought} - t_{drought\_end} \quad (4)$$

Where, D_{recov} is the time in months between the drought ending month ($t_{drought\_end}$) and the post drought month under consideration ($t_{post\_drought}$).

4.3.2 GWS change estimation using multiple methods in the recent decades

In order to characterize GWS depletion and recovery in the recent decade (2003–2019), we used GWS estimates made by four different methods. The GWS change estimation methods considered in this study are: (1) GRACE, (2) Wells, (3) WB, and (4) hydrologic model simulation (C2VSIM). The key input datasets used in each method are listed in Table 4.1.

Table 4.1. List of datasets used for estimating GWS change.

Data type	Data source	Spatial distribution/ resolution	Reference/note
Groundwater level	California Statewide Groundwater Elevation Monitoring (CASGEM)	Total stations in CV: 23,048	CASGEM (2021)
Terrestrial Total Water Storage Anomaly (TWSA)	GRACE and GRACE-FO MasCon. Two sources: (1) Jet Propulsion Laboratory (JPL-m) and (2) Center of Space Research (CSR-m)	0.5 degree	Save (2020); Save (2016); Watkins et al. (2015)
Reservoir storage	California Data Exchange Center	~50 reservoirs	CDEC (2020)
Streamflow	Inflow data from United States Geological Survey (USGS); outflow data from Dayflow	52 inflow locations and delta outflow	CDWR (2020); Dayflow (2020); USGS (2020)
Land use	USDA National Agricultural Statistics Service Cropland Data Layer	30 m	USDA-NASS (2020)
Precipitation	PRISM DAYMET Livneh et al. (L13)	4 km 1 km ~6 km (1/16th degree)	Daly et al. (2008) Thornton et al. (2017) Livneh et al. (2013)
Evapotranspiration, snow water equivalent, and soil moisture	Variable Infiltration Capacity (VIC) simulations	~6 km (1/16th degree)	VIC-4.1.2.g model simulated for this study
C2VSIM-FG simulated GWS	GWS obtained from C2VSIM simulation (2002-2015). We extended the simulation to September-2019.	Central Valley-wide	CDWR (2020)
Specific yield (Sy)	C2VSIM-FG model field CVHM model field	~1.65 km^2 (avg.) FE cells 1.61 km FD grids	CDWR (2020) Faunt et al. (2009)

4.3.2.1 GRACE-based estimate of GWS change

We used GRACE/GRACE-FO release (RL06) level 3 mass concentration (MasCon) solutions from two sources, NASA Jet Propulsion Laboratory (JPL-m) and University of Texas

Center for Space Research (CSR-m). In contrast to the traditional processing method (i.e., spherical harmonics) (Bettadpur, 2012; Wahr et al., 1998), MasCon solutions can be applied at regional scale as they better distinguish land and ocean signals, thus reducing leakage errors (reducing leakage of signal from land to ocean) (Long et al., 2016). Also constraining MasCon solutions with geophysical data during processing makes it suitable for the non-geodetic community. MasCon solutions parameterize the gravity field with regional concentration functions and have been applied globally in numerous studies (Save et al., 2016; Scanlon et al., 2016; Watkins et al., 2015). CSR and JPL MasCon solutions vary in the scale of grid cells; CSR uses ~1° (or ~120 km at the equator) hexagonal tiles of geodesic equal area (Save et al., 2016), and JPL solves the gravity field at a 3° spherical cap (~330 km at the equator) (Watkins et al., 2015). Details about CSR and JPL MasCon data processing are provided by Save et al. (2016) and Watkins et al. (2015).

We used the GRACE/GRACE-FO data for the period April-2002 through September-2019 to estimate GWS changes. The GRACE/GRACE-FO data provide the total water storage (TWS) anomaly at monthly time steps. TWS includes storages in snow, surface reservoir, soil moisture, and groundwater. We subtracted all of the storage terms from the TWS measurement to estimate the GWS change time series (see SI, Text C1 for detail). Because the GWS change in the CV (Figure 4.1a) is higher than that in the surrounding region (Xiao et al., 2017), we used the original 3-degree mascon tiles following (Ojha et al., 2019) to conduct an analysis that takes into account the groundwater signal potentially distributed inside each mascon tile. Figure 4.1c shows the GRACE analysis region (hereafter, we refer to GWS change in the GRACE analysis region as the change in the CV for GRACE/GRACE-FO based calculations). The GRACE/GRACE-FO based GWS change (ΔGWS) is computed by subtracting the soil moisture storage anomaly (ΔSMA),

snow water equivalent anomaly ($\Delta SWEA$), and surface water storage anomaly ($\Delta SWSA$) from the terrestrial water storage anomaly ($\Delta TWSA$) obtained from JPL-m and CSR-m dataset:

$$\Delta GWS = \Delta TWSA - \Delta SMSA - \Delta SWEA - \Delta SWSA \qquad (5)$$

4.3.2.2 Water balance method

ΔGWS was estimated as a residual in the WB method. The WB components are precipitation, ET, storage changes (soil moisture, snow water equivalent, reservoir storage), streamflow into and out of the CV:

$$\Delta GWS = P + Q_{in} - Q_{out} - \Delta SMS - \Delta SWE - ET - \Delta SWS \qquad (6)$$

where P, Q_{in}, Q_{out}, and ET are precipitation, surface water inflow to the CV, delta outflow from the CV and ET. ΔGWS, ΔSMS, ΔSWE and ΔSWS are changes in GWS, soil moisture storage, snow water equivalent and surface water storage (reservoirs), respectively. Table 4.1 provides a summary of data type, sources, and references (detailed descriptions in SI, Text C1).

4.3.2.3 Model simulations (C2VSIM)

We used an integrated groundwater-surface water simulation model, known as California Central Valley Surface-Groundwater Simulation Model (C2VSIM), to estimate GWS change for 2002 through 2019. C2VSIM, developed by California Department of Water Resources (CDWR), simulates all important hydrologic processes including streamflow, surface runoff, root-zone and vadose zone processes and groundwater flow (Brush, 2013; Dogrul et al., 2015). Its core is a finite element solver of the groundwater flow equations for finite element grids. Several previous studies have used the model to simulate groundwater-surface water dynamics in the CV region (Alam et al., 2020; Brush, 2013; Ghasemizade et al., 2019; Kourakos et al., 2019; Miller et al., 2009). The model is available at https://data.cnra.ca.gov/dataset/c2vsimfg-version-1-0 (last accessed: March

2021). We used version 1.0 of the C2VSIM fine grid model (IWFM-2015 version), which is the most updated version of the model (hereafter, referred as C2VSIM) (CDWR, 2020; See SI ,Text C3 and S4 for more detail).

4.3.2.4 GWS change calculation using well-measurements

We calculated GWS changes for the entire CV using groundwater head time series obtained from wells. We assembled groundwater level data from CDWR for 2002 through 2019 (CASGEM, 2021). There are 43,987 wells in the CASGEM database with multiple purposes (irrigation, domestic, monitoring, and others), including 23,014 groundwater wells are located in CV (Figure 4.1c). However, well records are not continuous at most locations and records are missing in many months. In general, the highest number of records are available for March and October (see SI, Figure C2, S3 for well numbers).

We computed volumetric GWS changes as the product of groundwater level changes, CV area, and storage coefficient (i.e., volume of water released from aquifer per unit decrease in head). Both groundwater level changes and the storage coefficient are uncertain. Groundwater level measurements from observation wells are generally a preferred option for calculating GWS changes, however, observation wells in CV are sparse in places, the number of measurements is below 500 in most of the months, and measurements are discontinuous. In contrast, there are numerous head measurements from pumping wells (e.g., well used for irrigation, industrial, residential, and other sectors), but they are pumped, which is reflected in the associated groundwater levels. That said, drawdowns due to pumping are expected to be small in winter, offering the possibility of the selective use of pumped wells.

Another complication is that there is limited knowledge of the storage coefficient in CV that is required to compute GWS from head change. There are stacked unconfined and confined

aquifers within the CV. For unconfined aquifers the storage coefficient is the specific yield (Sy) - the volume of water released due to drainage from an unconfined aquifer per unit decline in groundwater level. In the CV, typical values range from 0.06-0.3 (Faunt et al., 2009). The storage coefficient in confined aquifers is typically 2 – 3 orders of magnitude less than that in unconfined aquifers (Faunt, 2009). In the unconfined aquifers, the groundwater surface (water table) is at atmospheric pressure and it declines as water drains through the porous media. In contrast, confined aquifers are bounded by an impermeable capping layer and groundwater is under pressures exceeding one atmosphere. Because the actual storage coefficient (both confined and unconfined) in the CV is unknown and there is limited knowledge of how much groundwater being extracted from unconfined versus confined aquifers, we used multiple storage coefficients and compare GWS estimation with other methods to obtain a sense of GWS trend and variability (more information in SI, Text C5).

We followed four steps to estimate GWS changes from well data: (1) spatial interpolation of groundwater levels using Inverse Distance Weighing (GWL, 10 km resolution) for each month from 2002 through 2019; (2) calculation of the month-to-month changes in GWL for each grid cell; (3) multiplication of GWL changes by storage coefficients and area to obtain volumetric GWS changes; (4) calculation the cumulative GWS changes. Similar to Scanlon et al. (2012), we added a 2% uncertainty to our estimates to account for errors associated with interpolation. To identify suitable sets of well data capable of representing CV GWS changes, we generated two monthly GWS time series using: (1) only observation wells, (2) all types of wells (observation and pumped)

4.3.3 Numerical experiment for estimating groundwater recovery under multiple climate and water management scenarios

We conducted numerical experiments to quantify the recovery time for drought-associated groundwater overdraft for multiple droughts, recovery percentage, water management, and climatic conditions. Among the four GWS change estimates discussed earlier, we used WB method for numerical experiment as it is computationally efficient for a very large numbers of iterations necessary for this study. In order to consider a range of post-drought climate scenarios, we performed sampling experiment from past climate data that could represent the following scenarios:

- Recent climatology (2003–2019): Sampling of WB components from this period represents recent-decade climatology that includes different types of years (e.g., droughts 2007–2009, 2012–2016; wet years: 2011, 2017 and others)
- Long-term climatology (1982–2019): Sampling of WB components from this period represents long-term climatology.
- No-drought climatology (2003–2006, 2010–2011, 2017, 2019): Sampling of WB components from this period represents optimistic scenario where droughts do not occur.
- Wet climatology (2005-2006, 2011, 2017, 2019): Sampling of monthly WB components from this period represents wet climatic condition where Standardized Precipitation Index exceeds 0.5. This scenario provides an upper bound for the GWS recovery.

In order to consider water management options, we considered the following scenarios:

- No cap on groundwater extraction, which is the current situation in the CV.
- Cap on groundwater extraction, which is likely the future scenario following the implementation of SGMA that regulates groundwater usage. We considered different caps on groundwater extraction: 30^{th}, 40^{th}, and 50^{th} percentile of groundwater depletion rate.

Our numerical experiment approach is detailed in Figure 4.2.

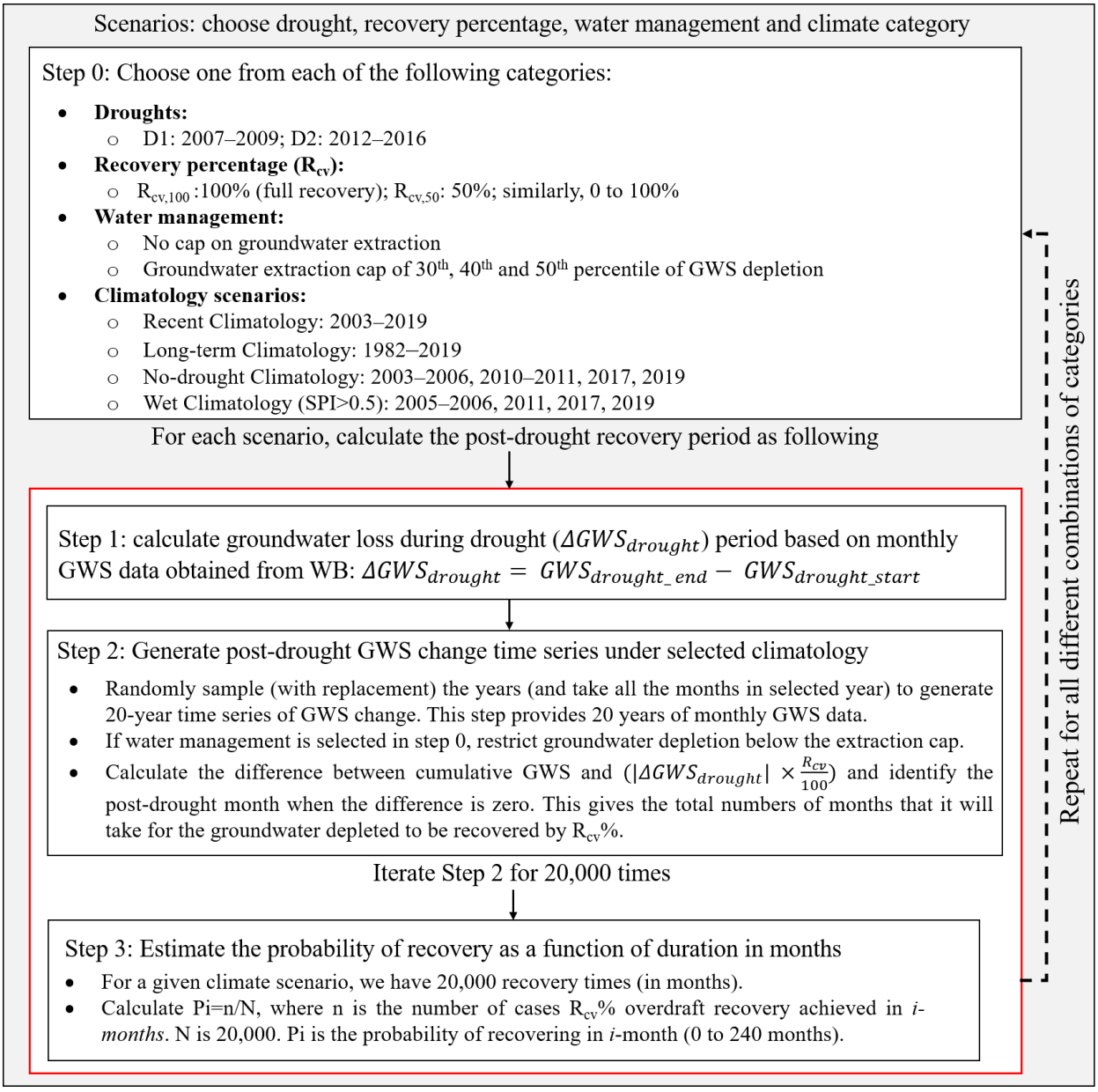

Figure 4.2. Steps of numerical experiments conducted to estimate post-drought groundwater storage recovery time for two droughts, recovery percentage, two water management options, and four climate scenarios.

4.3.4 Post-drought groundwater recovery under future climate change scenarios

We conducted synthetic experiments to assess the sensitivity of recovery times to water availability (i.e., inflow and precipitation over the CV) and evaporative demand and compare with projected changes under future change scenarios. The base scenario assumes that the inflow (and

precipitation) is similar to the monthly median of the years 1982 through 2019. We generated an array of GWS time series for different percentage changes in inflow (and precipitation) and ET, and calculated recovery times for all combinations. This analysis produced a matrix of recovery times that show its sensitivity to inflow and ET. Furthermore, we compare these with projected changes for 20 Global Climate Models and 2 RCP scenarios: modest global emission (RCP4.5) and high global emission (RCP8.5) (Stocker et al., 2014). Similar method for climate change impact assessment has been found effective in earlier studies (Brown et al., 2012; Poff et al., 2016).

4.4 Results and Discussion

4.4.1 GWS depletion and recovery assessment in the recent decades

4.4.1.1 GWS depletion and recovery estimates from different methods

GWS changes estimated by the four methods show similar depletion and recovery patterns during 2002-2019 (Figure 4.3a and Table 4.2). All methods indicate lower groundwater storage in 2019 compared to 2003, with relatively mild decline during the first drought (2007–2009) and severe decline during the second drought (2012–2016). However, there are important differences in the magnitude, depletion/recovery rates, and seasonal variations for the different methods. GRACE produce relatively higher seasonal GWS variations, whereas WB and C2VSIM produce much lower seasonal amplitudes. While the GWS from well data is computed for winter months only to reduce potential errors sourcing from pumping wells. GRACE shows relatively high groundwater storage at the end of the study period (2019). The WB and C2VSIM GWS time series are close to each other. C2VSIM GWS is intermediate between WB, GRACE and Well throughout the period. Compared to April-2003, the GWS in March-2019 changed by -19.1 km^3 (GRACE), -32.4 km^3 (WB), -34.1 km^3 (C2VSIM), and -27.1 km^3 (Well). All methods show close agreement in post-drought recovery period when the uncertainty in GWS estimates is 3.9 km^3 and 1.5 km^3

during 2010–2011 and 2017–2019, whereas the uncertainty in GWS change during drought periods are 2.7 km^3 and 3.9 km^3 for 2007–2009 and 2012–2016 droughts, respectively (Table 4.2). Uncertainties in GWS estimates can be attributed to the limitation of different GWS estimation methods to represent the groundwater dynamic associated with CV-wide groundwater extraction and land use activities. All methods show a depletion in GWS during the 2007–2009 and 2012–2016 droughts, and GWS recovery during post-drought years 2010–2011 and 2017–2019.

During the first drought (2007–2009) period, GWS changes from Jan-2007 to Dec-2009 were in the range -24 to -16.5 km^3, depending on the method used, with C2VSIM indicating the greatest depletion (-24 km^3), and the WB indicating the least depletion (-16.5 km^3) (Figure 4.3b). During the subsequent post-drought period (2010–2011), GWS increased in 2011 compared to 2010 ranged from 2.4 to 11.6 km^3, with C2VSIM indicating the highest recovery (11.6 km^3), followed by GRACE (9.2 km^3), with WB (3.2 km^3) and Well (2.4 km^3) showing lowest recovery. Comparison of the post-drought (2010–2011) and drought (2007–2009) periods GWS estimates from four methods (in the order Well, WB, CVISIM, and GRACE) showed on median 34% of the GWS depleted during the drought was recovered during the post-drought years (Figure 4.3c).

Table 4.2. GWS changes during drought and post-drought years. Drought periods are Jan-2007 to Dec-2009 and Jan-2012 to Dec-2016. Post-drought periods are Jan-2010 to Dec-2011 (or Pd1) and Jan-2017 to Feb-2019 (or Pd2). Percentage post-drought recoveries for Pd1 and Pd2 are shown in columns $R_{f,Pd1}$ and $R_{f,Pd2}$, respectively.

Methods	2007–2009 [km^3]	2010–2011 [km^3]	Recovery $R_{f,Pd1}$ [%]	2012–2016 [km^3]	2017–2019 [km^3]	Recovery $R_{f,Pd2}$ [%]
GRACE	-18.8	9.2	49.1	-27.5	4.0	14.5
WB	-16.5	3.2	19.3	-23.5	6.8	29.1
C2VSIM	-24.0	11.6	48.4	-33.6	3.5	10.3
Well	-19.5	2.4	12.2	-24.6	2.7	10.9
Median	-19.2	6.2	33.9	-26.1	3.8	12.7
Average	-19.7	6.6	32.3	-27.3	4.3	16.2
St. dev.	2.7	3.9	16.7	3.9	1.5	7.6

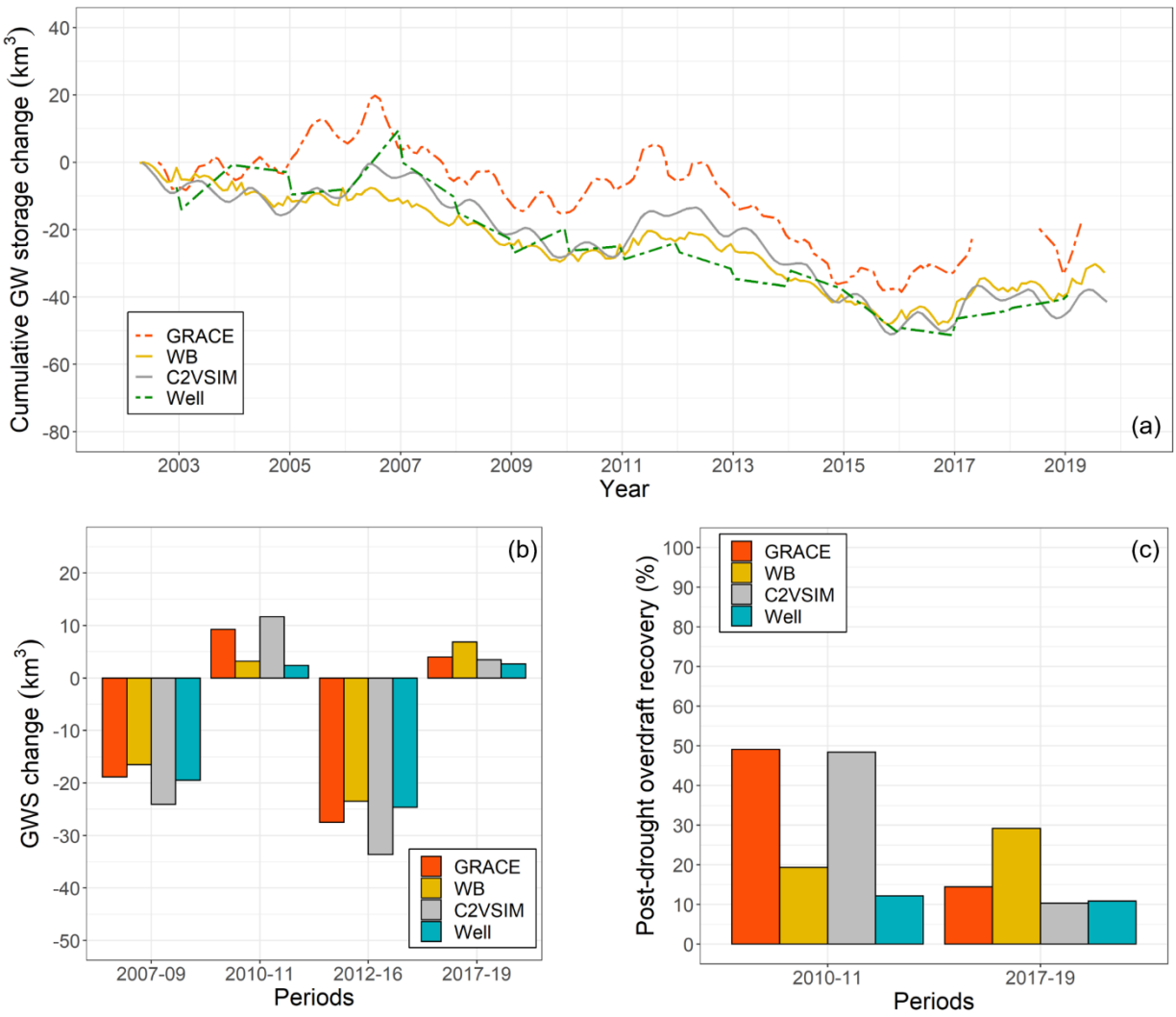

Figure 4.3. (a) Monthly GWS time series (median estimates) for the CV for April 2002 to September 2019 estimated using the four methods. GRACE GWS is 5-month moving averages to reduce seasonal variability. Well-based GWS is plotted only for winter months: December and January (5-month moving averages), (b) GWS change (km^3) estimates during drought and post-drought years. (c) Percent recovery of GWS from drought during post-drought years.

In the second and more-severe drought (2012–2016), the GWS changes from to Jan-2012 to Dec-2016 ranged from -23.5 to -33.6 km^3, with GRACE, WB and Well data showing relatively similar changes (-27.5, -23.5, and -24.6 km^3, respectively), while C2VSIM showed relatively higher depletion (-33.6 km^3) (Table 4.2). High GWS depletion in 2012–2016 is attributed to a longer dry period and greater drought-affected area that strongly increased groundwater dependence (Alam et al., 2019). During the subsequent post-drought years (2017–2019), the GWS

increase was low compared to the large overdraft created during the drought of 2012–2016 for all methods. GWS in Feb-2019 increases relative to Jan-2017 ranged from 2.7 to 6.8 km^3, with WB showing largest recovery (6.8 km^3), while GRACE, C2VSIM and Well data indicated similar and small recoveries (4, 3.5, and 2.7 km^3). Overall, the groundwater storage recoveries from the 2012–2016 drought were relatively small (on median 13%). As noted above, post-drought recoveries from the 2007–2009 drought were mostly higher than for the 2012–2016 drought, although all estimates in this case as well were less than 50% of the GWS loss during the prior drought period.

4.4.1.2 Uncertainties in GWS estimation methods

Despite the variations among the methods, we find the GWS recovery magnitude ranges 2.4–11.6 km^3 during 2010–2011 and 2.7–6.8 km^3 during 2017–2019 (Table 4.2), which is relatively small compared to drought period GWS changes of -16.5 km^3 to -24 km^3 and -23.5 km^3 and -33.6 km^3 during the 2007–2009 and 2012–2016 droughts. In terms of percentages, the post-drought GWS recovery ranges 12.2–49.1% during 2010–2011 and 10.3–29.1% during 2017–2019. In the previous section, we presented the median GWS changes from each method. Here, we discuss how the uncertainty in different methods affects the GWS estimates.

The GRACE-based GWS estimate in our analysis could be estimated from two different sources of GRACE datasets (JPL-m versus CSR-m). There are differences in GRACE-based GWS estimates between CSR-m and JPL-m. We find that the GWS estimate from JPL-m more closely matches GWS estimates from other methods (both depletion and recovery), whereas the CSR-m based estimate shows less groundwater depletion than other methods and very high groundwater recovery during 2010–2011 (69.4%). Differences between JPL-m and CSR-m increased after applying the scaling factor provided by JPL intended to reduce signal error (Wiese et al., 2016), whereas no scaling factor is available for CSR-m. Therefore, JPL-m based GWS estimate can be

used (after applying scaling factor) to reasonably to represent GWS depletion and recovery in the CV. However, we cannot conclusively state one GRACE MasCon product as the best one based on comparison over only the CV region, especially due to CV's small size, north–south orientation, and location near the coast. Although CSR-m shows relatively lower depletion, we follow a conservative approach and take the average of JPL-m and CSR-m to represent GRACE based GWS estimate. The difference in JPL-m and CSR-m estimates caused the GWS recovery percentage to vary from 38% to 69% during 2010–2011 and from 12% to 16% during 2017–2019.

The well-based GWS estimation is sensitive to the storage coefficient, interpolation method, and well selection criteria. The CV consists of both semi-confined and confined aquifers where knowledge of the storage coefficient is limited. The storage coefficient is the largest source of uncertainty when estimating GWS change from well data (Scanlon et al., 2012). We compared GWS estimates for three different storage coefficients and settled on an effective storage coefficient (Se = 0.06). The difference in the storage coefficients from multiple sources affect the magnitude of change, while keeping the percentage recovery same (as similar head change used with different storage coefficients). Regarding interpolation, although we used the IDW method, we also tested Kriging and found that the uncertainty associated with the interpolation method is much less than the uncertainty associated with the storage coefficient. We used all types of well data (pumped as well as observation) to generate well-based GWS time series, which means some measurements are affected by the cone of depression from pumping. However, groundwater pumping is typically less during the wet season (November through March) and hence well observations during this period should be much less affected by pumping. In our calculation of GWS changes during drought and post-drought years, we compared GWS values for months in the wet season only (i.e., December or January, in the interest of omitting "shoulder" months) after

taking a 5-month moving average (which captures GWS signal during the entire wet season). Therefore, well-based GWS changes estimated during and after drought years (Figure 4.3b) should be relatively unaffected by pumping. Furthermore, we computed GWS changes using observation wells, and found that the observation-well based GWS time series does not capture the seasonal pattern. This limited capacity of the observation well data is attributed to significantly lower numbers of measurements compared to the large area of the CV. Different approaches (interpolation methods, varying moving average time window) caused the GWS recovery percentage to vary from 0% to 44% during 2010–2011 and from 4% to 13% during 2017–2019.

The WB-based GWS estimation in CV depends on the storage (i.e., soil moisture, SWE, and reservoir) and flux terms (i.e., inflow, outflow, ET). Average changes in storage term during 2003–2019 is close to zero, and the magnitude of changes are relatively smaller than flux terms. Among the flux terms, we find the inflow to CV has greater uncertainty (standard deviation of 3 km^3/year) than precipitation (standard deviation of 1.42 km^3/year) over the CV. Relatively high uncertainty associated with inflow is intuitive as headwater inflow supply volume is higher than the net precipitation over CV, and multiple sources of inflow data. Since we are using measured outflow, the outflow term does not add uncertainty in our estimation. Difference in WB components caused GWS recovery percentage to vary from around 8% to 69% during 2010–2011 and from 13% to 81% during 2017–2019.

The C2VSIM GWS estimation is affected by uncertain inputs from multiple sources: model parameters (e.g., storage coefficient, hydraulic conductivity, irrigation efficiency), surface water deliveries at different locations, groundwater pumping rates (and location of pumps), and input flux variables (e.g., precipitation, inflow, ET) (CDWR, 2020). In this study, we only used C2VSIM simulations publicly available and have not assessed the uncertainty in overdraft recovery

introduced by model inputs and parameters. However, we estimated uncertainty from surface water delivery (relatively low to high surface water allocation) for the 2016-2019 period of C2VSIM simulation that we extended for this study, where we find the GWS recovery percentage during 2017–2019 vary between 2% to 30%.

4.4.2 GWS recovery assessment under varying climate and water management scenarios

4.4.2.1 Recovery time under different climatology

We calculated the probability of fully recovering from drought-related groundwater overdraft up to 20-years after drought termination (Figure 4.4a). The purpose of conducting such an experiment is to understand the response of the aquifer to different climatic conditions and get a sense of the feasibility of recovery from historical groundwater overdraft. The cumulative probability distribution (CDF) of full GWS recovery for the 2007–2009 and 2012–2016 droughts vary significantly for different climatic conditions (i.e., long term climatology, recent climatology, no-drought, and wet years) (Figure 4.4a). In general, the recovery time for the 2012–2016 drought is longer than that from the 2007–2009 drought, which is attributable to the greater groundwater overdraft during the 2012–2016 drought.

The cumulative distribution of post-drought recovery time shifts significantly from drier (recent climatology) to wetter (wet climatology) conditions, indicating high sensitivity of GWS change to the precipitation and inflow to the CV (Figure 4.4a). There is less than 10% chance to recover 2007–2009 overdraft in 5 post-drought years under recent climatology, while the chance is much lower for 2012–2016 overdraft (~3%) (Figure 4.4a). The precipitation and inflow under recent climatology scenario are around 359 ± 26 mm/year and 30 ± 4 km^3/year, respectively. The recent climatology scenario consists of drought events similar to the recent past (2003–2019), therefore drought recovery will be less likely occur as we have already found that the CV GWS

has been declining over recent decades (Figure 4.3a). A similar situation is the case for long-term climatology as the GWS has been declining over past decades due to frequent droughts and increased agricultural water use (Faunt et al., 2009). The recovery time curve for the long-term climatology scenario is close to the recent climatology with relatively longer recovery times (Figure 4.4a). In the long-term scenario, the existence of longer period droughts (e.g., 1986-1992) in addition to recent droughts results greater recovery times than for any other scenarios. There is only 15% (or less) chance to fully recover 2007–2009 drought overdrafts in 20 years (much less chance for 2012–2016 drought). In contrast, there is around 95% chance to recover 2007–2009 overdraft in 5-years under wet climatology, which is around 85% for 2012–2016 overdraft. The precipitation and inflow during the wet climatology are around 513 ± 6 mm/year and 52 ± 3.5 km^3/year, respectively. Under no-drought climatology, there is around 48% chance to recover 2007-2006 overdraft in 5-years (~20% for 2012–2016 overdraft). At a relatively higher probability level (i.e., 80%), it would require 13-18 years to recover from both droughts under the no-drought conditions. Here, the precipitation and inflow during no-drought climate are around 451 ± 17 mm/year and 40 ± 4 km^3/year, respectively. Comparing the recovery times between wet climatology and no-drought climatology, we find that the recovery time for the no-drought climatology is on average 2.3 and 3.5 times the recovery time for wet climatology at for 50% and 80% chances, respectively (Figure 4.4b-e).

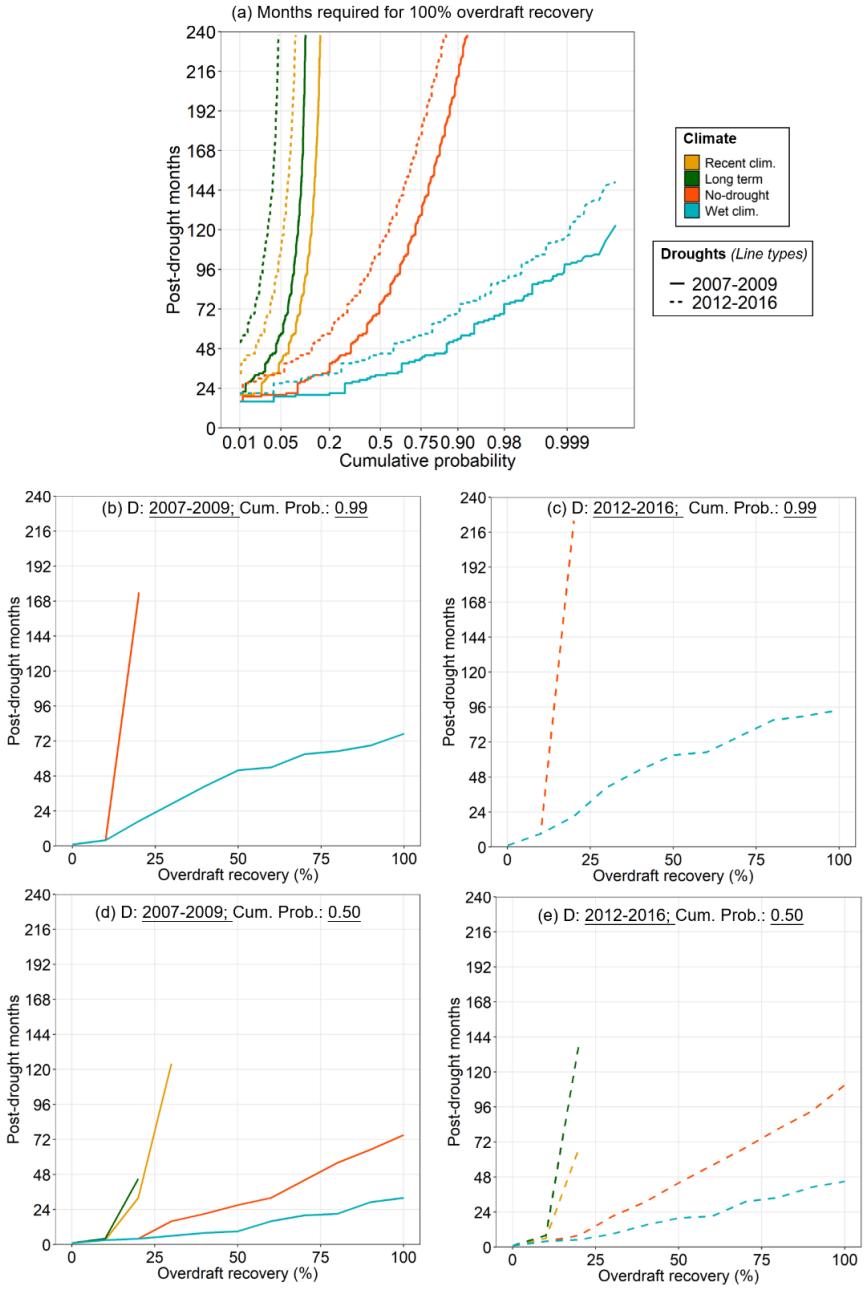

Figure 4.4. Cumulative probability distribution of months required for 100% recovery of 2007–2009 and 2012–2016 overdrafts. The horizontal axis is plotted on a normal probability scale. (b-e) Months required for varying percentages of overdraft recovery for two droughts (D: 2007–2009 and 2012–2016) and cumulative probabilities (Cum. Prob.: 0.99 and 0.5).

The post-drought recovery time increases almost linearly with recovery percentage (0-100%), where the slope increases with the cumulative probability considered (e.g., higher slope for a cumulative probability of 0.99 than 0.5) (Figure 4.4b-e). The relationship between recovery

time and recovery percentage indicates that it is difficult (if not impossible) to recover drought overdraft. Result shows that it would take 6-8 years to fully recovery overdraft under wet climatology, while it is less likely to have 6-8 consecutive wet years in reality. This indicates that the wet climate spells in California cannot fully recover drought caused overdraft under current water management conditions. From the above analysis, we infer that the CV aquifer is not resilient to droughts (less likely to fully recover) and will require appropriate management strategies to establish groundwater sustainability (as mandated by SGMA).

4.4.2.2 Recovery times for restricted groundwater use scenarios

We calculated overdraft recovery times for scenarios where a groundwater extraction cap is implemented. We analyzed three extraction cap scenarios equal to the 30^{th}, 40^{th} and 50^{th} percentiles of historic GWS depletion. For a given scenario (e.g., 30^{th} percentile restriction), ΔGWS below the threshold is restricted. To estimate the cap magnitude for a given percentile, we first identified negative GWS changes during 2003–2019. Then we estimated the 30^{th}, 40^{th}, and 50^{th} percentiles of these negative GWS changes. The resultant magnitudes are -1.44 km^3/month, -1.19 km^3/month and -1.02 km^3/month for 30^{th}, 40^{th} and 50^{th} percentile, respectively (below which groundwater depletion is restricted under selected scenarios). Figure 4.5 shows the cumulative probability distribution of groundwater recovery times for (a) 2007–2009 and (b) 2012–2016 droughts after applying extraction caps. The extraction caps strongly affect the recovery times under the no-drought, recent, and long-term climatology scenarios, whereas they make little difference in the wet climatology scenario. The volume of reduced groundwater extraction under no-drought, recent, and long-term climatology scenarios vary between 2.1-2.6 km^3, 1.5-2.1 km^3, and 1-1.5 km^3/year for 50^{th}, 40^{th}, and 30^{th} percentile groundwater extraction caps, the value of which are 1.9, 1.5, and 1 km^3/year respectively for wet climatology. The limited effects of the caps

under wet climatology are attributable to a much lower number of times when ΔGWS goes below the cap, hence the cap is rarely implemented. To demonstrate how effective the extraction cap would be, we extracted recovery times for cumulative probability levels 0.5 (moderate) and 0.8 (high chance) from Figure 4.5. For these probability levels the recovery times for recent and long-term climatology are beyond maximum time period of the analysis (240 months or 20 years; Figure 4.4), in other words, there is less than 50% chance to recover in less than 20 years under these scenarios. Therefore, we compared recovery times for no-drought and wet climatology scenarios.

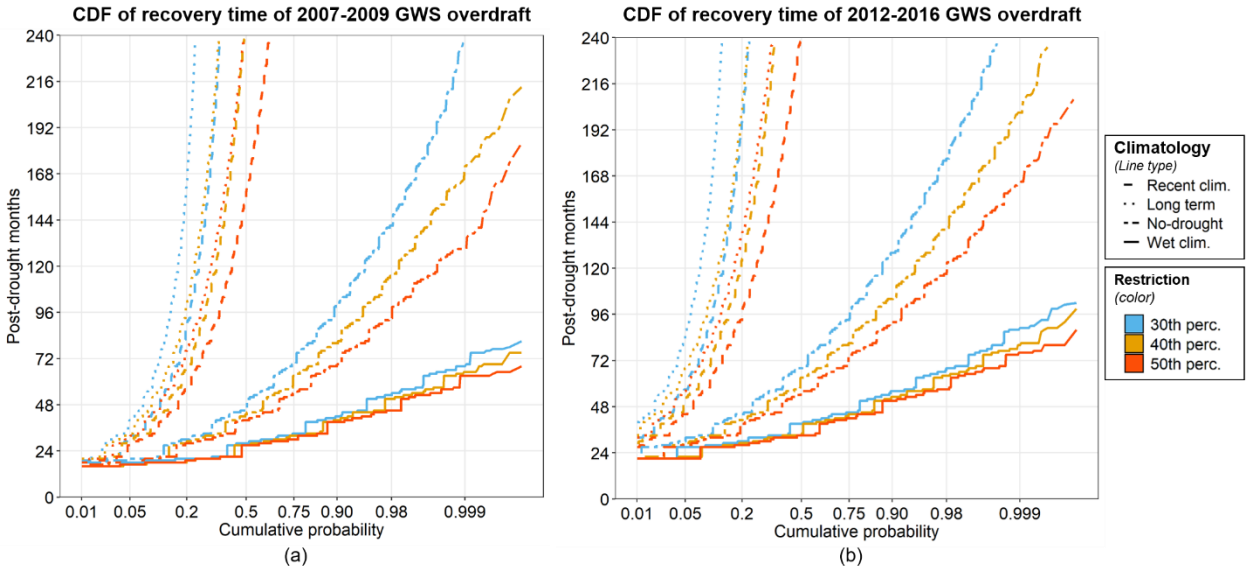

Figure 4.5. Cumulative distribution of recovery times for groundwater overdraft during (a) 2007–2009 and (b) 2012–2016 droughts. Recovery time is shown after implementation of 30th, 40th, and 50th percentile groundwater extraction caps.

The results show that the groundwater extraction caps significantly reduce the drought-linked GWS recovery time under the no-drought scenario. Groundwater recovery times for full recovery decreases by factors of 1.8 ± 0.1 (3.3± 0.8 years reduced) and 2.3 ± 0.3 (8.1± 1.4 years reduced) after applying an extraction cap for probability levels of 0.5 and 0.8, respectively. The recovery time for the 50th percentile restriction reduces recovery times by 0.4-1 year and 1.8-2.2 years more than for the 30th percentile under 0.5 and 0.8 probability levels, respectively. In

contrast, recovery times is reduced by factors of 1.2-1.3 under the wet climatology, which is relatively small as discussed above. Furthermore, recovery times were reduced significantly under recent and long-term climatology. For instance, at a probability level of 0.2 the recovery times (for full recovery) under recent and long-term climatology exceeded 20 years (Figure 4.4), whereas they were reduced to 5-10 years under the extraction cap (lower recovery time for 50% extraction cap), which is a reduction by a factor of 2-4 times or more. This is due to the greater number of occurrences when GWS depletion goes below the threshold (thereby, extraction cap being implemented). Although our results show that implementation of groundwater extraction caps can improve aquifer resilience to drought, we acknowledge that the impact can vary regionally (south versus north CV), and the actual recovery times can vary. In particular, the southern CV has greater groundwater overdraft and groundwater dependence than the north. Therefore, the impact of extraction caps on the southern CV is expected to be higher. Moreover, reduction of groundwater extraction implies that there will be less water for irrigation, suggesting a decline in crop production.

4.4.3 Evaluate the impact of climate change on post-drought recovery time

We evaluated the relative influence of ET and inflow changes on groundwater overdraft recovery time and predicted how the recovery time is expected to change under future climate change. Figure 4.6 shows the changes in recovery times for different ET and inflow changes. Under historical average condition (average of 1982–2019), 2012–2016 groundwater overdraft was impossible to fully recover as evident from the location of black dot in the unsustainable zone (Figure 4.6a). However, a marginal increase in average inflow can have a major impact on recovery time when moving from the no-recovery zone to the recovery zone (recovery zone is shown by color shades in Figure 4.6a). For instance, a 10% increase in average inflow (assuming ET remains

the same) will have a recovery time of ~30 years, whereas a 20% increase will have a recovery time of ~9 years (~5 years for 30% increase). However, reducing the recovery time to 1-2 years requires a much greater increase in average inflow. Increases in inflow of around 43% and 60% (compared to the average condition and assuming no ET change) are required for recovery times of 1 and 2 years, respectively. In the past two decades, inflows for almost all years (except years 2010, 2011, 2017, and 2019) were less than the long-term average. While past inflow variability was high (coefficient of variation of annual inflow = 0.32), ET variations were much less (coefficient of variation of annual ET = 0.05).

The projected changes in the recovery time map move further from the average condition into the no-recovery zone, where the negative impact is higher for RCP8.5 (Figure 4.6c) compared with RCP4.5 (Figure 4.6b). Overall, it is evident that historical conditions led to chronic groundwater depletion where drought recovery will be difficult to achieve, whereas future climate will exacerbate the problem manyfold. Therefore, in addition to reducing groundwater use (as shown in section 3.4.2), increasing recharge of excess water can potentially have important impacts under future climate. Because future climate will change the seasonality of surface water inflow to the CV (increased winter flow and decreased summer flow) (Gergel et al., 2017; Li et al., 2017), more water is expected to leave the CV region during the winter season without being used or stored for later use. Earlier studies show that strategies, such as managed aquifer recharge, can recharge excess surface water (Alam et al., 2021; Gailey et al., 2019; Scanlon et al., 2016; Wendt et al., 2021) and can potentially act as an important adaptation strategy to climate change. The method developed in this study to generate recovery time sensitivity map (Figure 4.6) can be a useful tool for water managers and planners to estimate post-drought duration required for

overdraft recovery. This drought recovery time map is unique from any previous study and can be used to identify potential strategies to minimize the groundwater overdraft recovery times.

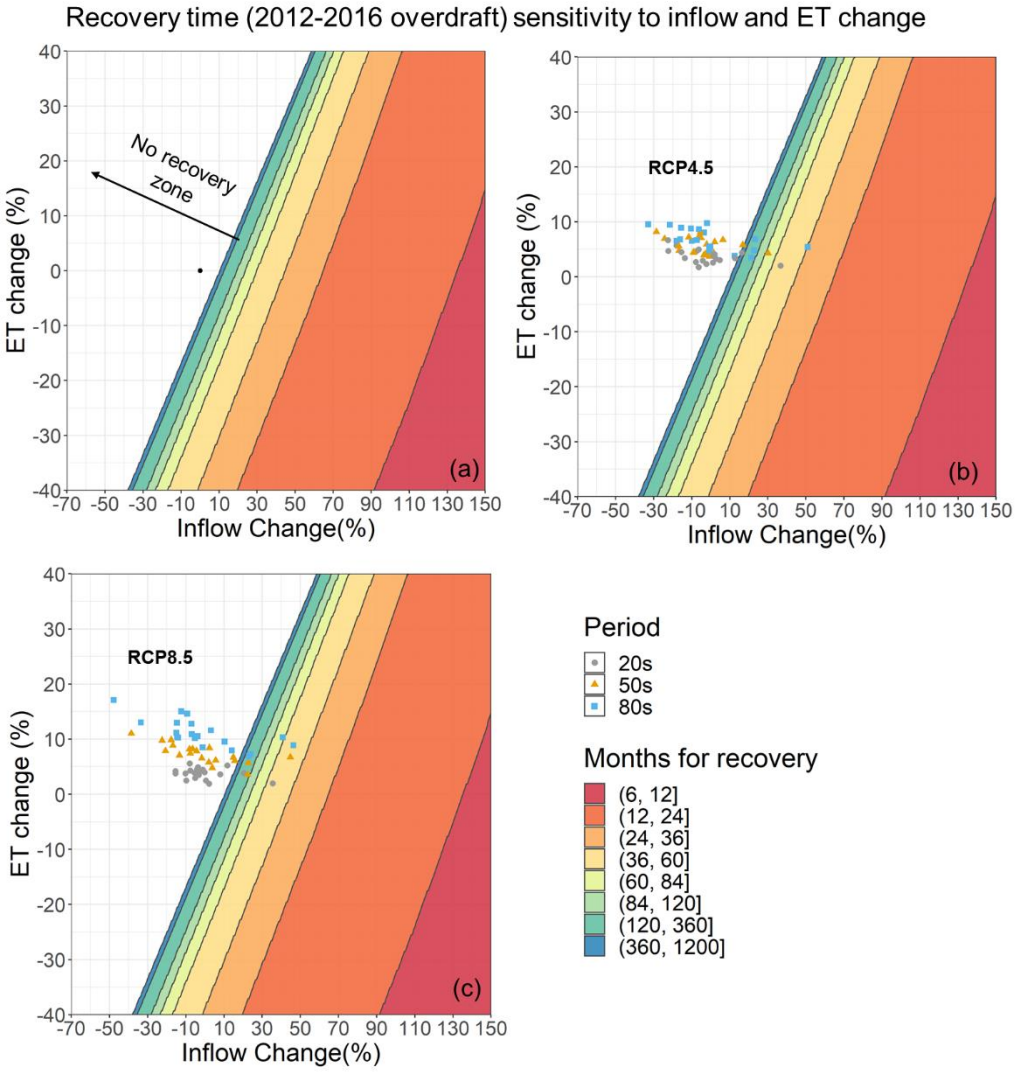

Figure 4.6. Sensitivity of GWS overdraft (from 2012–2016 drought) recovery time to changes in inflow and ET (a-c). The colors show recovery time bands for different ranges of months. (a) The black dot represents the average historic condition (1982–2019). Projected changes in inflow and ET are shown for (b) RCP4.5 and (c) RCP8.5 scenarios over the sensitivity map (projected changes were obtained from Alam et al. (2019)). The color of the dots (b-c) represents projected changes for three periods 2020s (2010-2039), 2050s (2040-2069), and 2080s (2070-2099).

4.5 Summary and conclusions

Groundwater is a critical source of the CV's water supply; however, the resource has been used unsustainably in the past, particularly during droughts, leading to progressive groundwater depletion. Quantifying drought-related groundwater depletion and post-drought recovery and understanding the role of climate and water management in recovering from overdraft is key to establishing a more sustainable management program. We have addressed these issues by quantifying drought-associated groundwater depletion and recovery for two recent droughts (2007–2009 and 2012–2016) using four methods, (GRACE satellite data, water balance approach, the C2VSIM model, and well-measurements). The study reveals the value of considering multiple methods for GWS estimation. Additionally, we used numerical experiments to estimate the probability of post-drought recovery times under different climatic conditions. Based on our analysis, we conclude that:

- Groundwater storage in the CV declined by a median of 19 km^3 (17-24 km^3) and 26 km^3 (24-35 km^3) during the 2007–2009 and 2012–2016 droughts, respectively based on the four methods. The median drought-related overdraft recovery was 34% and 13% during the post-drought years 2010–2011 and 2017–2019, respectively. The relatively low recovery from the 2012–2016 overdraft is attributable to the very large overdraft compared to limited surface water availability during post-drought years. In general, estimates of GWS changes using different methods show similar patterns, but different magnitude. Because there is variability in GWS estimates from different methods that is expected to vary between regions, no one method can be identified as the best. Instead, the multi-method ensemble provides a better overall picture of GWS depletion and post-drought recovery.

- Surface water availability (surface inflows to the CV and precipitation) greatly influence the recovery of drought-associated groundwater overdraft. Recovery from drought-related overdrafts is unlikely if the recent climatology (2003–2019) continues after the drought ends (less than 20% chance to fully recover in 20 years). This is because drought-related overdraft in the CV continues and accelerates long-term GWS depletion. Relative to replicated historical climatology, projected drought recovery times decrease by a factor of up to 3.6 for futures with no drought years and by a factor of 7.8 for futures with wet years only. The practical implication is that under current management policies, the CV aquifers are not resilient to drought events — appropriate management measures are needed to establish sustainability.
- A cap on groundwater depletion would accelerate groundwater recovery considerably, especially if post-drought conditions are relatively dry. This is because groundwater extraction volume is larger during dry years and tends to exceed any extraction cap more often than for the case of wet climatology when the cap is rarely implemented. Overdraft recovery times decreases by ~2x with implementation of pumping restrictions to constrain groundwater depletion relative to no restrictions under no-drought climatology, with ~2-4x or more if climatology remains at the historical levels. This indicates the important role of reducing groundwater extraction to accelerate overdraft recovery and establish groundwater sustainability.

The CV aquifer is currently managed unsustainably, hence full post-drought recovery is difficult (if not impossible) under the historical average (2003–2019) headwater inflows and crop water use conditions. A marginal increase in average inflow can have a substantial impact on drought recovery time. An increase in headwater inflow from 10% to 20% (of historic average)

would reduce the drought recovery time from 30 years to 9 years. In addition, climate change will make it more challenging to recover from drought-related overdrafts.

Acknowledgements

We thank Hyongki Lee at University of Houston for helpful discussions and advice regarding GRACE MasCon solutions. The University of California Research Initiatives Award LFR-18-548316 supported this work. GRACE CSR RL06 MasCon solutions were obtained from http://www2.csr.utexas.edu/grace and JPL MasCon solutions were obtained from https://podaac-tools.jpl.nasa.gov. The VIC-4.1.2.g code is available at https://doi.org/10.5281/zenodo.4695040. The VIC model parameter and forcing can be obtained from ftp://livnehpublicstorage.colorado.edu/public/ and ftp://livnehpublicstorage.colorado.edu/public/Livneh.2015.NAmer.Dataset/nldas.vic.params/ respectively. Data used in this study are archived at https://doi.org/10.6084/m9.figshare.14544381.v1.

CHAPTER 5

Conclusions and Future Work

The main objective of this dissertation was to improve the understanding of the climatic and anothropogenic drivers of groundwater depletion and recovery in California's Central Valley. In this regard, the dissertation has three original contributions: (1) the prediction of future groundwater storage changes in Central Valley under multiple climate change scenarios and an improved understanding of relative contribution of surface water supply and crop water use on groundwater storage changes, (2) the assessment of how regionwide managed aquifer recharge implementation to mitigate Central Valley's groundwater overdraft and management measures to increase the overdraft recovery, and (3) an improved understanding of groundwater overdraft recovery during post-drought years and the role of precipitation and water management groundwater overdraft recovery during post-drought years. In this section, a summary of the conclusions drawn from the research described in Chapter 2 through Chapter 4 is presented. Finally, possible future research is presented.

5.1 Conclusions and original contributions

Chapter 2 addressed a fundamental question: how does climate change impact groundwater storage in the semi-arid Central Valley of California? A suite of unidirectionally connected physically based models were applied to predict future groundwater storage changes under moderate and extreme climate change scenarios. Results show that climate change will cause additional groundwater depletion in Central Valley. Numerical experiments were conducted to evaluate the relative contribution of headwater watershed flow and crop water use on groundwater storage changes. To my knowledge, this is probably the first study that reveals the impacts of

future crop water use, surface water volume and seasonality change on the groundwater system in the Central Valley.

In Chapter 3, the impact of large scale implementation of managed aquifer recharge (MAR) on groundwater storage has been assessed. Many arid and semi-arid aquifers globally have experienced chronic groundwater depletion over the past many years due to a large increase in demand compared to limited surface water supply. Managed aquifer recharge has been proposed to halt groundwater depletion in many regions, however, the effectiveness of MAR to solve regional groundwater depletion problem was unknown. This is the first study that investigates the impact of large scale MAR impletation on groundwater overdraft recovery, flood peak, low flow, and water logging through numerical experiments. Results show that MAR has limited capacity to recovery historical groundwater overdraft in Central Valley due to the lack of surface water availability in the south. Delivering excess surface water from the delta to the Tulare and San Joaquin region can significantly solve the groundwater overdraft problem. Moreover, research shows MAR can reduce flood peaks, and increase summer flow.

Chapter 4 addressed the fundamental question: How much has drought-caused groundwater overdraft in Central Valley recovered during post-drought years and how do climate and water management affect the rate of overdraft recovery? An ensemble of groundwater storage change estimates has been made using multiple methods and numerical experiments conducted to understand the role of climate versus water management. Result reveals that the Central Valley aquifer is not resilient to drought under existing condition and it is very challenging to recover drought-caused groundwater overdraft. However, water management measures that restrict groundwater extraction can significantly reduce the recovery time.

5.2 Future work

Groundwater storage loss pose serious threat to sustainable future development. Although the dissertation addresses important problems, several important issues require further investigation in the future. Potential future works are discussed below that are related to the research carried out in this dissertation:

Climate change impact on groundwater storage was investigated (Chapter 2), but the relative impact on confined and unconfined aquifers is not well known. Future work involves improving the understanding of the influence of seasonal and annual climate variability on groundwater in confined and unconfined aquifers. Although the effectiveness of managed aquifer recharge to mitigate groundwater overdraft has been investigated (Chapter 3), the efficacy of large-scale managed aquifer projects on water quality needs to be evaluated. In particular, a study needs to be done to assess the impact of different land use (e.g., agricultural land use; also known as Ag-MAR). To halt groundwater depletion, a comprehensive strategy is required that combines more than one water management technique, such as, managed aquifer recharge, land-use change, policy restriction on groundwater extraction. Future work involves developing a framework that combines hydrologic models with an optimization model to identify the optimum combination of management strategies that can halt ongoing groundwater depletion. Recovery of drought-linked groundwater overdraft was investigated in the Central Valley region (Chapter 4). The groundwater recovery process depends on multiple factors like climate type, land use, aquifer, and soil properties that vary between aquifers globally. The future study involves the investigation of drought recovery in confined versus unconfined aquifers in regions with varying climatology, hydrogeologic properties, land use, and other physical properties. Moreover, it is critically important to know how the changes in recovery time under future climate would affect the number

of dry wells. Since the increase in dry wells is a threat to water and health security, future research should identify locations that are susceptible to an increase in groundwater recovery time and identify potential management strategies to increase the resilience of such aquifers.

Appendix A

This appendix provides supporting information for Chapter 2. This chapter has been published in the Climatic Change. © Springer Nature. Used with permission.

Alam, S., Gebremichael, M., Li, R. et al. Climate change impacts on groundwater storage in the Central Valley, California. Climatic Change 157, 387–406 (2019). https://doi.org/10.1007/s10584-019-02585-5 – Supporting Information.

Text A1: Comparison between VIC simulated runoff and unimpaired flow

We compare VIC simulated runoff with California Department of Water Resources (CDWR) unimpaired flows (UF) for 13 major watersheds, where VIC shows good agreement with UF. Fig S1 shows comparisons for three of the 13 watersheds; the Kling-Gupta Efficiency (KGE) and correlation coefficients (R^2) for all 13 watersheds are included in Table S1.

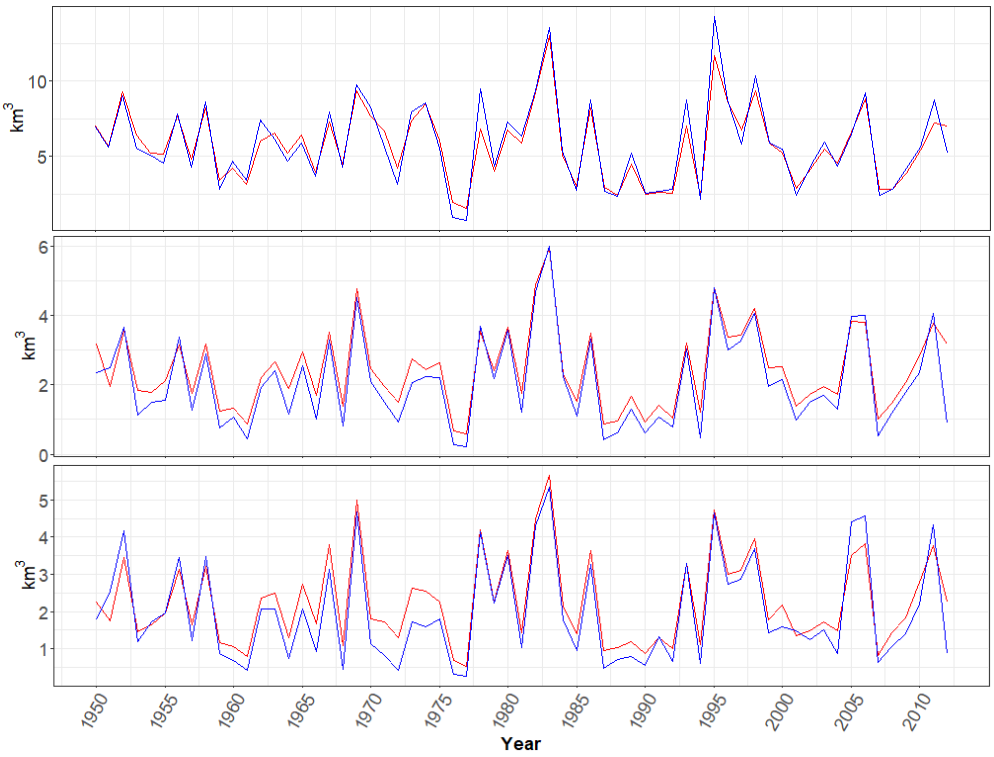

Figure A1. Annual time series of VIC runoff (blue) and UF (red) at (a) Feather River near Oroville, (b) Tuolumne River near Don Pedro and (c) San Joaquin River near Millerton. Plot of three rivers shown here, others are also in good agreement as shown in Table S1.

Table A1. Comparison between annual unimpaired (UF) and VIC runoff for selected locations in the headwater watershed

River (location)	R^2	KGE	River (location)	R^2	KGE
American (Fair Oaks)	0.93	0.93	Mokelumne (Pardee reservoir)	0.88	0.79
Calaveras (Jenny lind)	0.93	0.82	Sacramento (Shasta)	0.94	0.58
Chowchilla (Buchanan reservoir)	0.87	0.78	San Joaquin (Millerton reservoir)	0.91	0.80
Cosumnes (Michiganbar)	0.93	0.66	Stanislaus (Melons reservoir)	0.90	0.77
Feather (Oroville)	0.94	0.83	Tolumne (Don pedro)	0.93	0.81
Fresno (Daulton)	0.87	0.73	Yuba (Smartville)	0.93	0.96
Merced (Exchequer reservoir)	0.92	0.75			

Text A2. CVmod performance evaluation

We compared observed vs simulated reservoir releases for 16 major reservoirs simulated by CVmod, this includes reservoirs form the previous version of the model (Van Rheenen et al. 2004) and four new reservoirs in Tulare . Observed reservoir releases are from California Data Exchange Center (CDEC, http://cdec.water.ca.gov). We obtained reservoir releases that were not available from CDEC from the CALSIM model (see https://water.ca.gov). We performed calibrations using STELLA (CVmod is developed in STELLA), where the objective was to minimize the squared difference between simulated and observed reservoir storage. Table S2 summarizes the performance statistics of simulated releases from the major reservoirs (Fig S2 shows scatterplots of simulated vs observed releases). We calculated Kling-Gupta Efficiency (KGE) and correlation coefficients (R^2), which shows that observed and modelled releases generally are in good agreement.

Table A2. Comparison of simulated (CVmod) and observed reservoir releases for the major headwater reservoirs.

Reservoirs	River	Calibration		Validation	
		R^2	KGE	R^2	KGE
Shasta	Sacramento	0.80	0.82	0.80	0.78
Folsom	American	0.63	0.75	0.88	0.89
Oroville	Feather	0.67	0.77	0.65	0.53
Pardee/Camanche	Mokelumne	0.82	0.75	0.45	0.55
New Hogan	Calaveras	0.70	0.81	0.58	0.76
New Melons	Stanislaus	0.49	0.68	0.37	0.44
New Don Pedro/Lake McClure	Tuolumne/Merced	0.84	0.90	0.88	0.93
Milerton/Eastman/Hensley	San Joaquin/ Chowchilla/Fresno	0.79	0.78	0.79	0.77
Pine Flat	Kings	0.83	0.58	0.80	0.53
Isabella	Kern	0.86	0.76	0.84	0.83
Success	Tule	0.76	0.64	0.70	0.68
Terminus	Kaweah	0.80	0.71	0.71	0.76

Note: Calibration and validation periods are 10/1979 to 10/1994 and 11/1994 to 12/2017 respectively (except New Hogan and New Melons whose validation period is 11/1994 to 09/2009, and Pine Flat, Isabella, Success, and Terminus calibration periods are 10/1994-10/2009 and validation 11/2009-12/2017).

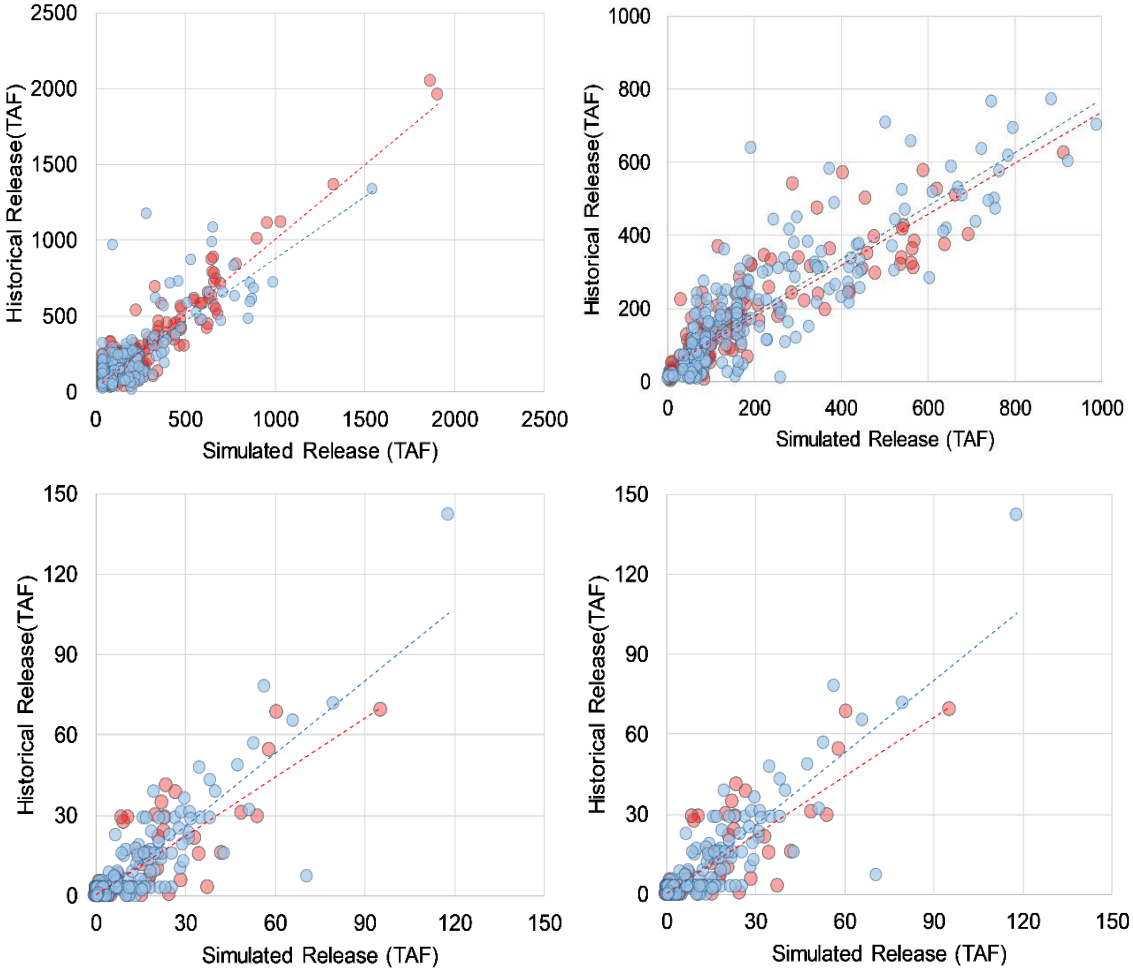

Figure A2. Simulated vs observed reservoir releases at (a) Folsom, (b) Milerton/Eastman /Hensley, (c) Success, and (d) Isabella Reservoirs. Blue circles are for calibration period and red circles are for validation period.

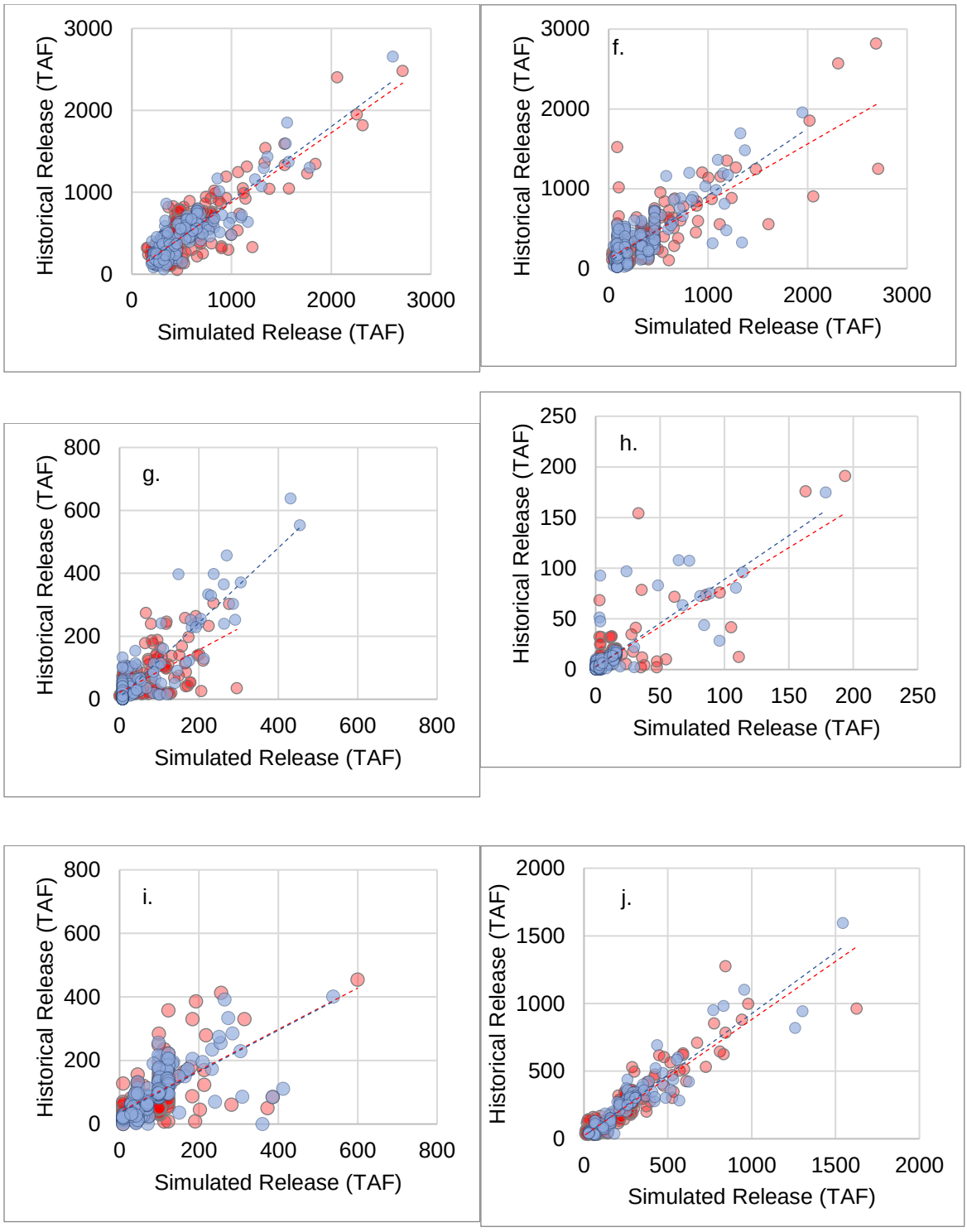

Figure A2. Continued. (e) Shasta, (f) Oroville, (g) Pardee-Camanche, (h) New Hogan, (i) New Melons, (j) New Don Pedro. Blue circles are for calibration period and red circles are for validation period.

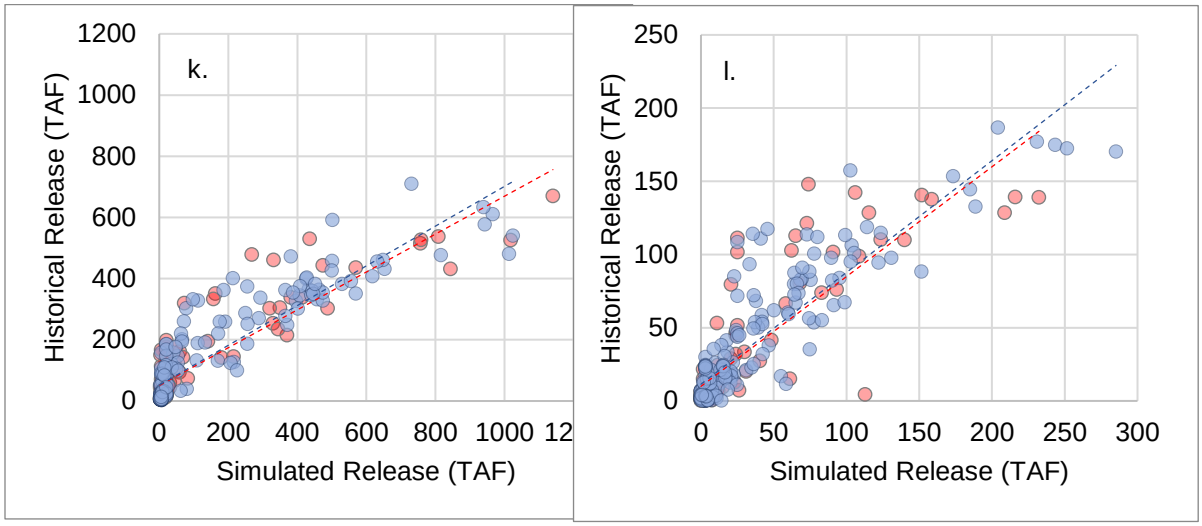

Figure A2. Continued. (k) Pine Flat, (l) Terminus. Blue circles are for calibration period and red circles are for validation period.

Text A3. Background of LP model

The objective of the linear programming (LP) model is to maximize the surface water diversion subject to constraints of mass balance, maximum diversion and minimum instream flow. As described in the main text, C2VSIM uses the diversion input to meet agricultural/municipal requirement, the part of total demand that is unmet by surface water is pumped from GW. So, maximizing the surface water diversion will ensure minimum GW pumping. The surface water network and distribution locations are same as the C2VSIM model (detail description of all the diversion network is available at Brush and Dogrul (2013).

$$\text{Maximize } Z = \sum_{i}^{i=n} \sum_{j}^{12} D_{i,j}$$

Subject to,

Mass balance, $\sum_{k}^{k=m}\sum_{j}^{12} I_{i,j} - \sum_{i}^{i=n}\sum_{j}^{12} D_{i,j} = \sum_{k}^{k=m}\sum_{j}^{12} O_{i,j}$

Max diversion constraint, $D_{i,j} \leq D\_max_{i,j}$

Nonnegativity constraint, $D_{i,j} \geq 0$; $O_{i,j} \geq 0$

Where,

D= diversion, D_max= maximum allowed diversion,

i= diversion nodes = 1,2,3…n, j= months=1,..,12, k= reach number=1,2,…m

We determined the maximum diversion constraint for each node based on historical values between 2001-2009 (assuming the water management practice during this period will be same in future). The LP model is written in python language using PuLP package, where PuLP is a linear programming module for python (Mitchell et al. 2011). We compared the surface water diversion estimated by the LP model between 2001-2009, which shows simulated diversion is in good agreement with historical diversion used in C2VSIM; around 90% and 66% of the locations have greater than 0.5 correlation and KGE respectively.

Text A4. Background on climate model selection

Rupp et al. (2013) ranked GCMs that performed best over an historical period (1950-99) in reproduction of key aspects of the climate of the Pacific Northwest. A similar analysis was performed by CDWR (2015) for the U.S. Southwest from which 10 GCMs were selected as most suitable for water resources studies in California (the Southwest work used essentially the same methods as Rupp et al., 2013). We compared the empirical cumulative distribution function (ECDF) of mean annual runoff (VIC-simulated annual total runoff averaged over 2006-2099 for

RCP 8.5 for the Sacramento, San Joaquin, and Kings Rivers) for 32 GCMs archived in cal-adapt (http://cal-adapt.org/) and 10 GCMs from CDWR (2015) (Fig S3). We found that the full range of variability over all 32 GCMs is not well captured by the 10 "best" models according to the CDWR (2015) criteria, so we instead selected 20 GCMs that simulated future climate flows for the above river basins and best captured the full range of variability as indicated by the ECDFs (the 10 "best" models based on the CDWR (2015) criteria were among the 20 selected models). The selected models are listed in Table S3; their ECDFs are shown in Fig S3.

Table A3. Selected 20 GCMs for this study (see Rupp et al. (2013) for more information)

1.	ACCESS1-0	6.	CESM1-BGC	11.	GFDL-ESM2G	16.	MIROC-ESM
2.	ACCESS1-3	7.	CMCC-CMS	12.	GISS-E2-R	17.	MIROC5
3.	bcc-csm1-1-m	8.	CNRM-CM5	13.	HadGEM2-AO	18.	MPI-ESM-LR
4.	CanESM2	9.	EC-EARTH	14.	HadGEM2-CC	19.	MRI-CGCM3
5.	CCSM4	10.	GFDL-CM3	15.	HadGEM2-ES	20.	NorESM1-M

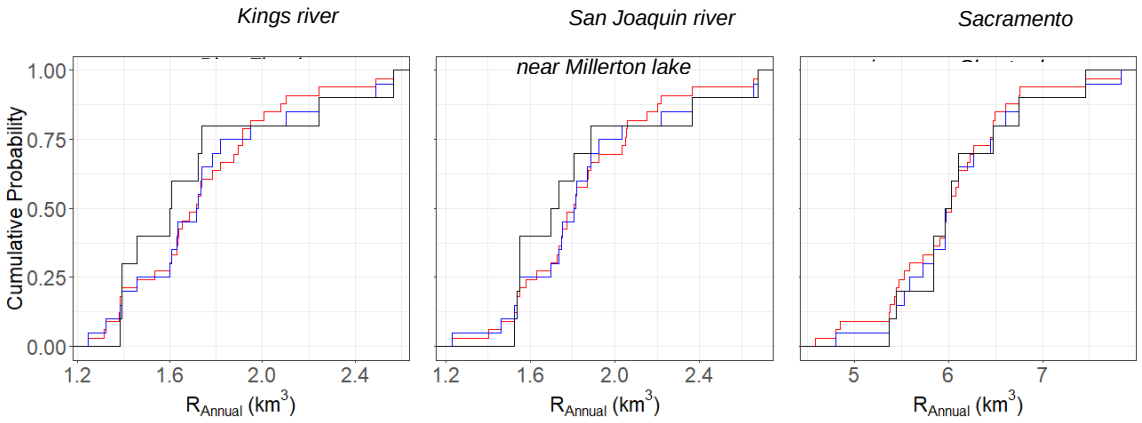

Figyre. A3. Cumulative distribution functions of projected mean annual runoff (RCP 8.5) between (a) all 32 GCMs (red line) (b) 10 GCMs recommended using the CDWR (2015) criteria (black line) (b) 20 GCMs used in this study (blue line)

Table A4. Multimodel median changes and ensemble standard deviation of precipitation, runoff and ETo changes over CV for future periods (all units are % of historic values).

Region		RCP 4.5			RCP 8.5		
		ΔP	ΔETo	ΔI	ΔP	ΔETo	ΔI
Central Valley	BOC	-3.65(8.7)	3.59(1.3)	-2.40(13)	-3.87(6.5)	3.85(1)	-4.11(10)
	MOC	-2.98(8)	5.86(1.5)	-4.20(12)	-1.94(11.3)	7.24(1.8)	-4.37(19)
	EOC	-2.22(9)	6.6(2)	-3.59(16)	-4.4(15.2)	10.45(2.6)	-8.19(23)
Sacramento	BOC	-2.76(7.9)	4.19(1.3)	-2.33(11)	-2.59(6.3)	4.22(1.1)	-2.65(9)
	MOC	-0.73(7.9)	6.29(1.5)	-2.76(11)	-1.37(10.7)	7.71(1.6)	-3.92(17)
	EOC	-0.15(9)	7.33(1.9)	-3.35(15)	-1.57(13.9)	11.03(2.4)	-4.78(19)
San Joaquin	BOC	-2.87(10.3)	3.88(1.4)	-3.08(15)	-4.04(7.1)	4.22(1.1)	-7.43(12)
	MOC	-2.62(9)	6.42(1.7)	-6.38(13)	-1.76(12.4)	7.66(2.2)	-4.85(21)
	EOC	-3.59(10)	7.05(2.3)	-6.23(18)	-5.39(17.2)	11.52(3.3)	-11.83(27)
Tulare	BOC	-5.98(10)	3.31(1.2)	-3.40(19)	-7.01(6.9)	3.72(1)	-4.11(10)
	MOC	-6.27(9.1)	5.23(1.4)	-6.29(16)	-6.04(12.6)	6.73(1.8)	-4.37 (19)
	EOC	-7.67(9.1)	5.76(1.9)	-8.46(20)	-10.46(16.9)	9.93(2.6)	-8.19(23)

Note: P denotes precipitation, I is headwater inflow, ETo is reference evapotranspiration. All values are percentage changes. Values in the parenthesis are standard deviation of multi-model estimation.

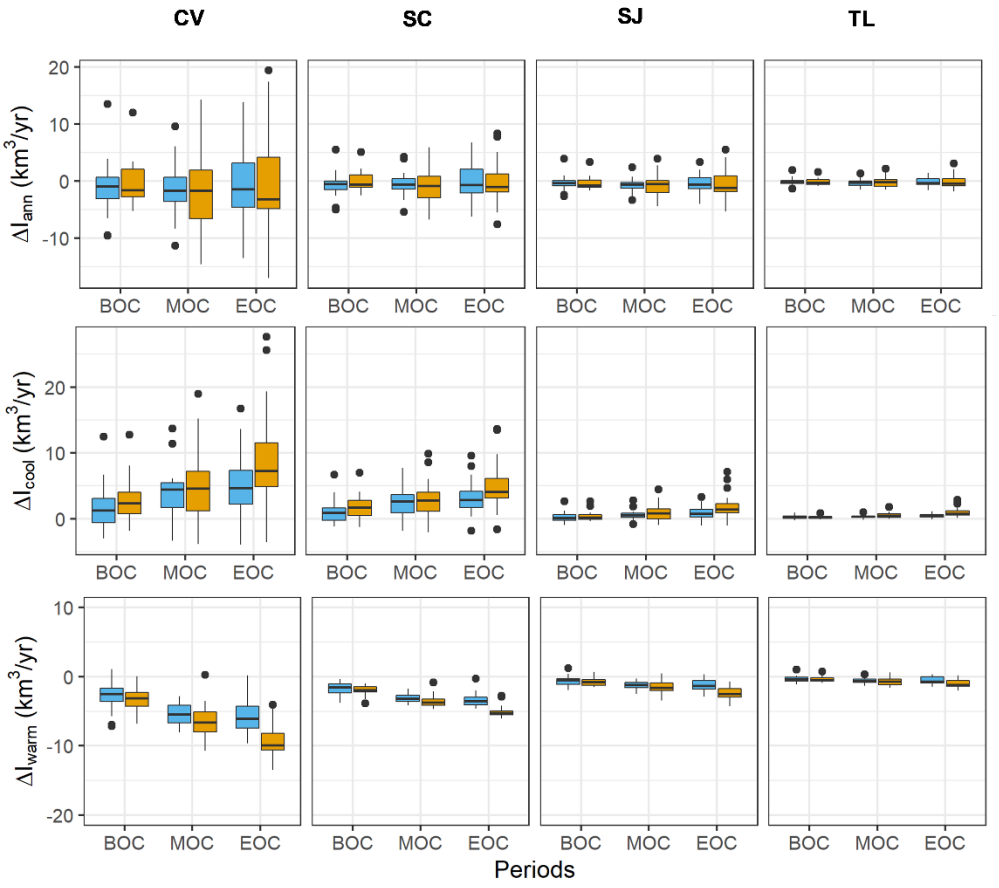

Figure A4. Changes in annual, cool season and warm season inflows during three future periods. Box represent first and third quartile, horizontal line in the box is median and whiskers represent min (max) value or 1.5 times interquartile range from first (third) quartile, whichever is bigger (smaller).

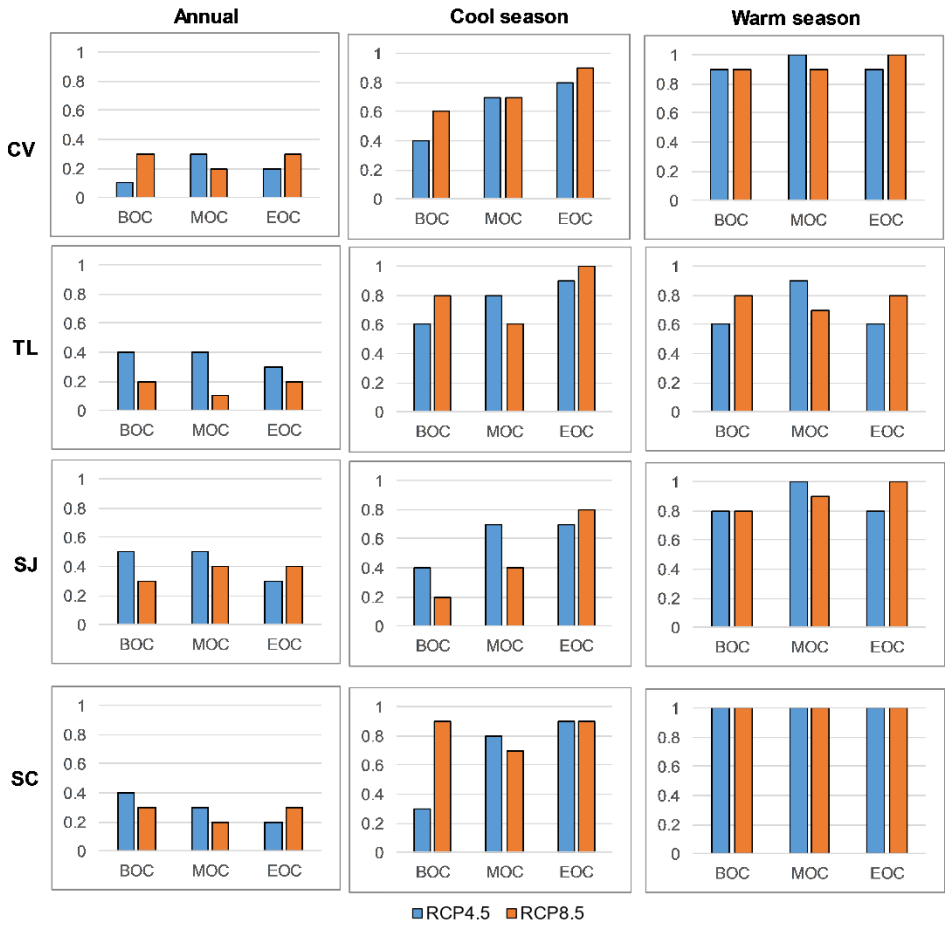

Figure A5. Comparing uncertainty in change direction (sign) for annual and seasonal inflows. The values represent number of concordant minus discordant pairs, divided by the numbers of pairs. For annual and warm season inflow it is concordant if a model estimates future decrease (vice versa in case of discordant). For cool season, it is concordant if a model estimates increase (vice versa in case of discordant).

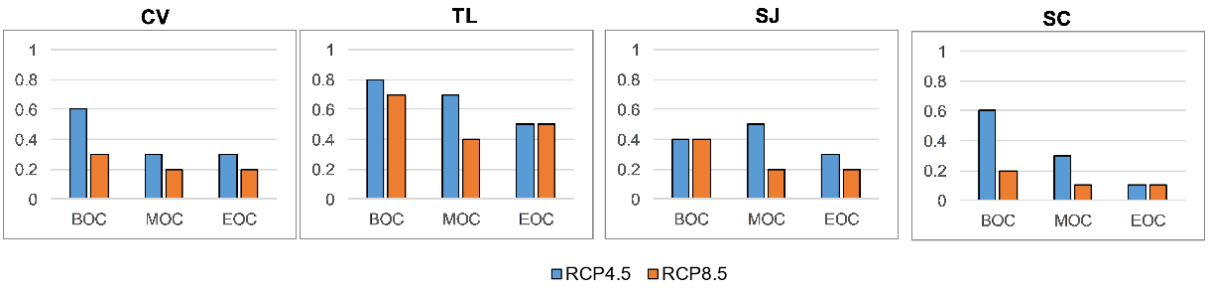

Figure A6. Comparing uncertainty in change direction (sign) for annual precipitation. The values represent - number of concordant minus discordant pairs, divided by the numbers of pairs. For annual and warm season inflow it is concordant if a model estimates future decrease (vice versa in case of discordant). For cool season, it is concordant if a model estimates increase (vice versa in case of discordant).

Appendix B

This appendix provides supporting information for Chapter 3. This chapter has been published in the Water Resources Research. © American Geophysical Union.

Alam, S., Gebremichael, M., Li, R., Dozier, J. and Lettenmaier, D.P., 2020. Can Managed Aquifer Recharge Mitigate the Groundwater Overdraft in California's Central Valley?. Water Resources Research, 56(8), p.e2020WR027244. https://doi.org/10.1029/2020WR027244 – Supporting Information.

Text B1. Selection of surface water diversion nodes:

This text provides additional information regarding the selection of surface water diversion nodes, as discussed in the main text (Section XX). We assume that subregions with one incoming stream receive water from one diversion point, whereas subregions with multiple incoming streams receive water from multiple diversion points (one on each stream). We select surface water diversion locations so as to minimize the distance from the recharge sites. There are multiple benefits in minimizing this distance, e.g. less evaporative loss, less expense if infrastructure development is required, and faster conveyance to the site. To determine the diversion locations for subregions with one incoming stream (i.e. subregion 1, 3, 4, 5, 7, 10, 11, 15, 16, 17, 19, 20 and 21), we first calculated the sum of the distance of each stream node to all recharge sites in that subregion. Then we identified the stream node with a minimum sum of distances and used that as a diversion location. To determine the diversion location for subregions with multiple incoming streams, we followed a two-step method. First, we identified the closest stream to each recharge site. We did so by calculating the distance of all stream nodes

from each recharge site, where we selected a stream (containing the reach node) for each recharge site. Second, we used the method followed for subregions with one incoming stream (described above) to identify diversion locations with minimum distance to recharge sites. Figure 4a of the manuscript shows the diversion locations identified using the above method. For the MAR experiments, we haven't allocated water for SR14 and SR9, in both cases there is no incoming stream from headwater watersheds like any other subregions (as we assumed MAR diversion stream for any subregion should head just upstream of the subregion and flow through it).

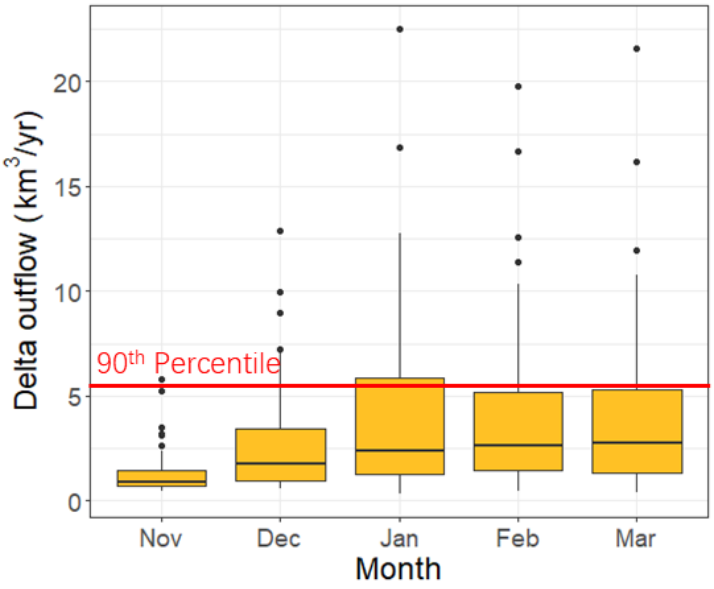

Figure B1. Winter Delta outflows to San Francisco Bay during 1960-2015.

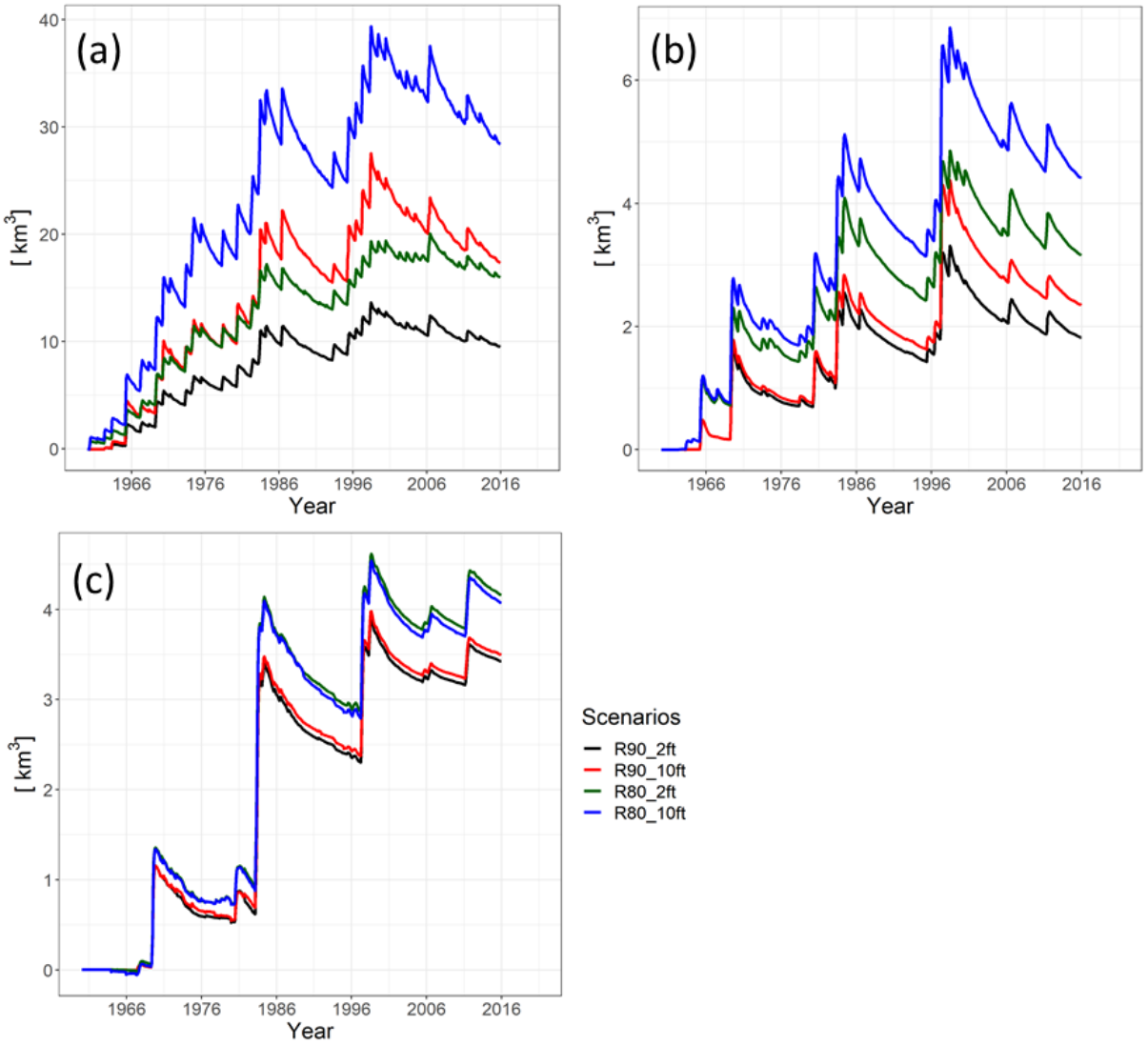

Figure B2. Difference in groundwater storage between MAR scenarios and base simulation in (a) SC_EZ, (b) SJ and (c) TL.

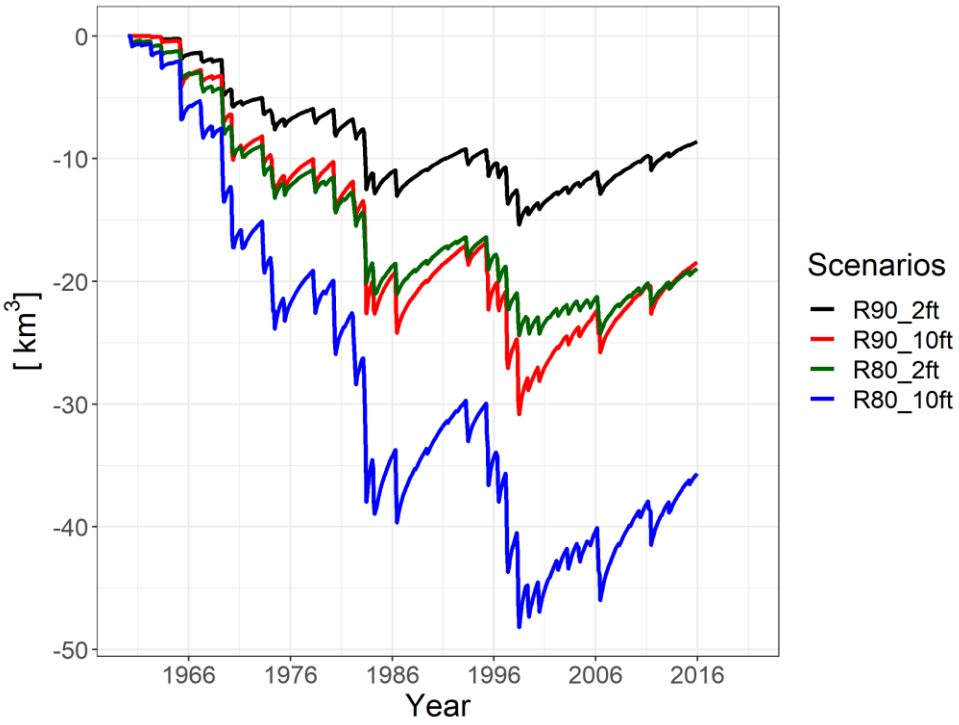

Figure B3. Cumulative difference in Delta outflow between MAR scenarios and base simulation. Negative values indicate that the Delta outflow decreased compared to the base simulation.

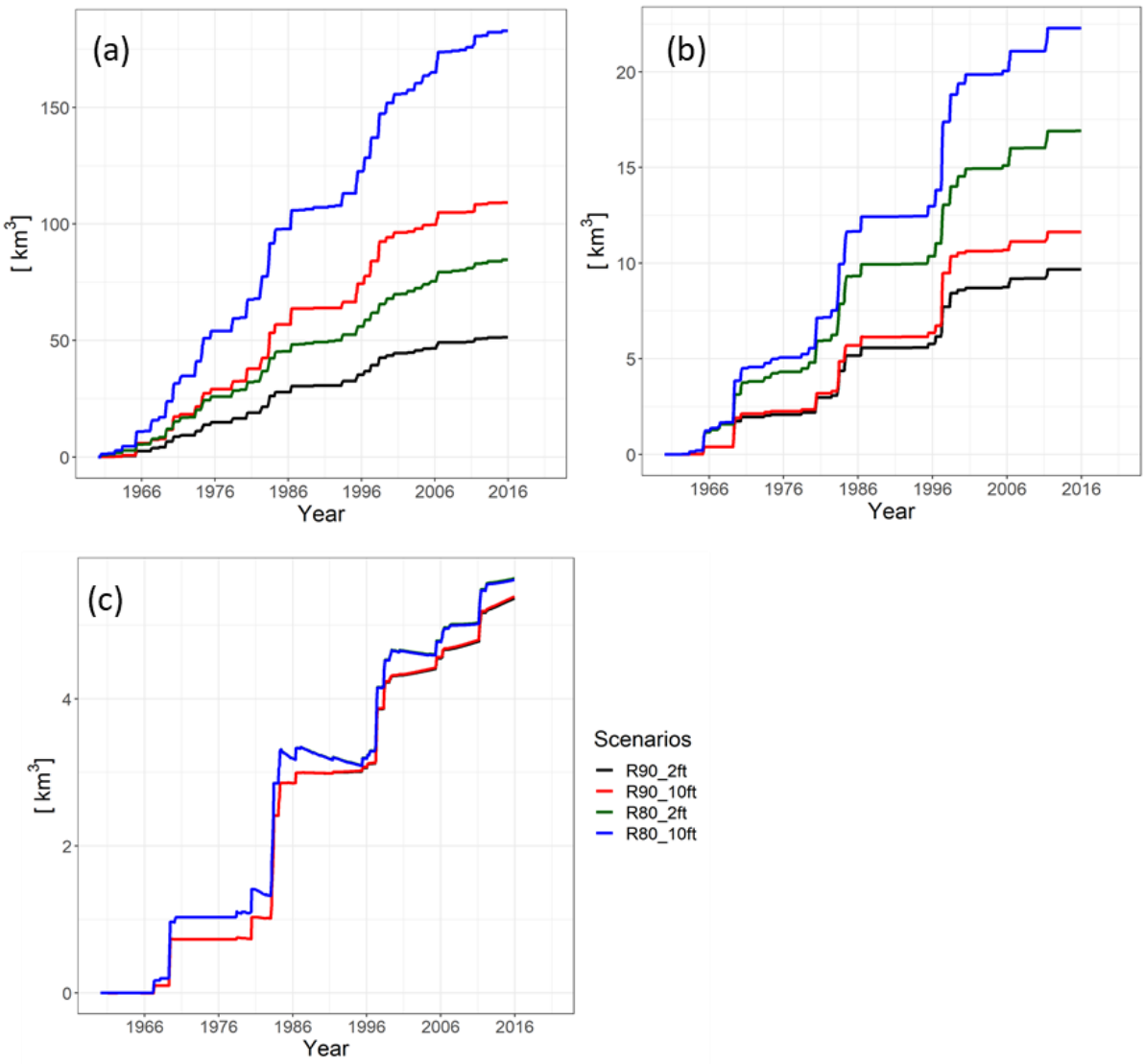

Figure B4. Cumulative difference in deep percolation between MAR scenarios and base simulation in (a) SC_EZ, (b) SJ and (c) TL.

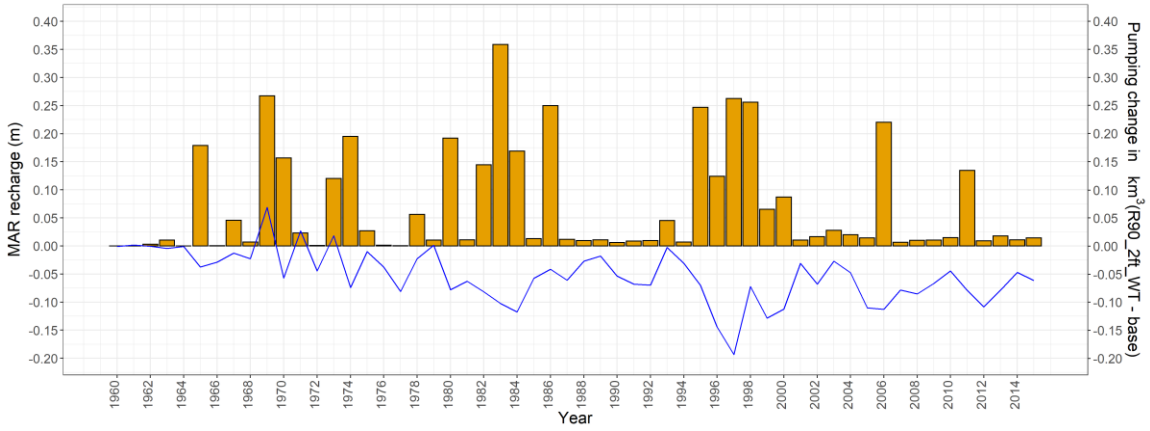

Figure B5. Temporal distribution (annual) of MAR recharge (barplot) and change in pumping (between R90_2ft_WT and base) over the entire CV

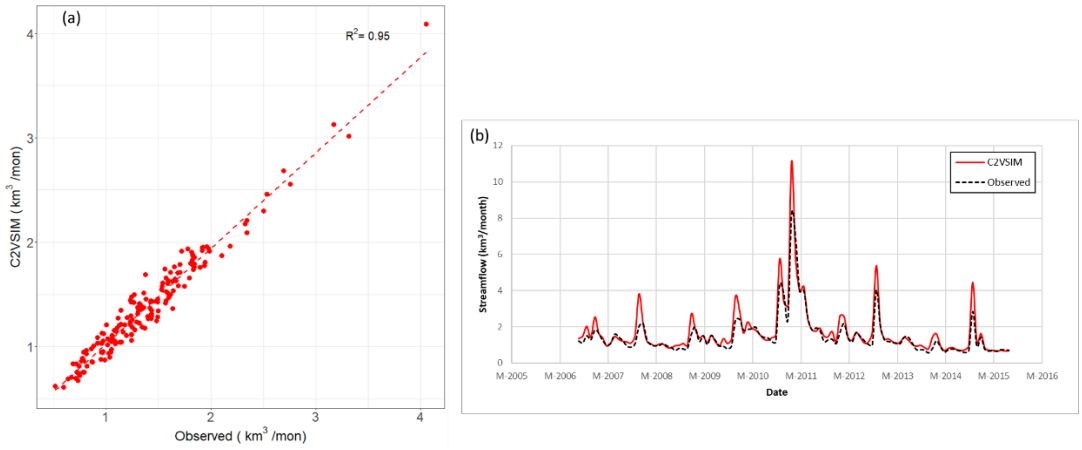

Figure B6. Comparison of C2VSIM simulated and observed delta inflow. (a) Scatterplot of flows during summertime (July-Sep.) for years 1960-2015, (b) time series delta inflow comparison during recent drought of 2007-2009 and 2012-2015.

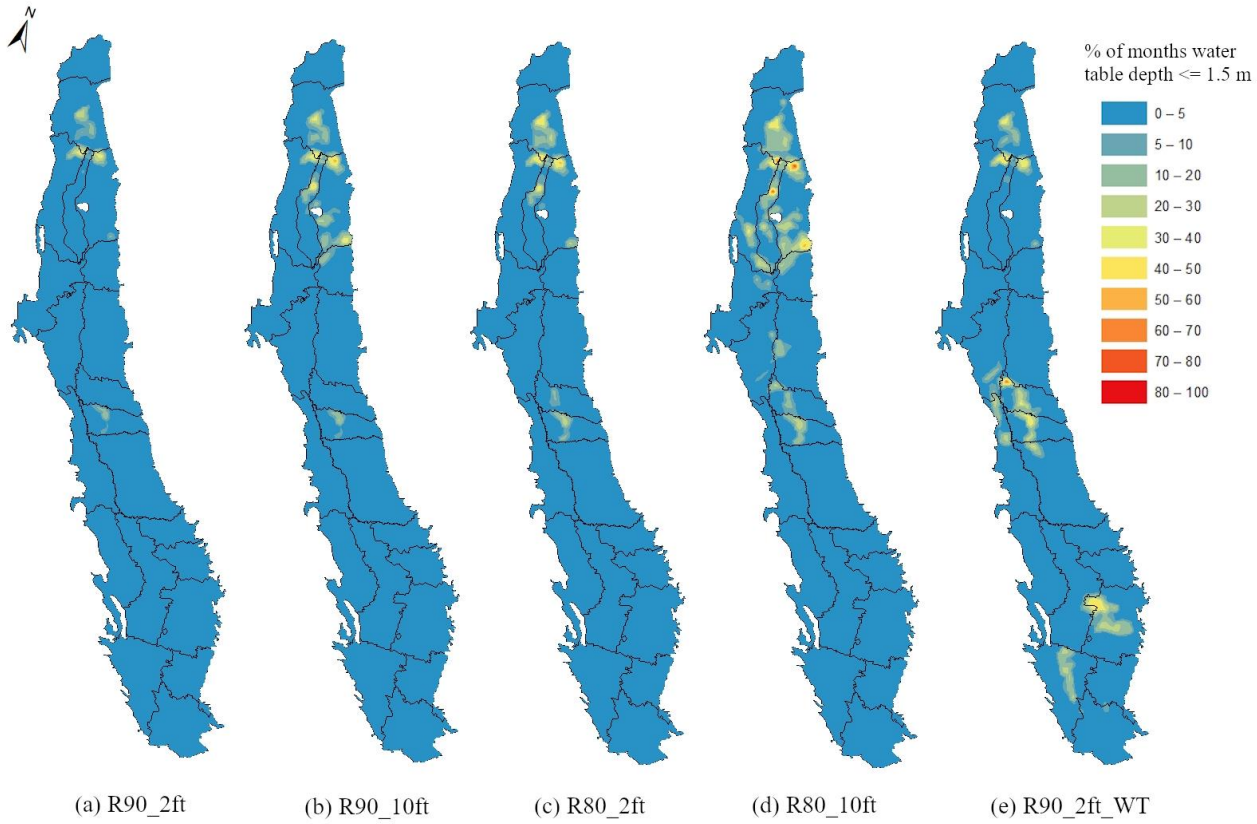

Figure B7. Percent of winter season months (Nov through Mar) for which the water table enters the rootzone due to the implementation of different MAR scenarios.

Table B1. Names of the streams from which surface water diversions can be made for MAR for each subregion.

Subregion	Diversion stream	Subregion	Diversion stream
1	Cottonwood Creek	12	Tuolumne River and Merced River
2	Elder Creek, Thomes Creek, Big Chico Creek and Deer Creek	13	Bear Creek, Deadman's Creek, Chowchilla River and Fresno River
3	Stony Creek	14	None
4	Butte Creek	15	Kings River (downstream of Island Weir)
5	Feather River and Yuba River	16	San Joaquin River
6	Cache Creek and Putah Creek	17	Kings River (upstream of Island Weir)
7	Bear River	18	Kaweah River, Tule River, Deer Creek and White River
8	American River, Cosumnes River, Dry Creek, Mokelumne River and Calaveras River	19	Kern River
9	None	20	Poso River
10	Orestimba Creek	21	Kern River
11	Stanislaus River		

Appendix C

This appendix provides supporting information for Chapter 4. This chapter has been submitted Water Resources Research.

Text C1. Description of datasets

1) **Precipitation:** We used gridded precipitation data from four sources, (1) PRISM (Daly et al., 2008), (2) DAYMET (Thornton et al., 2017), (3) UCLA Drought Monitor, and (4) Livneh et al. (2013) (hereafter L13) (see Table 1). PRISM data are available at 4 km spatial resolution for the period 1895-2020. DAYMET is available at 1 km spatial resolution for the period 1980-2020. The UCLA Drought Monitor precipitation is available at 1/16th degree (~6 km in the north-south direction) spatial resolution for the period 1980-2020. L13 precipitation data are available at 1/16th degree spatial resolution for 1950-2013, extended to 2018 by (Su et al., 2021) (available at ftp://livnehpublicstorage.colorado.edu/public/sulu). All precipitation data were aggregated to the monthly time scale.
2) **Evapotranspiration:** We extracted evapotranspiration (ET) estimates from the Variable Infiltration Capacity (VIC) land surface model (Liang et al., 1994). We forced the VIC model with the precipitation, temperature, downward solar and longwave radiation, humidity, and surface wind from L13. VIC-simulated outputs are available at the same 1/16th degree spatial resolution as precipitation. In the CV, irrigation strongly affects ET. VIC only simulates actual ET for non-irrigated vegetation. Therefore, we used the VIC-simulated ET only for the non-irrigated portion of the CV, and estimated ET for irrigated areas using the product of reference evapotranspiration (ETo) and crop coefficients (Kc) by FAO (Allen et al., 1998) and Brush et al. (2004) respectively (this is the same approach as was used by Xiao et al. (2017)). Table C1

of supplemental information shows the Kc values used. We obtained crop types and non-irrigated areas from the CropScape database (Han et al., 2012). CropScape provides geospatial cropland data over CV for the period 2007 through 2018. Because we require data from 2002 through 2019, we assumed that the crop types for the pre-2007 period were the same as 2007, and crop types in 2019 were the same as in 2018. Similar assumptions were made by Xiao et al. (2017); however, they only divided the crop land use into two periods: pre- and post-2011 (where pre-2011 land use was assumed to be the same for all years, and post-2011 land use assumed to be similar for all years). In contrast, we used crop land use time series for each year separately (when available). Finally, to estimate net ET over CV for each year, we summed the ET over the non-irrigated and irrigated areas.

3) **Soil Moisture:** We used soil moisture (SM) simulated by the VIC model for the non-irrigated portion of the CV. For the irrigated portion, we assumed that the soil moisture was close to the field capacity and did not vary from year to year. We found that variations in soil moisture were relatively small compared to variations in precipitation and ET. A similar approach was taken in calculating GWS changes by (Xiao et al., 2017). We ignored interannual variations in soil moisture in non-irrigated areas, as those variations are small and should have little impact on our calculations.
4) **Snow Water Equivalent:** We used VIC-simulated snow water equivalent (SWE) to estimate storage changes attributable to snow. SWE changes are negligible in the CV as essentially all of the snow falls in the upstream headwater watersheds. Therefore, we omitted ΔSWE from equation 1. However, SWE changes are non-negligible across the GRACE footprint which extends into the headwater watersheds (more discussion in section 3.1.4).

5) **Surface water inflow to CV and outflow from CV:** Almost all of the surface water that flows in the rivers or creeks of the CV originates in the upstream watersheds (headwater watersheds) that surround the CV. There are a total of 52 rivers and creeks that enter the CV at different locations. We collected inflow data from U.S. Geological Survey (USGS) and DWR records. For gages with discontinuous measurements, we used VIC simulations (unimpaired locations) and regression to estimate streamflow. A detail description of surface water inflow data processing is provided in Text C2. Surface water flow in the CV that remains after subtracting all diversions reaches the Delta region to be discharged to San Francisco Bay or diverted south to the California Aqueduct. The outflow from the CV is available from DWR at Dayflow (http://www.water.ca.gov/dayflow/) (see Figure C4).

6) **Reservoir storage:** There is only one reservoir in the CV proper (Camanche) which is relatively small in size (0.5 km^3), therefore, we omitted the ΔSW term from equation 1. There are 93 dams and reservoirs with storage capacities greater than 10^5 m^3) in the Sacramento-San Joaquin-Tulare (SSJT) basin that regulate flow in the rivers and canals. According to DWR, the total storage capacity of these reservoirs is about 37 km^3 (http://cdec.water.ca.gov/misc/resinfo.htm). These dams and reservoirs have multiple purposes including water supply, flood protection, environmental flows, and hydroelectric power generation. The 22 largest reservoirs account for about 85% of the total usable storage. We extracted reservoir storage data for these 22 reservoirs from the California Data Exchange Center (CDEC) for the period 2002-2019 (http://cdec.water.ca.gov/misc/monthly_res.html and http://waterdata.usgs.gov/nwis/uv/?referred_module=sw). We created a single (monthly) time series representing total surface water storage during 2002-2019. We used this storage time series to calculate GWS change from GRACE (see section 3.1.4). Although there are many

reservoirs, only one of them lies within the CV proper. Therefore, we omitted the ΔSW term from equation 1.

Text C2. Surface water inflow data processing

There are a total of 52 rivers and creeks that enter the CV at different locations. Of the 52 inflow locations, 35 have U.S. Geological Survey (USGS) or CDWR gauges that monitor streamflow. However, the gauge data are not continuously available (Table C2 provides the gauge list). A total of 19 out of 35 stations have data available for the entire study period (2002-2019); these stations represent about 90% of the long term mean flow of all these stations (Xiao et al., 2017). For the remaining 16 USGS stations we used the inflow data available from CDWR for the period up to 2015-September, which are inputs to the California Central Valley Surface-Groundwater Simulation model (C2VSIM) (available at https://data.cnra.ca.gov/dataset/c2vsimfg-version-1-0). For 2015-October to 2019-September, we estimated the inflow from VIC simulations and/ or regression on gauged flows nearby. There are 28 creeks/rivers that are mostly unimpaired and relatively small that appear to be well represented by VIC simulations. We compared the VIC runoff with the inflow obtained from C2VSIM (for the pre-2016 period) and found good agreement in seasonality. We multiplied the VIC runoff by a scaling factor where there were substantial differences in estimated volumes. To estimate the total inflow to the CV from surrounding watersheds for the entire 2002-2019 period, we used USGS observed streamflow for the above-mentioned 19 inflow locations, and for the remaining inflow locations we estimated flows using model simulations or regression. For stations where USGS data were not available post-2015 and correlations with VIC runoff were low, we estimated the flows from the best performing linear regression equation developed using flows at nearby gauge locations as predictors. We used DWR

inflow data (only available up to 2015-September) for all the inflow locations where USGS observations were not available.

Text C3. C2VSIM model

The core of C2VSIM model is a finite element solver. The subsurface is divided into four vertical layers, where the top two layers are unconfined and the bottom two are confined. The unconfined and confined layers are separated by thin Corcoran clay in places where it exists. In the horizontal direction, the model is discretized into irregular polygons with varying size. See CDWR (2020) for more detail about C2VSIM.

The user inputs to the model are precipitation, land use and crop distribution, irrigation method, evapotranspiration, population, surface water delivery and boundary inflows to CV region at monthly time steps. The original C2VSIM model simulation is available for the period 1973 through 2015 (water year). However, we needed model simulation through 2019 (water year) to match with GWS estimates from other three methods used in this study. Therefore, we extended the original version of the model through 2019-September (see Text C4 for details of the model extension)

Text C4. Extending the C2VSIM simulation

We extended a previous C2VSIM simulation from 2015-October through 2019-September. We did so by creating three inputs for the extended period: precipitation, surface water inflow to the CV and surface water diversions. We used precipitation data from the PRISM data set (Daly et al., 1994) at a monthly time step using the same sources as for the base model (CDWR, 2020). We created inflow time series for the extended period using observations and simulated outputs

from the VIC model. C2VSIM requires inflows at 52 locations, which we estimated as described in Text C1. The third input we created was surface water deliveries for multiple purposes, including agricultural, industrial, and residential sectors. Surface water deliveries in the CV depend on multiple factors, including water availability, water demand, conveyance capacity, water rights, and minimum flow requirements. We made assumptions to estimate surface water deliveries for the period 2002-2019 that yielded a range of delivery values rather than a fixed value. We followed the approach of (Hanson et al., 2012) with slight modifications. Hanson et al. (2012) first divided the historical water years into dry and wet years based on precipitation anomalies and then calculated the median surface water delivery during those two types of years at each diversion location. Later, they classified future water years into dry and wet types and assigned diversions for those periods. In our case, we divided the historical water years into wet and dry years and calculated the 25^{th}, 50^{th} and 75^{th} percentile deliveries during those years. We then determined the year types for 2016-2019 and ran the model with different diversion percentiles assigned according to the water year types. The simulated GWS change provides a range of estimates arising from variable surface water diversions. We assumed that other variables, such as land use and irrigation method, remained the same as for 2015.

Text C5. Storage coefficient selection

Sy values for the CV region from the C2VSIM-FG model (CDWR, 2020), and CVHM (Faunt et al., 2009), average 0.11 and 0.18 respectively (see Figure C4 of supporting information for the spatial distribution of Sy). We first calculated GWS change in CV using only Sy values from C2VSIM-FG and CVHM. Using Sy for GWS calculation is sufficient when the majority of groundwater is pumped from unconfined aquifers, but groundwater in CV is pumped from both

unconfined, semiconfined, and unconfined aquifers. In confined aquifers, specific storage (Ss) is 2-3 orders of magnitude less than Sy (where Ss is the water released from a unit volume of aquifer for a unit decrease in head). However, the average of Sy and Ss in the CV is 0.05 based on the C2VSIM-FG model. We therefore adopted another method to estimate the storage coefficient to supplement the C2VSIM and CVHM Sy estimates. In particular, we adjusted the CV-wide average storage coefficient value to match the GWS time series from wells with the GWS anomaly from GRACE observations. We term the storage coefficient that results in the best overall match the effective storage coefficient. Because the effective storage coefficient (S_e) represents both unconfined, semiconfined, and confined aquifers, we hypothesize that the value of S_e should be less than Sy values in the unconfined aquifers. We acknowledge that the use of S_e is applicable for large scale GWS estimation in the CV only, spatially varying S_e may not be a realistic option due to lack of reference GWS estimates at higher spatial resolution to validate the estimation (Table C3 shows specific storage used in other studies).

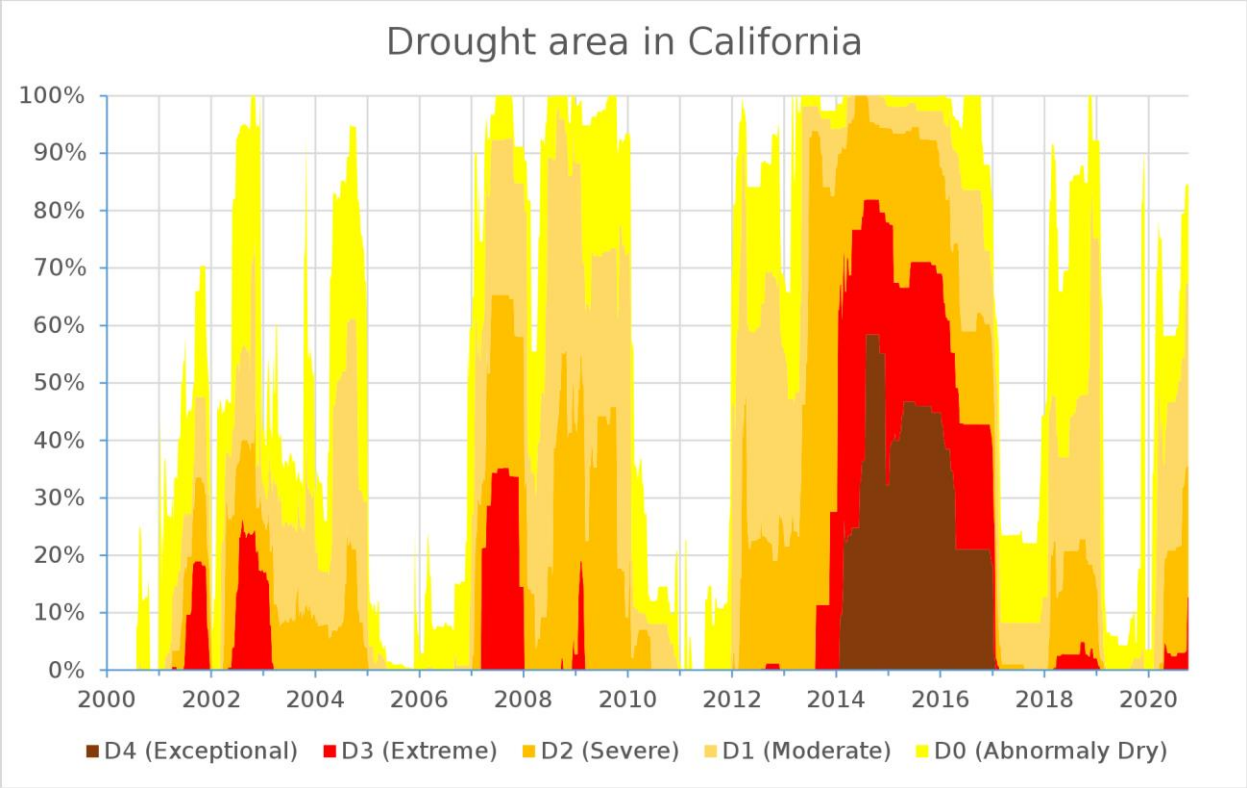

Figure C1. Drought area classification according to US drought monitor classes (https://droughtmonitor.unl.edu/), The 2007-2009 and 2012-2016 periods have at least 20% of the area of CA under D1 to D4 drought, therefore, we consider these periods as drought years in our analysis.

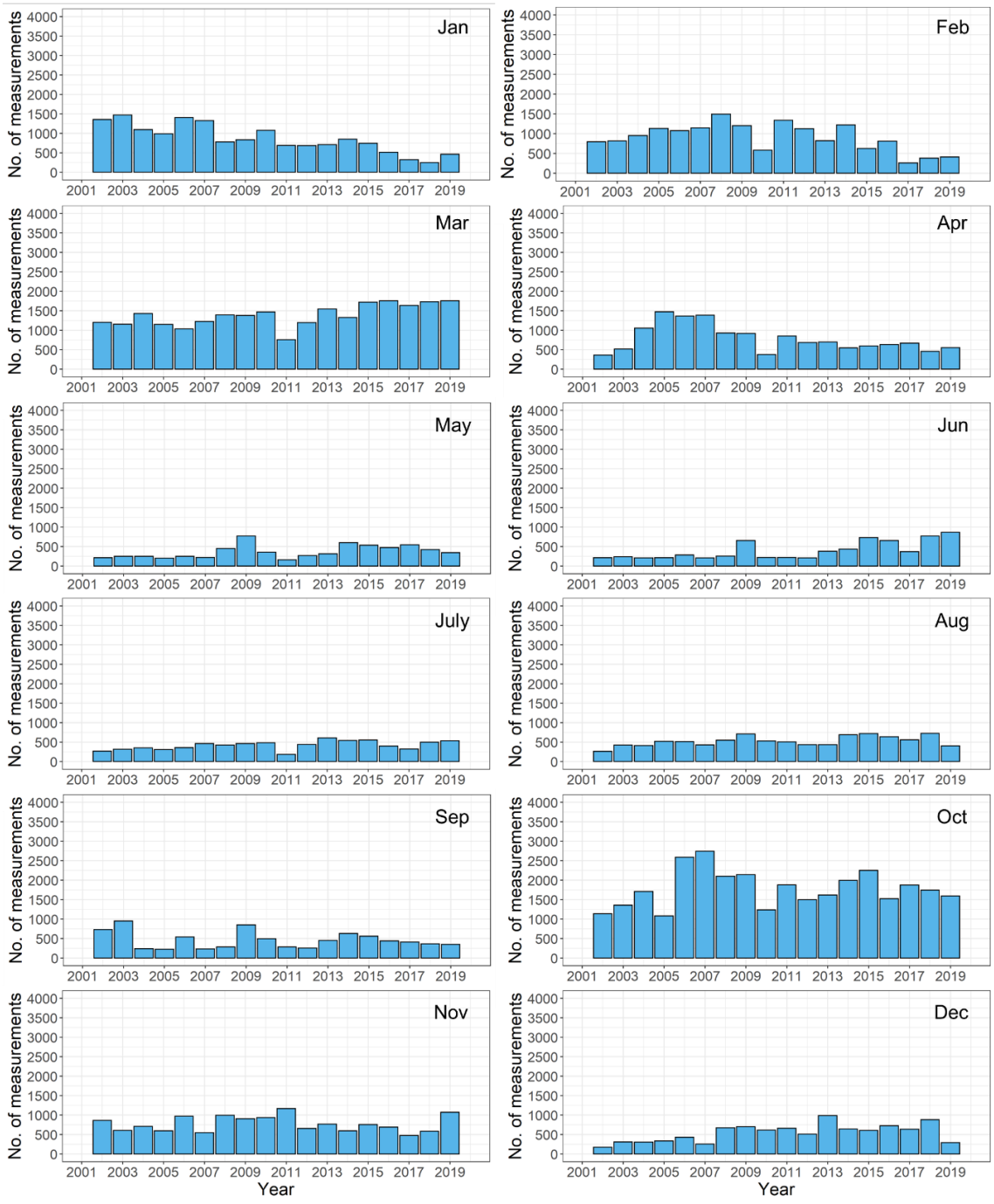

Figure C2. Number of well measurements available in each month for different years in CASGEM datasets. The data include all types of wells (observation, irrigation, residential and others). The wells are a subset of all well data available that are considered representative. The information used to select these wells comes from CDWR.

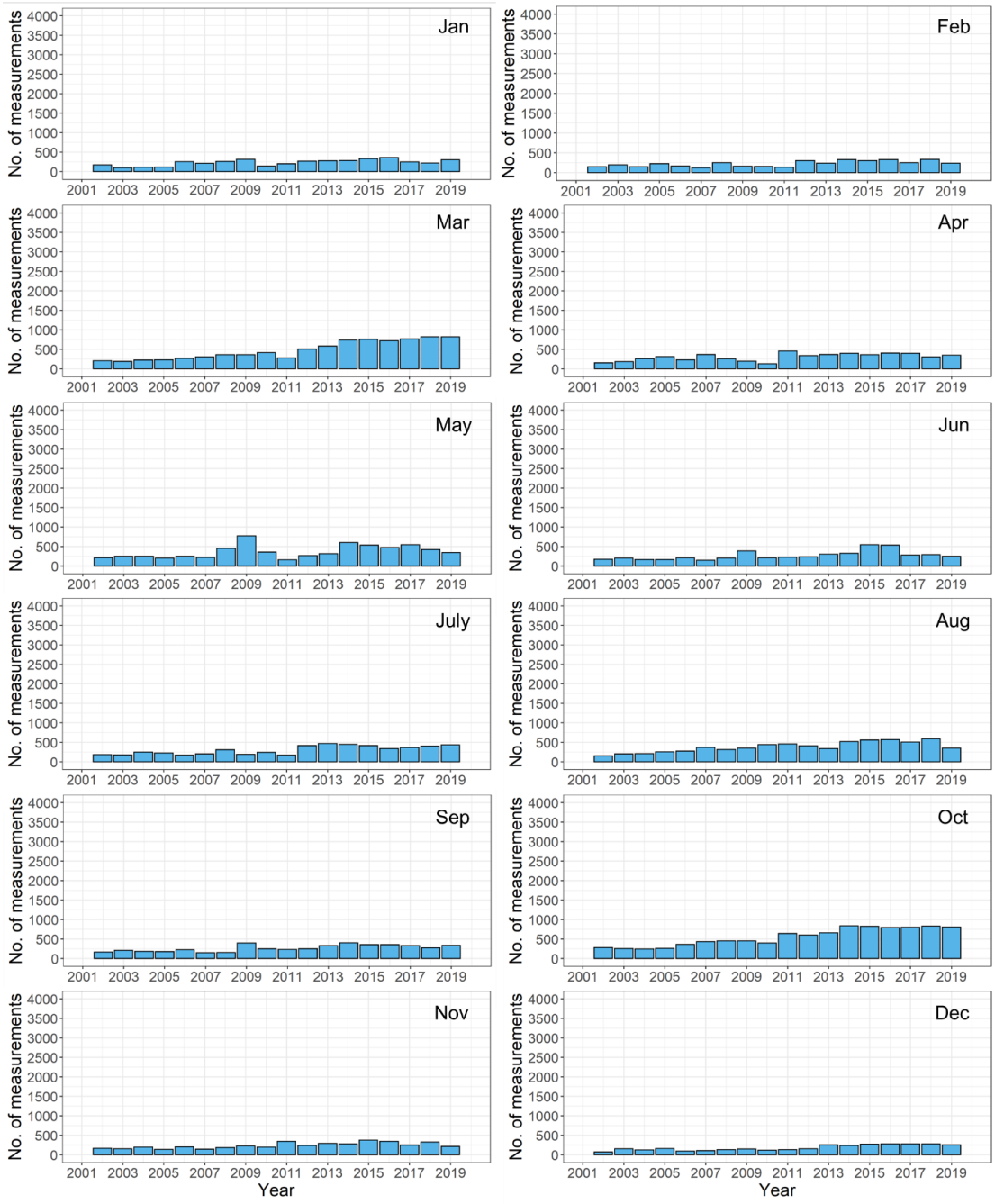

Figure C3. Number of observation well measurements available in each month for different years in CASGEM datasets.

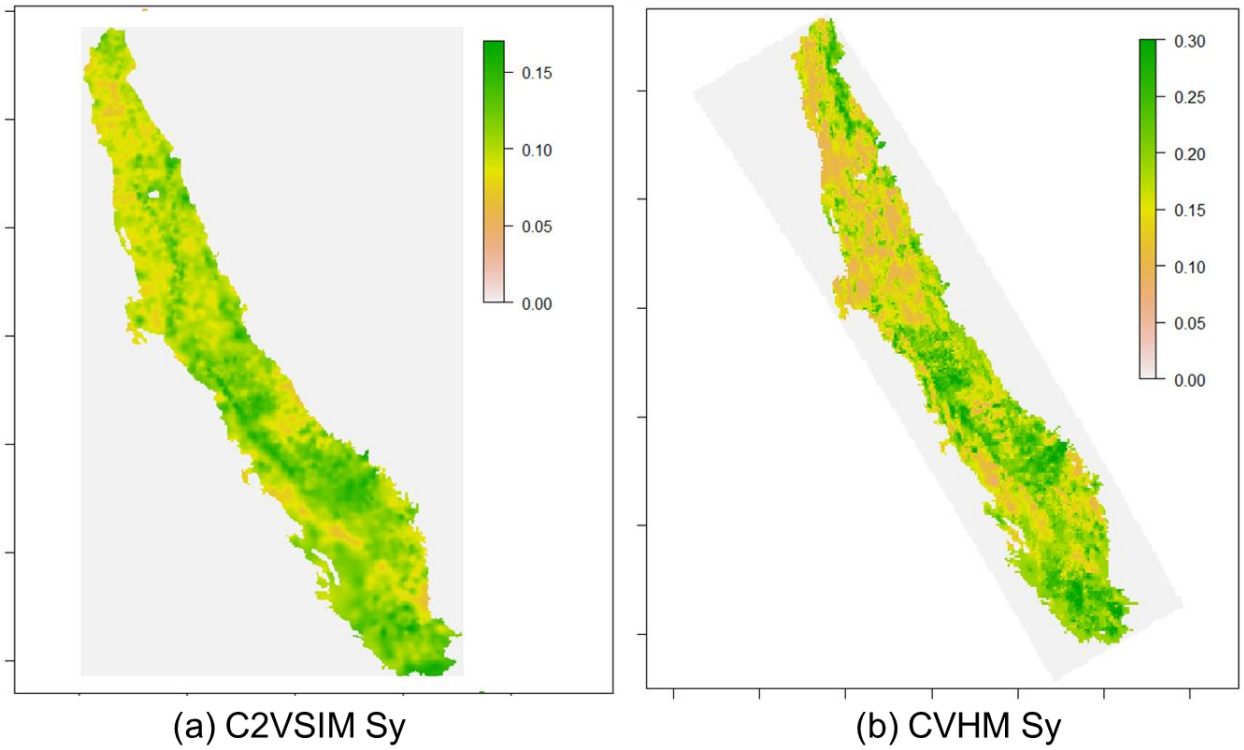

Figure C4. Specific yield data obtained from (a) C2VSIM-FG model (available at https://data.cnra.ca.gov/dataset/c2vsimfg-version-1-0), and (b) CVHM model (available at https://ca.water.usgs.gov/projects/central-valley/central-valley-hydrologic-model.html).

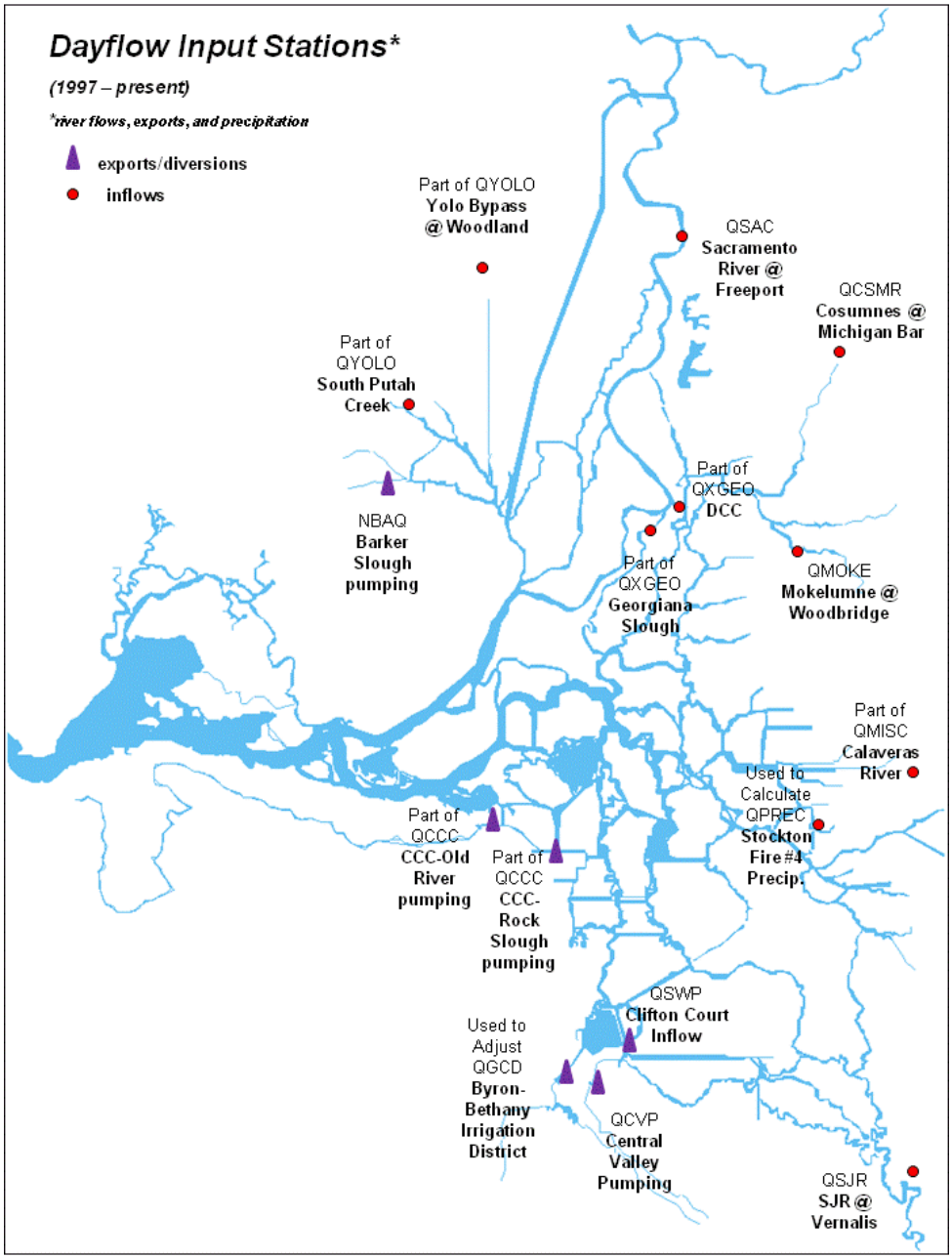

Figure C5. Dayflow station map per California DWR. Source: https://water.ca.gov/Programs/Environmental-Services/Compliance-Monitoring-And-Assessment/Dayflow-Data

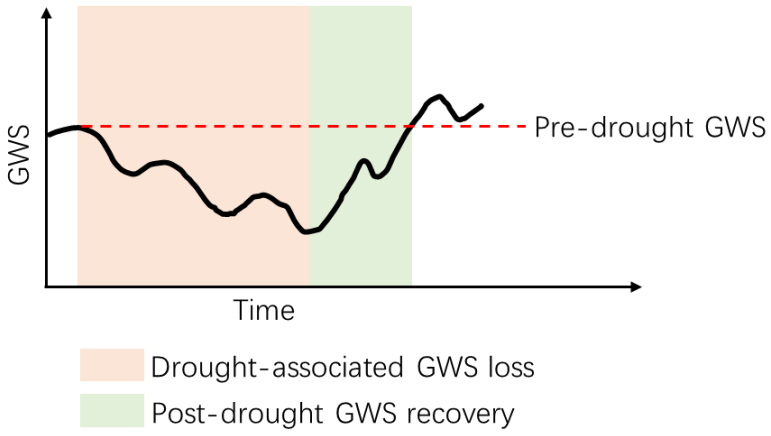

Figure C6. Schematic showing groundwater drought recovery. Here, the return of groundwater storage (GWS) to the pre-drought level is considered to be a full recovery from the drought. We used the USDM drought classifications to identify drought periods (shown in Figure C1). In our analysis, the drought periods are Jan-2007 to Dec-2009 and Jan-2012 to Dec-2016. The recovery period for the 2007-2009 drought is the time between Jan-2010 to Dec-2011. The recovery period for 2012-2016 starts immediately after drought ends (Jan-2017) and the end of the recovery period depends on data availability (Feb-2019).

Table C1. Crop coefficients for the CV, adapted from Brush et al (2004) and Allen et al (1998). We use average Kc for calculations following Xiao et al. (2017). Kc0, Kc1, Kc2 and Kc3 refers to states: initial, crop development, mid-season, and late-season.

Crop	Kc0	Kc1	Kc2	Kc3
Alfalfa	0.4	0.4	1.1	0.4
Cotton	0	0.16	1.05	0.4
Tomatoes	0	0.24	1.12	0.7
Pasture	0.06	0.9	0.9	0.9
Clover	0.06	1.05	1.05	1.05
Corn	0.06	0.23	0.87	0.65
Barley	0.06	0.24	0.87	0.65
Clover	0.06	0.52	0.87	0.65
Wheat	0.06	1.05	0.87	0.65
Grapefruit	0.65	0.65	0.65	0.65
Grapes	0.06	0.25	0.8	0.3
Oat	0.06	0.9	0.6	0.6
Artichokes	0.06	0.25	0.65	0.65
Asparagus	0	0.25	1	0.37
Broccoli	0	0.3	1	0.87
Cabbage	0	0.3	1	0.87
Carrots	0	0.85	0.95	0.83
Cauliflower	0	0.3	1	0.87
Citrus	0	0.14	1.1	0.1
Pecans	0	0.54	1.17	0.38
Apples	0.06	0.52	0.97	0.85
Apricots	0.06	0.52	0.87	0.65
Cherries	0.06	0.52	0.97	0.85
Pistachios	0.06	0.4	1.1	0.645
Walnuts	0.06	0.5	1.1	0.652
Peaches	0.06	1.05	1.05	1.05
Almonds	0.06	0.4	1.1	0.65
Average	0.05	0.51	1.05	0.65

Table C2. Name and Ids of USGS stations used to estimate inflow to CV.

Serial	Name	Station ID
1	American River at Fair Oaks (AFO)	11446500
2	Battle Creek (BAT)	11376550
3	BEAR R F REL BL CAMP FAR WEST RES NR WHEATLAND CA (CFW)	11423800
4	BIG CHICO C NR CHICO CA (BIC)	11384000
5	Butte Creek NR CHICO(BCK)	11390000
6	CACHE C AB RUMSEY CA (RUM)	11451760
7	CLEAR C NR IGO CA (IGO)	11372000
8	COSUMNES R A MICHIGAN BAR CA (MHB)	11335000
9	COTTONWOOD C NR COTTONWOOD CA (COT)	11376000
10	COW C NR MILLVILLE CA (COW)	11374000
11	DEER C NR VINA CA (DCV)	11383500
12	DRY C NR GALT CA (DCG)	11329500
13	DRY C NR LEMONCOVE CA (LCV)	11211300
14	DRY C NR WHEATLAND CA(DCW)	11424500
15	ELDER C NR PASKENTA CA (ECP)	11379500
16	FEATHER R NR GRIDLEY CA (GRL)	11407150
17	FRESNO R NR KNOWLES CA (FHL)	11257500
18	KAWEAH R A THREE RIVERS CA (TRR)	11209900
19	KERN R BL KERN CYN PH DIV DAM NR BAKERSFIELD CA (KRD)	11192950
20	LITTLE DRY C A MOUTH NR FRIANT CA (LDC)	11251600
21	LOS GATOS C NR COALINGA CA (LGC)	11225000
22	MERCED R BL MERCED FALLS DAM NR SNELL CA (MMF)	11270900
23	MILL C NR LOS MOLINOS CA (MLM)	11381500
24	MILL C NR PIEDRA CA (PDR)	11221700
25	MOKELUMNE R A WOODBRIDGE CA (WBR)	11325500
26	MUD C NR CHICO CA (MUC)	11384350
27	PUTAH C NR WINTERS CA (PUT)	11454000
28	SACRAMENTO R A KESWICK CA (KWK)	11370500
29	SAN JOAQUIN R BL FRIANT CA	11251000
30	STANISLAUS R BL GOODWIN DAM NR KNIGHTS FERRY CA (SKF)	11302000
31	STONY C BL BLACK BUTTE DAM NR ORLAND CA (SCG)	11388000
32	THOMES C A PASKENTA CA (THO)	11382000
33	TUOLUMNE R BL LAGRANGE DAM NR LAGRANGE CA (LGN)	11289650
34	WHITE R NR DUCOR CA (WRD)	11199500
35	YUBA R NR MARYSVILLE CA (MRY)	11421000

Table C3. Specific Yield used by other studies over CV.

Area/Aquifer	Specific yield (Sy)	Study domain	Reference
Central Valley	0.04	GRACE/InSAR	(Ojha et al., 2018)
Central Valley, San Joaquin	0.1	GRACE- In Situ	(Hanak et al., 2019)
Central Valley,	0.1	GRACE, GW/SW dynamics	(Gilbert & Maxwell, 2017)

Table C4. Comparing GWS change estimates during drought and post-drought years from multiple ensembles of GRACE, WB, and well-based GWS estimates. GRACE estimates are provided for JPL-m and

Methods	2007-2009 [km^3]	2010-2011 [km^3]	Recovery $R_{f,Pd1}$ [%]	2012-2016 [km^3]	2017-2019 [km^3]	Recovery $R_{f,Pd2}$ [%]
GRACE						
JPL-m	-25.1	9.5	38	-30.2	3.7	12.1
CSR-m	-14.4	10	69.4	-23	3.5	15.6
Average	-19.8	9.8	53.7	-26.6	3.6	13.9
Range	10.7	0.5	31.4	7.2	0.2	3.5

Bibliography

Aeschbach-Hertig, W., Gleeson, T., 2012. Regional strategies for the accelerating global problem of groundwater depletion. Nat. Geosci. 5, 853–861.

Alam, S., Borthakur, A., Ravi, S., Gebremichael, M., Mohanty, S., 2021. Managed aquifer recharge implementation criteria to achieve water sustainability. Sci. Total Environ. 144992. https://doi.org/10.1016/j.scitotenv.2021.144992

Alam, S., Gebremichael, M., Li, R., 2019. Remote sensing-based assessment of the crop, energy and water nexus in the Central Valley, California. Remote Sens. 11. https://doi.org/10.3390/rs11141701

Alam, S., Gebremichael, M., Li, R., Dozier, J., Lettenmaier, D.P., 2020. Can Managed Aquifer Recharge mitigate the groundwater overdraft in California's Central Valley? Water Resour. Res. e2020WR027244.

Alam, S., Gebremichael, M., Li, R., Dozier, J., Lettenmaier, D.P., 2019. Climate change impacts on groundwater storage in the Central Valley, California. Clim. Change 157, 387–406.

Allen, R.G., Pereira, L.S., Raes, D., Smith, M., 1998. Crop evapotranspiration-Guidelines for computing crop water requirements-FAO Irrigation and drainage paper 56. Fao Rome 300, D05109.

Alley, W.M., Healy, R.W., LaBaugh, J.W., Reilly, T.E., 2002. Flow and storage in groundwater systems. science 296, 1985–1990.

Argus, D.F., Landerer, F.W., Wiese, D.N., Martens, H.R., Fu, Y., Famiglietti, J.S., Thomas, B.F., Farr, T.G., Moore, A.W., Watkins, M.M., 2017. Sustained Water Loss in California's Mountain Ranges During Severe Drought From 2012 to 2015 Inferred From GPS. J. Geophys. Res. Solid Earth 122, 10,559-10,585. https://doi.org/10.1002/2017JB014424

Asoka, A., Gleeson, T., Wada, Y., Mishra, V., 2017. Relative contribution of monsoon precipitation and pumping to changes in groundwater storage in India. Nat. Geosci. 10, 109–117.

Bachand, P.A.M., Roy, S.B., Choperena, J., Cameron, D., Horwath, W.R., 2014. Implications of using on-farm flood flow capture to recharge groundwater and mitigate flood risks along the Kings River, CA. Environ. Sci. Technol. 48, 13601–13609.

Baker, D.B., Richards, R.P., Loftus, T.T., Kramer, J.W., 2004. A new flashiness index: Characteristics and applications to midwestern rivers and streams 1. JAWRA J. Am. Water Resour. Assoc. 40, 503–522.

Bales, R.C., Molotch, N.P., Painter, T.H., Dettinger, M.D., Rice, R., Dozier, J., 2006. Mountain hydrology of the western United States. Water Resour. Res. 42.

Bettadpur, S., 2012. UTCSR level-2 processing standards document for level-2 product release 0005. GRACE Rep 327, 742–742.

Brown, L.R., Kimmerer, W., Brown, R., 2009. Managing water to protect fish: a review of California's environmental water account, 2001–2005. Environ. Manage. 43, 357–368.

Brunner, P., Cook, P.G., Simmons, C.T., 2009. Hydrogeologic controls on disconnection between surface water and groundwater. Water Resour. Res. 45.

Brush, C.F., 2013. Historical Rim Inflows, Surface Water Diversions and Bypass Flows for the California Central Valley Groundwater-Surface Water Simulation Model (C2VSim), Version 3.02-CG. Bay-Delta Office, California Department of Water Resources.

Brush, C.F., Belitz, K., Phillips, S.P., 2004. Estimation of a Water Budget for 1972-2000 for the Grasslands Area, Central Part of the Western San Joaquin Valley, California. US Department of the Interior, US Geological Survey.

Brush, C.F., Dogrul, E.C., 2013. User's Manual for the California Central VAlley Groundwater-Surface Water Simulation Model (C2VSim), Version 3.02-CG. Calif. Dep. Water Resour. Tech. Memo. 134–134.

Brush, C.F., Dogrul, E.C., Kadir, T.N., 2013. Development and Calibration of the California Central Valley Groundwater- Surface Water Simulation Model (C2VSim), Version 3.02-CG. Calif. Dep. Water Resour. Tech. Memo. 2013, 193–193.

Cal-Adapt, 2018. Cal-Adapt is developed by the Geospatial Innovation Facility at University of California, Berkeley. Data downloaded from https://cal-adapt.org/ in 2018.

California State Legislature, 2014. Sustainable groundwater management act. https://www.opr.ca.gov/docs/2014_Sustainable_Groundwater_Management_Legislation_092914.pdf.

CASGEM, 2021. Periodic Groundwater level Measurements. Department of Water Resources California Statewide Groundwater Elevation Monitoring [Data file]. Retrieved from: https://data.cnra.ca.gov/dataset/periodic-groundwater-level-measurements.

CDEC, 2020. California Data Exchange Center - Reservoirs. Source: https://cdec.water.ca.gov/reservoir.html.

CDWR, 2020. C2VSimFG Version 1.0: Fine Grid California Central Valley Groundwater-Surface Water Simulation Model. Model last updated on December 8, 2020. Available at https://data.cnra.ca.gov/dataset/c2vsimfg-version-1-0.

CDWR, 2018a. Flood-MAR white paper: using flood water for managed aquifer recharge to support sustainable water resources. California Department of Water Resources, Sacramento, CA, USA.

CDWR, 2018b. Water Available for Replenishment. Appendix A: Water Available for Replenishment Information and Estimates.

CDWR, 2016. Estimates of Natural and Unimpaired Flows for the Central Valley of California: Water Years 1922–2014. Report from California Department of Water Resources.

CDWR, 2014. California State Water Project Overview California Dept. Water resources.

CDWR, 2013. California Department of Water Resources and California Natural Resources Agency, and State of California. California's groundwater update 2013, A Compilation of Enhanced Content for California (California: Department of Water Resources).

Chinnasamy, P., Muthuwatta, L., Eriyagama, N., Pavelic, P., Lagudu, S., 2018. Modeling the potential for floodwater recharge to offset groundwater depletion: a case study from the Ramganga basin, India. Sustain. Water Resour. Manag. 4, 331–344.

Christian-Smith, J., 2013. Improving water management through groundwater banking: Kern County and the Rosedale-Rio Bravo water storage district. Oakl. CA Pac. Inst.

Cooper, M.G., Schaperow, J.R., Cooley, S.W., Alam, S., Smith, L.C., Lettenmaier, D.P., 2018. Climate Elasticity of Low Flows in the Maritime Western U.S. Mountains. Water Resour. Res. 54. https://doi.org/10.1029/2018WR022816

Dahlke, H., Brown, A., Orloff, S., Putnam, D., O'Geen, T., 2018. Managed winter flooding of alfalfa recharges groundwater with minimal crop damage. Calif. Agric. 72, 65–75.

Dale, L.L., Dogrul, E.C., Brush, C.F., Kadir, T.N., Chung, F.I., Miller, N.L., Vicuna, S.D., Berkeley, L., 2013. Simulating the Impact of Drought on California ' s Central Valley Hydrology , Groundwater and Cropping 3, 271–291.

Daly, C., Halbleib, M., Smith, J.I., Gibson, W.P., Doggett, M.K., Taylor, G.H., Curtis, J., Pasteris, P.P., 2008. Physiographically sensitive mapping of climatological temperature and

precipitation across the conterminous United States. Int. J. Climatol. J. R. Meteorol. Soc. 28, 2031–2064.

Dayflow, 2020. Delta boundary hydrology available through California Natural Resources Agency. source: https://data.cnra.ca.gov/dataset/dayflow.

DeChant, C.M., Moradkhani, H., 2015. Analyzing the sensitivity of drought recovery forecasts to land surface initial conditions. J. Hydrol. 526, 89–100.

Deitch, M.J., Dolman, B., 2017. Restoring summer base flow under a decentralized water management regime: Constraints, opportunities, and outcomes in Mediterranean-climate California. Water 9, 29–29.

Dillon, P., 2009. Water recycling via managed aquifer recharge in Australia. Bol. Geológico Min. 120, 121–130.

Dillon, P., Stuyfzand, P., Grischek, T., Lluria, M., Pyne, R.D.G., Jain, R.C., Bear, J., Schwarz, J., Wang, W., Fernandez, E., Stefan, C., Pettenati, M., van der Gun, J., Sprenger, C., Massmann, G., Scanlon, B.R., Xanke, J., Jokela, P., Zheng, Y., Rossetto, R., Shamrukh, M., Pavelic, P., Murray, E., Ross, A., Bonilla Valverde, J.P., Palma Nava, A., Ansems, N., Posavec, K., Ha, K., Martin, R., Sapiano, M., 2019. Sixty years of global progress in managed aquifer recharge. Hydrogeol. J. 27, 1–30. https://doi.org/10.1007/s10040-018-1841-z

Dogrul, E.C., Kadir, T.N., Brush, C.F., 2015. DWR Technical Memorandum and User ' s Manual.

Dogrul, E.C., Kadir, T.N., Brush, C.F., Chung, F.I., 2016. Environmental Modelling & Software Linking groundwater simulation and reservoir system analysis models : The case for California ' s Central Valley. Environ. Model. Softw. 77, 168–182. https://doi.org/10.1016/j.envsoft.2015.12.006

Döll, P., Hoffmann-Dobrev, H., Portmann, F.T., Siebert, S., Eicker, A., Rodell, M., Strassberg, G., Scanlon, B.R., 2012. Impact of water withdrawals from groundwater and surface water on continental water storage variations. J. Geodyn. 59, 143–156.

Famiglietti, J.S., 2014. The global groundwater crisis. Nat. Clim. Change 4, 945–948.

Famiglietti, J.S., Lo, M., Ho, S.L., Bethune, J., Anderson, K.J., Syed, T.H., Swenson, S.C., De Linage, C.R., Rodell, M., 2011a. Satellites measure recent rates of groundwater depletion in California's Central Valley. Geophys. Res. Lett. 38, 2–5. https://doi.org/10.1029/2010GL046442

Famiglietti, J.S., Lo, M., Ho, S.L., Bethune, J., Anderson, K.J., Syed, T.H., Swenson, S.C., De Linage, C.R., Rodell, M., 2011b. Satellites measure recent rates of groundwater depletion in California's Central Valley. Geophys. Res. Lett. 38, 2–5. https://doi.org/10.1029/2010GL046442

Fan, Y., Li, H., Miguez-Macho, G., 2013. Global patterns of groundwater table depth. Science 339, 940–943. https://doi.org/10.1126/science.1229881

Farrar, C.D., Bertoldi, G.L., 1988. Region 4, central valley and pacific coast ranges. Hydrogeol. Geol. Soc. N. Am. Boulder Colo. 1988 P 59-67 4 Fig 28 Ref.

Faunt, C.C., Hanson, R.T., Belitz, K., Schmid, W., Predmore, S.P., Rewis, D.L., McPherson, K., 2009. Groundwater Availability of the Central Valley Aquifer, California, US. Geological Survey Professional Paper 1766.

Faunt, C.C., Sneed, M., Traum, J., Brandt, J.T., 2016. Water availability and land subsidence in the Central Valley, California, USA. Hydrogeol. J. 24, 675–684.

Feng, W., Shum, C.K., Zhong, M., Pan, Y., 2018. Groundwater storage changes in China from satellite gravity: An overview. Remote Sens. 10, 674–674.

Feng, W., Zhong, M., Lemoine, J., Biancale, R., Hsu, H., Xia, J., 2013. Evaluation of groundwater depletion in North China using the Gravity Recovery and Climate Experiment (GRACE) data and ground-based measurements. Water Resour. Res. 49, 2110–2118.

Fleming, S.W., Quilty, E.J., 2006. Aquifer responses to el Niño–Southern oscillation, southwest British Columbia. Groundwater 44, 595–599.

Flint, A.L., Flint, L.E., 2007. Application of the basin characterization model to estimate in-place recharge and runoff potential in the Basin and Range carbonate-rock aquifer system, White Pine County, Nevada, and adjacent areas in Nevada and Utah.

Flores-López, F., 2019. Managed Aquifer Recharge Using Floodwaters on Agricultural Fields. California Department of Water Resources. https://www.grac.org/media/files/files/c42cafa7/19-4-1-c-francisco-flores-lopez.pdf.

Fogg, G.E., 1986. Groundwater flow and sand body interconnectedness in a thick, multiple-aquifer system. Water Resour. Res. 22, 679–694.

Foster, S., Garduño, H., 2013. Groundwater-resource governance: are governments and stakeholders responding to the challenge? Hydrogeol. J. 21, 317–320.

Gailey, R.M., Fogg, G.E., Lund, J.R., Medellín-Azuara, J., 2019. Maximizing on-farm groundwater recharge with surface reservoir releases: a planning approach and case study in California, USA. Hydrogeol. J. 27, 1183–1206.

Garrote, L., Iglesias, A., Granados, A., Mediero, L., Martin-Carrasco, F., 2015. Quantitative assessment of climate change vulnerability of irrigation demands in Mediterranean Europe. Water Resour. Manag. 29, 325–338.

Gebremichael, M., Krishnamurthy, P.K., Ghebremichael, L.T., Alam, S., 2021. What Drives Crop Land Use Change during Multi-Year Droughts in California's Central Valley? Prices or Concern for Water? Remote Sens. 13, 650–650.

Ghasemizade, M., Asante, K.O., Petersen, C., Kocis, T., Dahlke, H.E., Harter, T., 2019. An integrated approach toward sustainability via groundwater banking in the southern Central Valley, California. Water Resour. Res. 55, 2742–2759.

Gleeson, T., Wada, Y., Bierkens, M.F.P., Van Beek, L.P.H., 2012. Water balance of global aquifers revealed by groundwater footprint. Nature 488, 197–200. https://doi.org/10.1038/nature11295

Gleick, P.H., 2000. Water: the potential consequences of climate variability and change for the water resources of the United States. Pacific Institute for Studies in Development, Environment, and Security.

Gorelick, S.M., Zheng, C., 2015. Global change and the groundwater management challenge. Water Resour. Res. 51, 3031–3051.

Hanak, E., 2011. Managing California's water: from conflict to reconciliation. Public Policy Instit. of CA.

Hanak, E., Escriva-Bou, A., Gray, B., Green, S., Harter, T., Jezdimirovic, J., Lund, J., Medellín-Azuara, J., Moyle, P., Seavy, N., 2019. Water and the future of the San Joaquin Valley. San Franc. Public Policy Inst. Calif.

Hanak, E., Jezdimirovic, J., Green, S., Escriva-Bou, A., 2018. Replenishing Groundwater in the San Joaquin Valley 50–50.

Hanak, E., Lund, J., Arnold, B., Escriva-Bou, A., Gray, B., Green, S., Harter, T., Howitt, R., MacEwan, D., Medellín-Azuara, J., 2017. Water stress and a changing San Joaquin Valley. Public Policy Inst. Calif. 1, 5–48.

Hanson, R.T., Flint, L.E., Flint, A.L., Dettinger, M.D., Faunt, C.C., Cayan, D., Schmid, W., 2012. A method for physically based model analysis of conjunctive use in response to potential climate changes. Water Resour. Res. 48, 1–23. https://doi.org/10.1029/2011WR010774

Hashemi, H., Berndtsson, R., Persson, M., 2015. Artificial recharge by floodwater spreading estimated by water balances and groundwater modelling in arid Iran. Hydrol. Sci. J. 60, 336–350.

Holman, I.P., Rivas-Casado, M., Bloomfield, J.P., Gurdak, J.J., 2011. Identifying non-stationary groundwater level response to North Atlantic ocean-atmosphere teleconnection patterns using wavelet coherence. Hydrogeol. J. 19, 1269–1269.

IPCC, 2007. Climate Change 2007: impacts, adaptation and vulnerability, Working Group II contribution to the fourth assessment report of the Intergovernmental Panel on Climate Change. International Panel on Climate Change, Geneva.

ITRC, 2003. California crop and soil evapotranspiration for water balances and irrigation scheduling/design. California Polytechnic State University, web: http://www.itrc.org/reports/pdf/californiacrop.pdf.

Johnson, H., 2009. California population: Planning for a better future,report, Public Policy Inst. of Calif., San Francisco.

Kapnick, S., Hall, A., 2010. Observed climate–snowpack relationships in California and their implications for the future. J. Clim. 23, 3446–3456.

Kocis, T.N., Dahlke, H.E., 2017. Availability of high-magnitude streamflow for groundwater banking in the Central Valley, California. Environ. Res. Lett. 12. https://doi.org/10.1088/1748-9326/aa7b1b

Kourakos, G., Dahlke, H.E., Harter, T., 2019. Increasing groundwater availability and seasonal base flow through agricultural managed aquifer recharge in an irrigated basin. Water Resour. Res. 55, 7464–7492.

Kuss, A.J.M., Gurdak, J.J., 2014. Groundwater level response in US principal aquifers to ENSO, NAO, PDO, and AMO. J. Hydrol. 519, 1939–1952.

Leblanc, M.J., Tregoning, P., Ramillien, G., Tweed, S.O., Fakes, A., 2009. Basin-scale, integrated observations of the early 21st century multiyear drought in southeast Australia. Water Resour. Res. 45.

Li, R., Ou, G., Pun, M., Larson, L., 2018. Evaluation of groundwater resources in response to agricultural management scenarios in the Central Valley, California. J. Water Resour. Plan. Manag. 144, 4018078–4018078.

Li, R., Pun, M., Bradley, J., Ou, G., Schneider, J., Flyr, B., Winter, J., Chinta, S., 2016. Evaluating hydrologically connected surface water and groundwater using a groundwater model. JAWRA J. Am. Water Resour. Assoc. 52, 799–805.

Liang, X., Lettenmaier, D.P., Wood, E.F., Burges, S.J., 1994. A simple hydrologically based model of land surface water and energy fluxes for general circulation models. J. Geophys. Res. Atmospheres 99, 14415–14428.

Livneh, B., Bohn, T.J., Pierce, D.W., Munoz-Arriola, F., Nijssen, B., Vose, R., Cayan, D.R., Brekke, L., 2015. A spatially comprehensive, hydrometeorological data set for Mexico, the US, and Southern Canada 1950–2013. Sci. Data 2, 1–12.

Livneh, B., Rosenberg, E.A., Lin, C., Nijssen, B., Mishra, V., Andreadis, K.M., Maurer, E.P., Lettenmaier, D.P., 2013. A long-term hydrologically based dataset of land surface fluxes and states for the conterminous United States: Update and extensions. J. Clim. 26, 9384–9392.

Maples, S.R., Fogg, G.E., Maxwell, R.M., 2019. Modeling managed aquifer recharge processes in a highly heterogeneous, semi-confined aquifer system. Hydrogeol. J. 27, 2869–2888.

Martos-Rosillo, S., Ruiz-Constán, A., González-Ramón, A., Mediavilla, R., Martín-Civantos, J.M., Martínez-Moreno, F.J., Jódar, J., Marín-Lechado, C., Medialdea, A., Galindo-Zaldívar, J., 2019. The oldest managed aquifer recharge system in Europe: New insights from the Espino recharge channel (Sierra Nevada, southern Spain). J. Hydrol. 578, 124047–124047.

Massoud, E.C., Purdy, A.J., Miro, M.E., Famiglietti, J.S., 2018. Projecting groundwater storage changes in California's Central Valley. Sci. Rep. 8, 1–9.

Miller, N.L., Bashford, K.E., Strem, E., 2003. POTENTIAL IMPACTS OF CLIMATE CHANGE ON CALIFORNIA HYDROLOGY 1. JAWRA J. Am. Water Resour. Assoc. 39, 771–784.

Miller, N.L., Dale, L.L., Brush, C.F., Vicuna, S.D., Kadir, T.N., Dogrul, E.C., Chung, F.I., Norman, L., Dale, L.L., Brush, C.F., Vicuna, S.D., Kadir, T.N., Dogrul, E.C., 2009a. Drought Resilience of the California Central Valley Surface-Groundwater-Conceyabce System 45. https://doi.org/10.1111/j.1752-1688.2009.00329.x

Miller, N.L., Dale, L.L., Brush, C.F., Vicuna, S.D., Kadir, T.N., Dogrul, E.C., Chung, F.I., Norman, L., Dale, L.L., Brush, C.F., Vicuna, S.D., Kadir, T.N., Dogrul, E.C., 2009b. Drought Resilience of the California Central Valley Surface-Groundwater-Conceyabce System 45. https://doi.org/10.1111/j.1752-1688.2009.00329.x

Niswonger, R.G., Morway, E.D., Triana, E., Huntington, J.L., 2017. Managed aquifer recharge through off-season irrigation in agricultural regions. Water Resour. Res. 53, 6970–6992.

Niu, G., Yang, Z., Mitchell, K.E., Chen, F., Ek, M.B., Barlage, M., Kumar, A., Manning, K., Niyogi, D., Rosero, E., 2011. The community Noah land surface model with multiparameterization options (Noah-MP): 1. Model description and evaluation with local-scale measurements. J. Geophys. Res. Atmospheres 116.

O'Geen, A., Saal, M., Dahlke, H., Doll, D., Elkins, R., Fulton, A., Fogg, G., Harter, T., Hopmans, J., Ingels, C., 2015. Soil suitability index identifies potential areas for groundwater banking on agricultural lands. Calif. Agric. 69, 75–84.

Ojha, C., Werth, S., Shirzaei, M., 2020. Recovery of aquifer-systems in Southwest US following 2012-2015 drought: evidence from InSAR, GRACE and groundwater level data. J. Hydrol. 124943–124943.

Ojha, C., Werth, S., Shirzaei, M., 2019. Groundwater loss and aquifer system compaction in San Joaquin Valley during 2012–2015 drought. J. Geophys. Res. Solid Earth 124, 3127–3143.

Olden, J.D., Poff, N.L., 2003. Redundancy and the choice of hydrologic indices for characterizing streamflow regimes. River Res. Appl. 19, 101–121.

Olmstead, A.L., Rhode, P.W., 2017. A history of California agriculture. Giannini Found. Agric. Econ. Univ. Calif.

Pan, M., Yuan, X., Wood, E.F., 2013. A probabilistic framework for assessing drought recovery. Geophys. Res. Lett. 40, 3637–3642. https://doi.org/10.1002/grl.50728

Perez-Valdivia, C., Sauchyn, D., 2011. Tree-ring reconstruction of groundwater levels in Alberta, Canada: Long term hydroclimatic variability. Dendrochronologia 29, 41–47.

Perez-Valdivia, C., Sauchyn, D., Vanstone, J., 2012. Groundwater levels and teleconnection patterns in the Canadian Prairies. Water Resour. Res. 48.

Perrone, D., Rohde, M.M., 2016. Benefits and economic costs of managed aquifer recharge in California. San Franc. Estuary Watershed Sci. 14, 0–13. https://doi.org/10.15447/sfews.2016v14iss2art4

Pierce, D.W., Cayan, D.R., Thrasher, B.L., 2014. Statistical Downscaling Using Localized Constructed Analogs (LOCA)*. J. Hydrometeorol. 15, 2558–2585. https://doi.org/10.1175/JHM-D-14-0082.1

Pierce, D.W., Kalansky, J.F., Cayan, D.R., 2018. Climate, drought, and sea level rise scenarios for the fourth California climate assessment. California's Fourth Clim. Change Assess. Calif. Energy Comm. Publ. Number CNRA-CEC-2018-006.

Planert, M., Williams, J.S., 1995. Groundwater atlas of the United States, California, Nevada. HA 730-B. US Geol. Surv. Rest. VA.

Ralph, F.M., Dettinger, M.D., 2012. Historical and national perspectives on extreme West Coast precipitation associated with atmospheric rivers during December 2010. Bull. Am. Meteorol. Soc. 93, 783–790.

Rateb, A., Scanlon, B.R., Pool, D.R., Sun, A., Zhang, Z., Chen, J., Clark, B., Faunt, C.C., Haugh, C.J., Hill, M., 2020. Comparison of Groundwater Storage Changes From GRACE Satellites With Monitoring and Modeling of Major US Aquifers. Water Resour. Res. 56, e2020WR027556-e2020WR027556.

Richey, A.S., Thomas, B.F., Lo, M., Reager, J.T., Famiglietti, J.S., Voss, K., Swenson, S., Rodell, M., 2015. Quantifying renewable groundwater stress with GRACE. Water Resour. Res. 51, 5217–5238.

Rodell, M., Famiglietti, J.S., 2002. The potential for satellite-based monitoring of groundwater storage changes using GRACE: the High Plains aquifer, Central US. J. Hydrol. 263, 245–256.

Rodell, M., Velicogna, I., Famiglietti, J.S., 2009. Satellite-based estimates of groundwater depletion in India. Nature 460, 999–1002.

Ronayne, M.J., Roudebush, J.A., Stednick, J.D., 2017. Analysis of managed aquifer recharge for retiming streamflow in an alluvial river. J. Hydrol. 544, 373–382. https://doi.org/10.1016/j.jhydrol.2016.11.054

Russo, T.A., Lall, U., 2017. Depletion and response of deep groundwater to climate-induced pumping variability. Nat. Geosci. 10, 105–108. https://doi.org/10.1038/ngeo2883

Save, 2020. CSR GRACE and GRACE-FO RL06 Mascon Solutions v02, doi: 10.15781/cgq9-nh24.

Save, H., Bettadpur, S., Tapley, B.D., 2016. High-resolution CSR GRACE RL05 mascons. J. Geophys. Res. Solid Earth 121, 7547–7569.

Scanlon, B. R., Faunt, C.C., Longuevergne, L., Reedy, R.C., Alley, W.M., McGuire, V.L., McMahon, P.B., 2012. Groundwater depletion and sustainability of irrigation in the US High Plains and Central Valley. Proc. Natl. Acad. Sci. 109, 9320–9325. https://doi.org/10.1073/pnas.1200311109

Scanlon, Bridget R, Faunt, C.C., Longuevergne, L., Reedy, R.C., Alley, W.M., McGuire, V.L., McMahon, P.B., 2012a. Groundwater depletion and sustainability of irrigation in the US High Plains and Central Valley. Proc. Natl. Acad. Sci. 109, 9320–9325.

Scanlon, Bridget R, Longuevergne, L., Long, D., 2012b. Ground referencing GRACE satellite estimates of groundwater storage changes in the California Central Valley, USA. Water Resour. Res. 48.

Scanlon, Bridget R., Reedy, R.C., Faunt, C.C., Pool, D., Uhlman, K., 2016. Enhancing drought resilience with conjunctive use and managed aquifer recharge in California and Arizona. Environ. Res. Lett. 11, 035013.

Scanlon, Bridget R, Zhang, Z., Save, H., Wiese, D.N., Landerer, F.W., Long, D., Longuevergne, L., Chen, J., 2016. Global evaluation of new GRACE mascon products for hydrologic applications. Water Resour. Res. 52, 9412–9429.

Siebert, S., Burke, J., Faures, J.-M., Frenken, K., Hoogeveen, J., Döll, P., Portmann, F.T., 2010. Groundwater use for irrigation–a global inventory. Hydrol. Earth Syst. Sci. 14, 1863–1880.

Sprenger, C., Hartog, N., Hernández, M., Vilanova, E., Grützmacher, G., Scheibler, F., Hannappel, S., 2017. Inventory of managed aquifer recharge sites in Europe: historical development, current situation and perspectives. Hydrogeol. J. 25, 1909–1922.

Taylor, R.G., Scanlon, B., Döll, P., Rodell, M., Van Beek, R., Wada, Y., Longuevergne, L., Leblanc, M., Famiglietti, J.S., Edmunds, M., Konikow, L., Green, T.R., Chen, J., Taniguchi, M., Bierkens, M.F.P., Macdonald, A., Fan, Y., Maxwell, R.M., Yechieli, Y., Gurdak, J.J., Allen, D.M., Shamsudduha, M., Hiscock, K., Yeh, P.J.F., Holman, I., Treidel, H., 2013. Ground water and climate change. Nat. Clim. Change 3, 322–329. https://doi.org/10.1038/nclimate1744

Thomas, B.F., Famiglietti, J.S., 2019. Identifying Climate-Induced Groundwater Depletion in GRACE Observations. Sci. Rep. 9, 4124–4124. https://doi.org/10.1038/s41598-019-40155-y

Thomas, B.F., Famiglietti, J.S., Landerer, F.W., Wiese, D.N., Molotch, N.P., Argus, D.F., 2017. GRACE groundwater drought index: Evaluation of California Central Valley groundwater drought. Remote Sens. Environ. 198, 384–392.

Thornton, P., Thornton, M.M., Mayer, B.M., Wei, Y., Devarakonda, R.S., Vose, R.S., Cook, R.B., 2017. Daymet: Daily Surface Weather Data on a 1-km Grid for North America, Version 3 ORNL DAAC Oak Ridge Tenn.

USBR, 2014. Central Valley Project U.S. Department of Interior Bureau of Reclamation.

USDA-NASS, 2020. National Agricultural Statistics Service Cropland Data Layer, Published crop-specific data layer. Available at https://nassgeodata.gmu.edu/CropScape/. USDA-NASS, Washington, DC.

USGS, 2020. National Water Information System data available on the World Wide Web (USGS Water Data for the Nation). source: http://waterdata.usgs.gov/nwis/.

USGS, 2016. Daily Streamflow Conditions, USGS Current Water Data for the Nation http://waterdata.usgs.gov/nwis/rt.

VanRheenen, N.T., Wood, A.W., Palmer, R.N., Lettenmaier, D.P., 2004. Potential implications of PCM climate change scenarios for Sacramento–San Joaquin River Basin hydrology and water resources. Clim. Change 62, 257–281.

Vorosmarty, C.J.;, Green, P., Salisbury, J., Lammers, B.R., 2000. Global Water Resources: Vulnerability from Climate Change and Population Growth. Science 289, 284–288. https://doi.org/10.1126/science.289.5477.284

Voss, K., Swenson, S., Rodell, M., Richey, A.S., Thomas, B.F., Lo, M.-H., Reager, J.T., Famiglietti, J.S., 2015. Quantifying renewable groundwater stress with GRACE. Water Resour. Res. 51, 1–22. https://doi.org/10.1002/2015WR017349.Received

Wada, Y., Van Beek, L.P.H., Van Kempen, C.M., Reckman, J.W.T.M., Vasak, S., Bierkens, M.F.P., 2010. Global depletion of groundwater resources. Geophys. Res. Lett. 37, 1–5. https://doi.org/10.1029/2010GL044571

Wahr, J., Molenaar, M., Bryan, F., 1998. Time variability of the Earth's gravity field: Hydrological and oceanic effects and their possible detection using GRACE. J. Geophys. Res. Solid Earth 103, 30205–30229.

Wang, J., Yin, H., Chung, F., 2011. Isolated and integrated effects of sea level rise, seasonal runoff shifts, and annual runoff volume on California's largest water supply. J. Hydrol. 405, 83–92. https://doi.org/10.1016/j.jhydrol.2011.05.012

Watkins, M.M., Wiese, D.N., Yuan, D., Boening, C., Landerer, F.W., 2015. Improved methods for observing Earth's time variable mass distribution with GRACE using spherical cap mascons. J. Geophys. Res. Solid Earth 120, 2648–2671.

Wendt, D.E., Van Loon, A.F., Scanlon, B.R., Hannah, D.M., 2021. Managed aquifer recharge as a drought mitigation strategy in heavily-stressed aquifers. Environ. Res. Lett. 16, 14046–14046.

Wilhite, D.A., Glantz, M.H., 1985. Understanding: the drought phenomenon: the role of definitions. Water Int. 10, 111–120.

Winter, T.C., Harvey, J.W., Franke, O.L., Alley, W.M., 1998. Ground water and surface water: a single resource. US geological Survey.

Woldeamlak, S.T., Batelaan, O., De Smedt, F., 2007. Effects of climate change on the groundwater system in the Grote-Nete catchment, Belgium. Hydrogeol. J. 15, 891–901.

Wu, W.-Y., Lo, M.-H., Wada, Y., Famiglietti, J.S., Reager, J.T., Yeh, P.J.-F., Ducharne, A., Yang, Z.-L., 2020. Divergent effects of climate change on future groundwater availability in key mid-latitude aquifers. Nat. Commun. 11, 1–9.

Xiao, M., Koppa, A., Mekonnen, Z., Pagán, B.R., Zhan, S., Cao, Q., Aierken, A., Lee, H., Lettenmaier, D.P., 2017. How much groundwater did California's Central Valley lose during the 2012–2016 drought? Geophys. Res. Lett. 44, 4872–4879.

Zektser, I.S., Loaiciga, H.A., 1993. Groundwater fluxes in the global hydrologic cycle: past, present and future. J. Hydrol. 144, 405–427.